UNIVERSITY OF TWENTE.

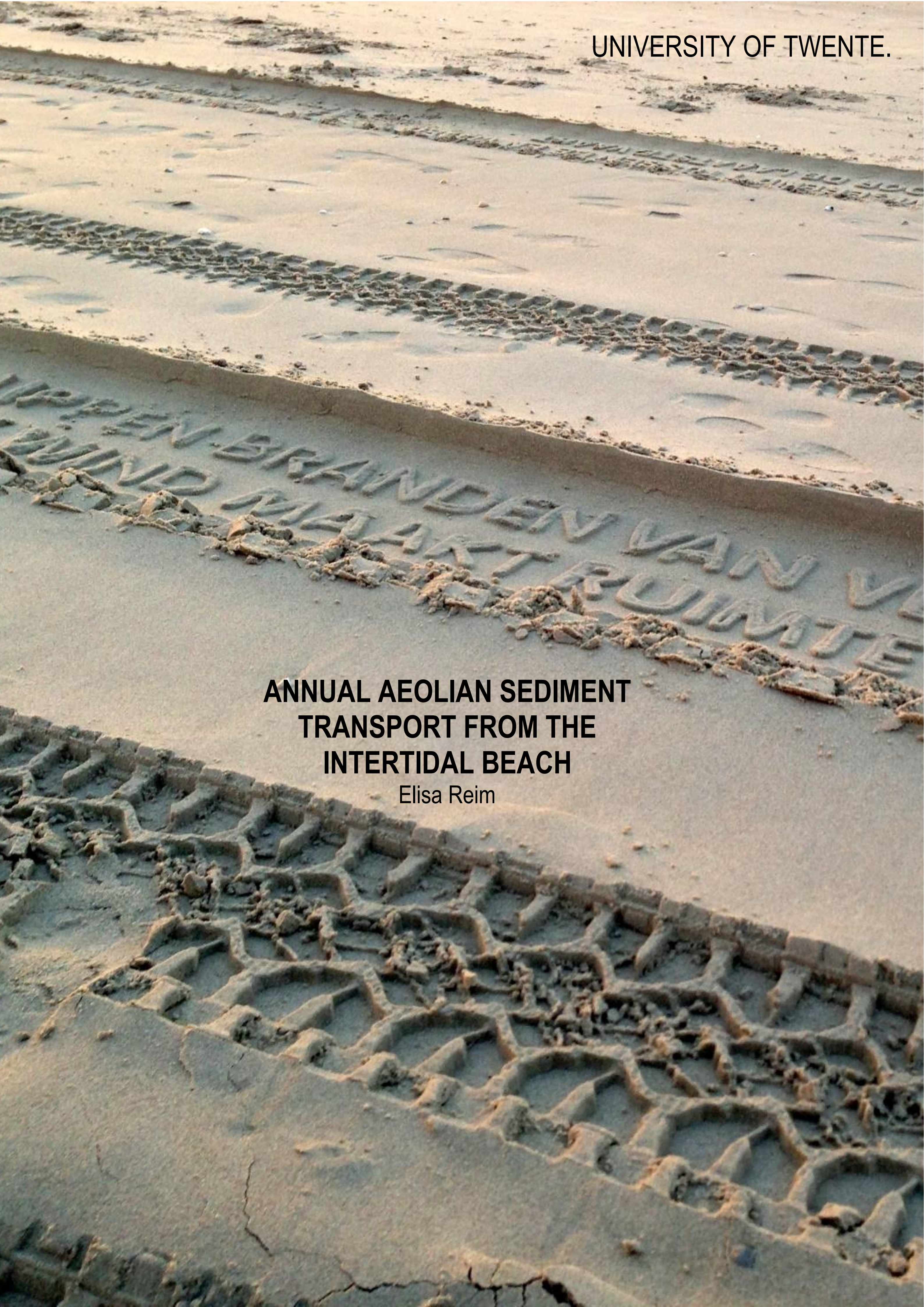

ANNUAL AEOLIAN SEDIMENT TRANSPORT FROM THE INTERTIDAL BEACH

Elisa Reim

MASTER THESIS

Water Engineering and Management

ANNUAL AEOLIAN SEDIMENT TRANSPORT FROM THE INTERTIDAL BEACH

AUTHOR

Elisa Reim

Faculty of Engineering Technology

Water Engineering and Management

Examination Committee

Chairperson: Dr. Ir. Jan S. Ribberink

Supervisor: Dr. Kathelijne M. Wijnberg

UNIVERSITY OF TWENTE.

November 26th 2013

PREFACE

'Siehst Du, Momo', sagte er, 'es ist so: Manchmal hat man eine sehr lange Straße vor sich. Man denkt, die ist so schrecklich lang, die kann man niemals schaffen, denkt man.' Er blickte eine Weile schweigend vor sich hin, dann fuhr er fort: 'Und dann fängt man an, sich zu eilen. Und man eilt sich immer mehr. Jedes Mal, wenn man aufblickt, sieht man, dass es gar nicht weniger wird, was noch vor einem liegt. Und man strengt sich noch mehr an, man kriegt es mit der Angst zu tun, und zum Schluss ist man ganz aus der Puste und kann nicht mehr. Und die Straße liegt immer noch vor einem. So darf man es nicht machen!'

Er dachte einige Zeit nach. Dann sprach er weiter: 'Man darf nie an die ganze Straße auf einmal denken, verstehst Du? Man muss nur an den nächsten Schritt denken, den nächsten Atemzug, den nächsten Besenstrich. Und immer wieder nur den nächsten.' Wieder hielt er inne und überlegte, ehe er hinzufügte: 'Dann macht es Freude; das ist wichtig, dann macht man seine Sache gut. Und so soll es sein.'

Michael Ende, Momo, 1973

Danke Mama und Jürgen.

Er haderte mit sich, bis er sich schließlich sagte, es sei eigentlich ganz normal, dass er nicht wisse, was er wolle. Man kann nie wissen, was man wollen soll, weil man nur ein Leben hat, das man weder mit früheren Leben vergleichen noch in späteren korrigieren kann. Es ist unmöglich zu überprüfen, welche Entscheidung die richtige ist, weil es keine Vergleiche gibt. Man erlebt alles unmittelbar, zum ersten Mal und ohne Vorbereitung. Wie ein Schauspieler, der auf die Bühne kommt, ohne vorher je geprobt zu haben. Was aber kann das Leben wert sein, wenn die erste Probe für das Leben schon das Leben selber ist? Aus diesem Grunde gleicht das Leben immer einer Skizze. Auch 'Skizze' ist nicht das richtige Wort, weil Skizze immer ein Entwurf zu etwas ist, die Vorbereitung eines Bildes, während die Skizze unseres Lebens eine Skizze von nichts ist, ein Entwurf ohne Bild.

Milan Kundera, Die unerträgliche Leichtigkeit des Seins, 1984

Danke Papa und Omi.

‘Je mag nooit vergeten: IJsberen hebben een rugzak nodig!’

Dank je Niels.

SUMMARY

This report presents a case study analysis of the quantification of sediment that is annually transported from the intertidal beach to the upper beach by wind at Egmond Beach in one particular year (2009). Special attention is paid to the relationship between the complex alongshore varying intertidal beach topography, which defines the fetch distance, and onshore directed aeolian sediment transport from the intertidal beach to the upper beach. The effect of a probable increased and varying moisture content was not yet accounted for.

Semi-hourly collected ARGUS (digital monitoring system) video images from Egmond Beach, The Netherlands, of the year 2009 were used to identify the occurrence of aeolian sediment transport. Hourly averaged wind speed and wind direction data from IJmuiden and precipitation data from Wijk aan Zee were used to get insight into the effect of those on aeolian sediment transport occurrences. The sediment transport equation of Kawamura (1951) was used to calculate the amount of sediment that could theoretically be transported from the intertidal beach towards the upper beach and dunes during conditions in which actual aeolian sediment transport was observed. Moisture content was accounted for using the equation of Dong et al. (2002) and the effect of fetch limitation was accounted for by using the equation of Delgado-Fernandez (2010).

It appeared that the hourly averaged wind speed data available from the long-term wind monitoring at IJmuiden was not an appropriate input value to calculate annual onshore aeolian sediment transport, as it lead to an underestimation. A new 'representative wind speed' was developed to account for gustiness of the wind throughout the hour. The translation to a representative wind speed value was developed based on an analysis of high resolution time series for wind speeds from wind stations near Salt Lake City, United States of America.

The most aeolian sediment transport occurrences were observed while wind was blowing alongshore or nearly alongshore the beach, which in the case of Egmond Beach means wind directions from South-West. No single velocity threshold for aeolian sediment transport occurrences valid for all wind direction has been found. Nevertheless, below an hourly averaged wind speed of 6 ms^{-1} almost no aeolian sediment transport occurrences have been identified.

The formula that is used in this study to calculate the annual aeolian sediment transport is most sensitive to changes in surface roughness length. Therefore, the surface roughness length is one of the key parameters of onshore annual aeolian sediment transport calculations.

The dune volume change per year at Egmond Beach is measured to be 10 $m^3m^{-1}y^{-1}$ (Arens, 2010). The total calculated onshore annual aeolian sediment transport in this study is 9.4 $m^3m^{-1}y^{-1}$ which is almost the same amount as found by Arens (2010). However, only in 5% of the aeolian sediment transport occurrences, the actual fetch distance was smaller than the theoretical critical fetch. However, the effect of the alongshore varying fetch distances on annual onshore aeolian sediment transport has been found, as 0.88 $m^3m^{-1}y^{-1}$. This is 8% of the total annual onshore aeolian sediment transport. It can be concluded that the small amount of cases, for which the actual fetch distance is smaller than the critical fetch distance, can result in a non-negligible difference in annual onshore aeolian sediment transport.

During the hours that transport was identified in the ARGUS images, 75% of the calculated annual aeolian sediment transport took place. During the hours that no transport was identified in the ARGUS images, 25% of the annual aeolian sediment transport was calculated (due to transport enabling wind conditions). Therefore, the identification of sediment transport occurrences on ARGUS images is an important part of the annual aeolian sediment transport calculation method.

Overall, in this study a method has been developed to calculate representative theoretical annual onshore aeolian sediment transport. This method consist of the analysis of ARGUS images, measurement of the fetch distances and development of a representative wind speed accounting for the gustiness of the wind.

TABLE OF CONTENTS

1. INTRODUCTION

1.1. CONTEXT – DUTCH COASTAL PROTECTION

At the Dutch coast, dunes function as a natural barrier protecting the hinterland from flooding during storm events. The advantages of dunes as coastal protection are that as well as being partly built by naturally occurring processes, they also provide space for recreation. The disadvantage of using such coastal protection structures is the fact that they are dynamic, meaning that the provided safety level varies in time.

At the most critical parts of the Dutch coast hard shore protection elements, such as dykes, groins, and seawalls, have been placed to secure the safety of land and people. Nevertheless, on average the Dutch coastline has more soft shore protection solutions than hard ones. Due to the fact that sediment can move freely along most parts of the Dutch coastline via transportation by wind or water, the coast can become weakened and the accepted safety standards are exceeded from time to time. These weak parts of the Dutch coastline were then fortified inter alia using hard structures as dykes and groins as well as using less interfering structures such as planting grass, placing sand trap fences and nourishing sand where needed. The idea was to interfere as little as possible with the natural processes occurring at the Dutch coastline. The interference had to be just enough to keep land and people safe and not to interfere more than needed with nature.

In the past dunes were reinforced in a reactive manner, meaning that the dunes where stabilized when safety criteria were not met. In contrast, recent flood management strategies in the Netherlands are meant to be proactive. In 1990, a formal policy for coastal management was adopted which is called the dynamic coastline preservation policy (Taal, et al., 2006). From 1990 onward the Dutch coast is nourished everywhere when it would otherwise move land inward compared to the situation in 1990. This nourishment strategy led to an annual nourishment volume of 12 million m^3 since 2000. Until now this strategy has been very effective, but keeping in mind the sea level rise the Delta Committee recommends to further extend the Dutch coastline to keep the inland safe in the long term. This extension should be made as effective and sustainable as possible. The Delta Committee continuously explores possibilities of how to use the natural processes at the coast to build, maintain and reinforce dunes. Coastal protection and natural coastal development are meant to be integrated to create an interdisciplinary flood management strategy. Long term safety of coasts is the goal that needs to be reached (Taal, et al., 2006). To be able to protect the Dutch coast in future in an effective and sustainable manner, the movement of sediment over and along the beach needs to be well understood. Until now only empirical data is available to assess the amount of sediment that reaches the dune. The empirically determined amount reaching the dune is around 10 $m^3m^{-1}y^{-1}$ near to Egmond Beach, (Arens, 2010). It is not possible yet to simulate and predict this amount of sediment from the physical process modelling using monitoring data of wind conditions and beach topography.

1.2. Objectives

This study aims to assess the amount of sediment that can theoretically be transported onshore annually from the intertidal beach to the upper beach by wind. Special attention is paid to the effect of alongshore varying intertidal topography on long term onshore directed aeolian sediment transport from the intertidal beach to the upper beach on Egmond Beach.

1.3. Research Questions

1. **What is the amount of sediment that can leave the intertidal beach by wind on an annual basis?**

    a. **How often and under which conditions does aeolian sediment transport occur?**
        i. How often does aeolian sediment transport occur per year?
        ii. At which wind speeds and wind direction does aeolian sediment transport occur?
        iii. What is the effect of the presence of precipitation on aeolian sediment transport?

    b. **How much aeolian sediment transport can occur in theory under these conditions?**
        i. What is the effect of the fetch distance on the annual aeolian sediment transport rate?
        ii. What is the effect of the wind speed on the annual aeolian sediment transport rate?

1.4. Research Approach

To answer the research questions a case study was done for Egmond Beach. During this case study a long term ARGUS video image database showing the intertidal beach and aeolian sediment transport occurrences was combined with long-term monitoring data on wind conditions. Given this dataset, annual aeolian transport at Egmond Beach was calculated. Aeolian sediment transport is defined as visible sediment movement over the beach, comparing two consecutive ARGUS images.

Firstly, the ARGUS images available for Egmond Beach in 2009 have been analysed. All ARGUS images showing aeolian sediment transport were linked to monitoring wind speed, wind direction, water level and precipitation data from IJmuiden. Having made this connection it has been looked for the effect of these parameters on visible aeolian sediment transport. In the whole study all references to aeolian sediment transport in any form are meant as visible aeolian sediment transport.

Secondly, a program was developed to be able to measure the fetch distances, alongshore Egmond Beach, from rectified ARGUS images. Using these images and the wind direction, the developed program is able to measure the fetch distances for every required location on the beach.

Thirdly, an algorithm was developed to translate the hourly averaged wind speeds to representative wind speeds. This has been done to be able to take the gustiness of the wind throughout the hour into account and calculate the annual onshore aeolian sediment transport. This translation is based on a large amount of high resolution time series for wind speeds from wind stations near Salt Lake City.

Thereafter, the annual onshore aeolian sediment transport was calculated using a mathematical model based on Kawamura (1951) taking into account the moisture content (Dong, et al., 2002) and the fetch distances for the cases where the actual fetch distance is smaller than the critical fetch distance (Delgado-Fernandez, 2010). Insight was gained into the amount of theoretical aeolian sediment transport from the intertidal beach to the upper beach.

Lastly, conclusions were drawn and recommendations for further research have been made.

2. AEOLIAN SEDIMENT TRANSPORT PROCESS ON BEACHES

Sediment transport caused by wind depends on several different and often interdependent variables. This chapter will give insight into the most important parameters that ought to have significant effect on aeolian sediment transport on beaches. The variables that will be explained in this chapter are: wind speed, fetch distance, and the combined effect of moisture and the beach topography.

The effect of wind speed, wind direction and moisture content of the beach surface on the magnitude of aeolian sediment transport on the beach is difficult to model. Therefore, the prediction of long term sediment delivery into the foredunes is a big challenge. So far, most insight has been gained in terms of short term aeolian sediment transport. It is found that short term variations in sediment transport occur because of short term changes in wind speed, variations in wind direction, precipitation intensity and tide level (Bauer, et al., 2009).

Because of the large amount of interacting environmental variables, operating at various spatial and temporal scales, studying aeolian sediment transport is challenging. It is not clearly understood how these variables operate individually and together. The missing knowledge of the aeolian sediment transport process including interacting environmental variables makes the quantification of these variables and interactions difficult. Modelling improved further and further but the proper validation using field data is still missing. The existing models try to cope with topographic variations (Bauer, et al., 1990), the effect of atmospheric considerations such as precipitation and air density, etc. (Sherman, et al., 1990), surface moisture and drying effects (Nordstorm, et al., 1992) and grain size variations (Rice, 1990). The preceding studies are mostly based on short term observations. Two variables that are often not taken into account during preceding theoretical studies are fetch distance and moisture content.

In the following sub-section, the main aeolian sediment transport influencing parameters will be explained in more detail.

2.1. CHARACTERISTICS ON A BEACH

EFFECT OF WIND SPEED

Wind speed is one of the most important parameters influencing aeolian sediment transport. Increasing wind speed causes a greater forward velocity of saltating grains. As a result the amount of sediment in motion increases. It was found that the rate of sediment transport by saltation ascends linearly with the third power of the wind speed. Sediment can be moved best at the highest wind speeds. Nevertheless, high wind speeds are infrequent and often go hand in hand with heavy precipitation that causes immobilization of the grains. Figure 1 shows the relationship between wind speed and sediment movement. It can be clearly seen that according to Warren (1979) the most sediment will be transported at about 16 ms^{-1} (Bagnold, 1941; Greeley, et al., 1985; Iversen, et al., 1999). Figure 1 states that the frequency curve of wind speeds has its peak at 8 ms^{-1} whereas the peak of the rate of sand movement in relation to wind speeds is given at 16 ms^{-1}. A more recent case study showed that most sediment has been transported between 8 ms^{-1} and 12 ms^{-1} (Delgado-Fernandez, et al., 2011). The difference between these two studies is probably due to the fact that results from Warren (1979) are just about the rate of sand movement in relation to wind speed, while the results of Delgado-Fernandez (2011) take the frequency of different wind speeds into account.

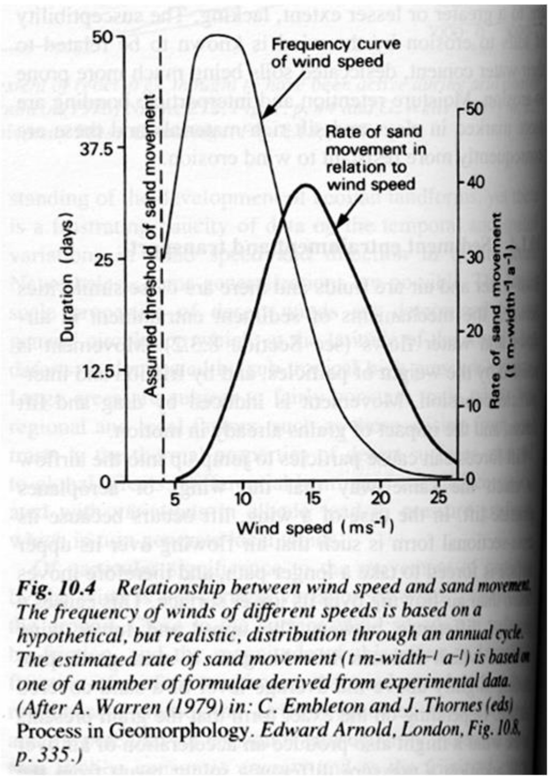

FIGURE 1: THE RELATIONSHIP BETWEEN WIND SPEED AND SEDIMENT MOVEMENT.

EFFECT OF FETCH DISTANCE

Aeolian sediment transport is assumed to depend on the fetch distance. The fetch distance is defined as the distance over the beach across which the wind blows. Longer fetch distances lead to higher transport rates under given wind conditions until a certain limit is reached. This limit is called the critical fetch. When the critical fetch is reached the wind transport is saturated. The maximum fetch length, which is defined in Figure 2, is limited by the beach width. The magnitude of the critical fetch depends on the wind speed, surface moisture content and the presence of lag deposits. The actual fetch distance is highly dependent on the wind direction (de Vries, et al., 2012). If the angle of the approaching wind is more oblique, the fetch distance increases. Therefore, there is a bigger opportunity for the saltation system to evolve toward an equilibrium transport state before the foredunes are reached. To reach the maximum transport equilibrium (predicted) rate the saltation system has to adjust over a downwind distance (Bauer, et al., 2009).

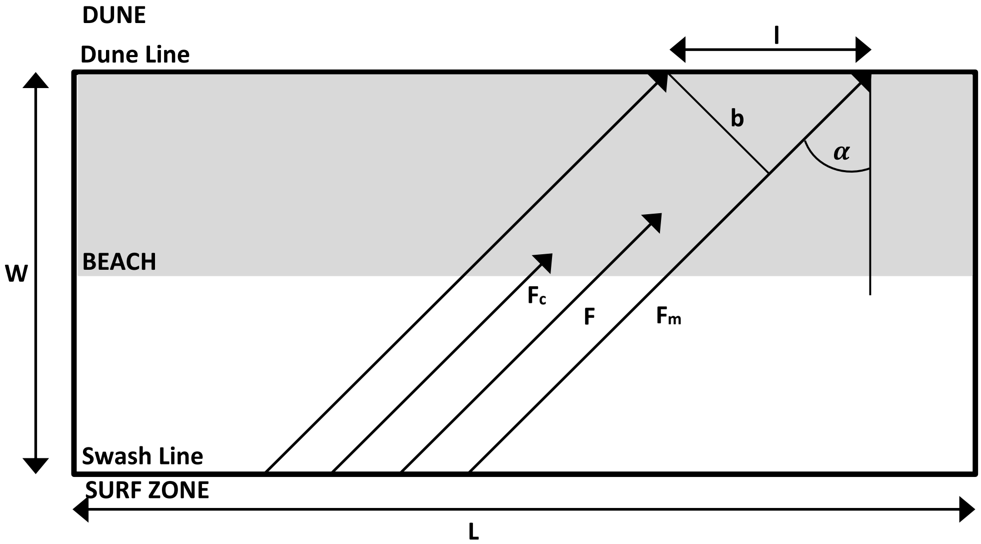

FIGURE 2: DEFINITION OF FETCH DISTANCE ON A RECTANGULAR BEACH OF LENGTH L AND WIDTH W. F_C IS THE CRITICAL FETCH AND F_M IS THE MAXIMUM FETCH RESULTING FROM THE RELATIONSHIP BETWEEN BEACH WIDTH AND ANGLE OF WIND APPROACH, α, RELATIVE TO SHORE NORMAL (BAUER, ET AL., 2002).

In Figure 3, the relationship between transport and the fetch distance is depicted. As can be seen, there are two curves presented until the critical fetch is reached. The blue dashed line shows the relationship as it is commonly known (Bauer, et al., 2002) whereas the black line shows the relationship as it has been found using the transport equation of Delgado-Fernandez (2010). For this study the transport formula of Delgado-Fernandez has been employed.

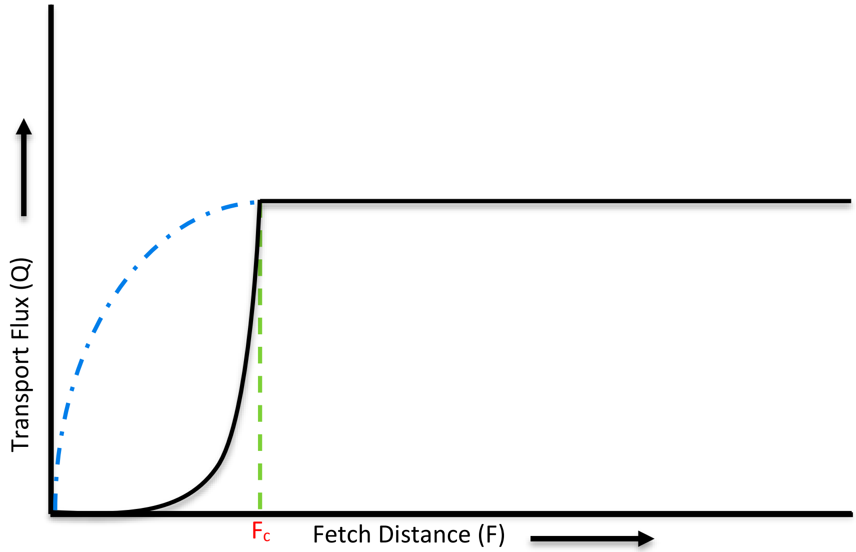

FIGURE 3: VISUALIZATION OF THE CRITICAL FETCH DISTANCE. THE REALTIONSHIP AS IT IS COMMONLY KNOWN (BLUE DASHED LINED) (BAUER, ET AL., 2002) AND THE RELATIONSHIP AS IT HAS BEEN FOUND USING THE TRANSPORT EQUATION OF DELGADO-FERNANDEZ (2010) (BLACK LINE).

Preceding wind tunnel and field studies showed that the critical fetch significantly depends on the wind speed. It is proven that the critical fetch increases with wind speed for dry and little moist sediment, and with moisture content as well. Nevertheless, it is not yet clear if the maximum sediment transport rate with moist sediment is less, the same or higher than the maximum sediment transport for dry sand (Davidson-Arnott, et al., 2008). The critical fetch is found to have a range from seven metres to several decametres. An increase of the critical fetch means an increase of distance that is needed to reach the maximum transport rate value. (Davidson-Arnott, et al., 1996; Davidson-Arnott, et al., 2008).

EFFECT OF BEACH TOPOGRAPHY AND MOISTURE

The beach geometry is usually stated to be a fixed boundary condition over time for aeolian sediment transport, but tidal excursions and storm surges have strong influence on the geometry of the beaches. Therefore, this geometry may not be seen as fixed and models should be developed which are able to deal with this situation (Bauer, et al., 2009).

The beach topography can also have significant influence on the fetch length and the aeolian sediment transport. Additionally, beach topography variations may cause variations in the development of the wind boundary layer, which may influence the aeolian sediment transport as well (Svasek, et al., 1974). On the beaches in the Netherlands a multitude of intertidal bars alternating with troughs can be found. This varying topography may cause variations in wind flow and therefore further variations in sediment transport. Strong cross shore variations in the surface moisture content can be seen at beaches that show large tidal ranges. Due to the topographical variations that cause variations in surface roughness and the variations in moisture content across the beach, the aeolian sediment transport may be affected (Anthony, et al., 2009).

Moisture reduces the transport of sediment (Bauer, et al., 2009; Davidson-Arnott, et al., 2005). The moisture content on the beach can be influenced by different factors: Rainfall, wave run-up, storm surge and tidal excursions. Short term fluctuations in sand transport are partly controlled by the episodic stripping of dry sand veneers and subsequent exposure of moist sand. Before further sand mobilization takes place the cohesive sand patches need to be dried. Due to the drying, a temporal variability in sand transport will take place. This might also be the case if the wind is steady (Bauer, et al., 2009).

The possible variation of surface moisture content over short distances should not be neglected. The variation depends on beach water hydraulics as well as on the grain sizes and their packing. In general: The beach water table shows a seaward slope during the falling tide and a landward slope during the rising tide. The tide and beach water table are sometimes decoupled. This phenomenon can be observed when beach drainage lags behind the falling tide, meaning that a seepage is formed expanding offshore during the falling of the tide. A cross shore pattern of groundwater zones can be seen between the seepage zone on the lower beach and the dry zone on the upper beach (Horn, 2002; Horn, 2006). The most advantageous area for aeolian sediment transport is the upper beach zone. This area is rather narrow and during spring tide, the moisture content of the beach surface may be so high that the sediment is immobilized (Oblinger, et al., 2008).

Additionally, the critical fetch will be influenced by the surface moisture content and the bed forms. It has been found that fetch segmentation may be reflected in the cross shore patterns of the bed form development that might embody moisture. Furthermore, fetch segmentation depends on the bar-trough distinction in surface moisture. If the troughs are permanently saturated, they will inhibit sediment transport. The dry fetch is interrupted or limited by the troughs, which means that the saltation process of the grains will likewise be limited or stopped. Therefore, the potential sediment supply from the beach to the foredune is dependent on and limited by the fetch segmentation. It is found that beach bars cause wind acceleration for onshore winds and deceleration for offshore winds (Anthony, et al., 2009).

3. METHODOLOGY

In this chapter, the equation to calculate aeolian sediment transport and the definition of aeolian sediment transport occurrences will be explained. Furthermore, the definition of the fetch distances and the determination of the representative wind speeds for the aeolian sediment transport calculation will be described.

3.1. CALCULATING THE AEOLIAN SEDIMENT TRANSPORT

In Table 1, the most common aeolian sediment transport equations can be seen. All the equations from Table 1 share a common structure. The horizontal mass transport rate Q is primarily defined by the cube of the shear velocity U_*. Bagnold (1941) and Zingg (1952) suggested that this relationship is modified by the particle diameter relative to a standard diameter for dune sand $D = 250\mu m$. Assuming a constant shear velocity, this means that higher mass transport rates are associated with a larger diameter of the sediment grains. Other models include a threshold shear velocity (U_{*t}) relative to U_* to express the effect of surface texture (Kawamura, 1951). This threshold shear velocity is required for the entrainment of grains. All sediment transport formulae include at least one parameter that has to be determined empirically. The equations assume a steady, uniform flow of air driving a homogeneous cloud of sand in horizontal direction (Nickling, et al., 2009).

	Formula	**Parameters**
Bagnold (1941, desert field study)	$Q = C_b \frac{\rho_a}{g} \sqrt{\frac{d}{D}} (U_*)^3$	Air density (ρ_a) assumed to be $1.22kgm^{-3}$, drag or friction velocity (U_*) in ms^{-1}, empirical coefficient (C_b) from 1.5 for nearly uniform sand over 1.8 for naturally graded to more than 3.5 for a relatively immobile sediment surface
Zingg (1952, wind tunnel experiments)	$Q = C_2 \left(\frac{d}{D}\right)^{\frac{3}{4}} U_*^3 \frac{\rho_a}{g}$	Based on measurements of vertical distribution of aeolian sediment transport in a wind tunnel $C_2 = 0.83$
Kawamura (1951, wind tunnel experiments)	$Q = K \frac{\rho_a}{g} (U_* + U_{*t})^2 (U_* - U_{*t})$	Critical shear velocity added, empirical coefficient $K \approx 2.78$

TABLE 1: THE MOST COMMON AEOLIAN SEDIMENT TRANSPORT EQUATIONS (GREELEY, ET AL., 1985).

The aeolian transport equation used in this study based on that defined by Kawamura (1951). It has been expanded to include the effect of fetch distance as well as moisture content, following Paul van Dijk (1996), Delgado-Fernandez (2010) and Dong et al. (2002).

Firstly, the threshold shear velocity U_{*tm} is adopted to include the effect of moisture. The threshold shear velocity is the minimal shear velocity required to initiate deflation of soil particles. Dong et al. (2002) defined the threshold shear velocity of moistened sand as follows:

$$U_{*tm} = U_{*tr} A[(\rho_s/\rho_a)gd]^{\frac{1}{2}} \text{ for } d \geq 0.1 \cdot 10^{-3}m \qquad (1)$$

With U_{*tm} being the threshold shear velocity of moistened sands. U_{*tr} is defined as dimensionless parameter called "the relative threshold shear velocity" (Dong, et al., 2002). *A* is a proportionality coefficient depending on the particle friction Reynolds number. The Reynolds number is dimensionless and characterizes the air flow turbulence close to the surface. According to Dong et al. (2002), the proportionality coefficient *A* decreases linearly with the square root of the particle friction Reynolds number at the threshold. Due to this relationship it can be said that the turbulence over the surface of the individual sand particles is important for the initiation of sand movement. ρ_s and ρ_a are the densities of sand and air in kg m^{-3}, *g* is the gravitational acceleration in m s^{-2} and *d* is the grain diameter in m.

A is calculated using formula (2) (Dong, et al., 2002), given a Reynolds number for a grain diameter of 0.25 mm, which is derived from wind tunnel experiments and is equal to 5.531 (Han, et al., 2009).

$$A = 0.172 - 0.0046 Re_{*t}^{0.05} = 0.167 \text{ for } d \geq 0.1 \cdot 10^{-3} m \tag{2}$$

The threshold shear velocity of moistened sand needs to be modified by the relative threshold shear velocity (Dong, et al., 2002).

$$U_{*tr} = \left(1 + K_g M\right)^{\frac{1}{2}} \tag{3}$$

With *M* being the moisture content in percentage and K_g a correlational factor according to the grain size. The values for K_g can be found in Table 2 (Dong, et al., 2002). The highlighted row shows the K_g value used according to the grain size.

A combination of equation (1) and (3) leads to a general equation for estimating the threshold shear velocity of moistened sand. In this study following definition of the threshold shear velocity has been used.

$$U_{*tm} = A\left[(\rho_s/\rho_a) g d \left(1 + K_g M\right)\right]^{\frac{1}{2}} \text{ for } d \geq 0.1 \cdot 10^{-3} m \tag{4}$$

(Dong, et al., 2002)

Serial number	**Mean size [mm]**	**K_g**	**R^2**
01	0.05	1.59	0.82
02	0655	1.85	0.90
03	0.0835	2.46	0.87
04	0.09	1.66	0.77
05	0.1175	2.51	0.83
06	0.1425	2.05	0.82
07	0.175	2.75	0.90
08	0.225	1.59	0.90
09	0.325	1.87	0.74
10	0.45	2.15	0.78

TABLE 2: THE RELATIVE THRESHOLD SHEAR VELOCITY FOR DIFFERENT GRAIN SIZES (DONG, ET AL., 2002). THE HIGHLIGHTED ROW CONTAINS THE K_G VALUE USED ACCORDING TO THE GRAIN SIZE.

In Figure 4, the threshold shear velocity over the moisture content for the different grain sizes can be seen. The maximum moisture content shown in Figure 4 is 5% (Dong, et al., 2002). The same relation between threshold shear velocity and moisture content, dealing with a maximum surface moisture content of 4%, has been found in Johnson (1963). In the present study the moisture content of the beach surface is assumed to be 0.25% in the upper part of the intertidal area. This value follows from a field study conducted in Canada using a Delta-T moisture probe. The probe measured the moisture content at the top 2 cm of surface (Yang, et al., 2005).

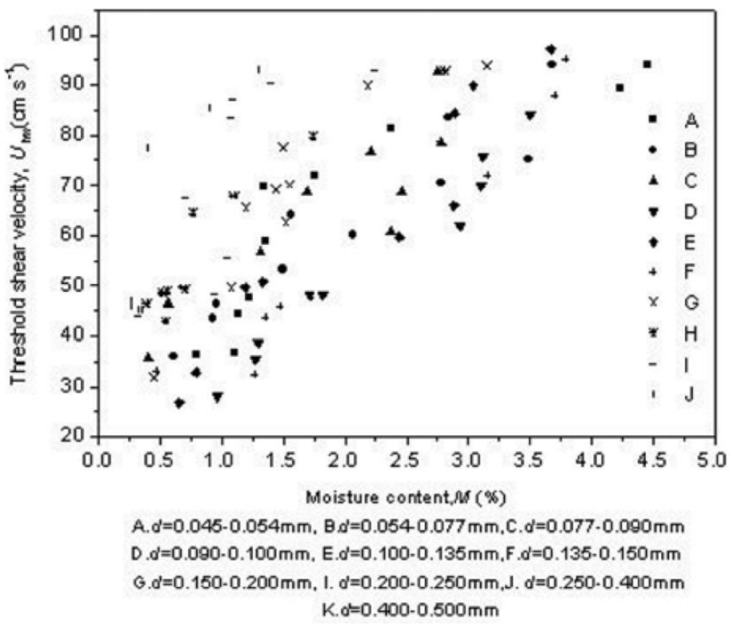

FIGURE 4: THE RESULTS OF THE WIND TUNNEL EXPERIMENT: THE THRESHOLD SHEAR VELOCITIES OF MOISTENED SANDS WITH DIFFERENT GRAIN SIZE (DONG, ET AL., 2002).

Van Dijk (1996) found a relationship between the critical fetch length and the grain size for the different shear velocities. This relationship can be seen in Figure 5.

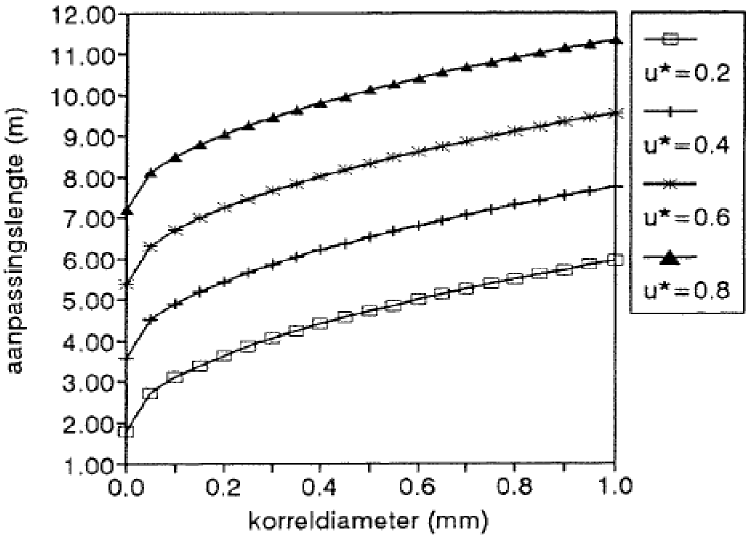

FIGURE 5: THE SALTATION LENGTH FOR THE DIFFERENT GRAIN SIZES DEPENDING ON THE SHEAR VELOCITY (VAN DIJK, 1996).

Van Dijk (1996) defines *L* as the distance traversed in one jump by grains of sand in motion, the saltation length. The saltation length increases with increasing shear velocity and grain size. This is due to the fact that larger grains get to faster moving air, leading to a higher horizontal velocity. In this study a linear relationship between *L* and $(U_* + U_{*t})$ is chosen (van Dijk, 1996). U_* is the shear velocity and U_{*t} the threshold shear velocity. This study includes the shear velocity of moistened sand. Therefore, it follows:

$$L = a(U_* + U_{*tm}) \tag{4}$$

With *a* being a certain coefficient not further defined (van Dijk, 1996). The relationship found by Kawamura (1964) gives that the critcal fetch length F_c is linearly related to *L*.

$$F_c = b(U_* + U_{*tm}) \tag{5}$$

With *b* being a coefficient defined to be 9 (van Dijk, 1996).

Combining the definitions of the critical fetch length (van Dijk, 1996) and the threshold shear velocity (Dong, et al., 2002) the critical fetch length F_c can be calculated.

Knowing these relationships, the sand flux can be calculated using the equation derived by Delgado-Fernandez, (2010):

$$Q = Q_m \frac{2}{\pi} sin^{-1}\left(\frac{F}{F_c}\right) \qquad \begin{array}{l} if \quad F = 0, \quad \sin^{-1}(0) = 0 \quad Q = 0 \\ if \quad F = F_c, \quad \sin^{-1}(1) = \left(\frac{\pi}{2}\right) \quad Q = Q_m \\ if \quad F > F_c, \quad Q = Q_m \\ if \quad F < F_c, \quad Q = Q_m \frac{2}{\pi} sin^{-1}\left(\frac{F}{F_c}\right) \end{array} \tag{6}$$

With Q_m being the maximum sediment transport rate for a given wind speed. The equation for the critical fetch length is based on an equation of Kawamura. Therefore, Q_m will also be calculated using Kawamura's equation for aeolian sediment transport:

$$Q_m = K \frac{\rho_a}{g}(U_* + U_{*tm})^2(U_* - U_{*tm}) \text{ if } U_* > U_{*tm} \tag{7}$$

K is an empirical constant defined in wind tunnel experiments by Kawamura to be 2.78 for a grain diameter of 0.25 mm. No other value has been found according to a grain diameter of 0.25 mm.

Combining equations (5), (6) and (7) following equation for the sediment transport has been found:

$$Q = K \frac{\rho_a}{g}(U_* + U_{*tm})^2(U_* - U_{*tm}) \frac{2}{\pi} sin^{-1}\left(\frac{F}{b(U_* + U_{*tm})}\right) \tag{8}$$

The only unknown left in this equation (8) is U_*.

The shear velocity U_* will be calculated using the "law of wall" equation (von Kármán, 1930):

$$U_Z = \frac{U_*}{\kappa} ln\left(\frac{z}{z_0}\right) \tag{9}$$

U_Z is defined as the wind speed at an elevation z, κ is the dimensionless von Kármán constant defined as 0.4, z_0 is the roughness length of the surface.

Combining equations (4), (8) and (9) the overall formula to calculate aeolian sediment transport during this study has been found to be:

$$Q = K \frac{\rho_a}{g}\left(\frac{U_Z \kappa}{ln\left(\frac{z}{z_0}\right)} + A\left[(\rho_s/\rho_a)gd\left(1 + K_g M\right)\right]^{\frac{1}{2}}\right)^2 \left(\frac{U_Z \kappa}{ln\left(\frac{z}{z_0}\right)} - A\left[(\rho_s/\rho_a)gd\left(1 + K_g M\right)\right]^{\frac{1}{2}}\right) \frac{2}{\pi} sin^{-1}\left(\frac{F}{b\left(\frac{U_Z \kappa}{ln\left(\frac{z}{z_0}\right)} + A\left[(\rho_s/\rho_a)gd\left(1 + K_g M\right)\right]^{\frac{1}{2}}\right)}\right) \tag{10}$$

The value of the roughness surface length was chosen from literature Hsu (1971), who measured values for the surface roughness length around 0.0003 m at the swash zone of a beach. The choice for this order of magnitude is confirmed by the study of Hansen (1993), who presented several tables containing different surface roughness lengths for different surface types. Hansen (1993) stated the surface roughness for a smooth desert to be equal to 0.0003 m.

3.2. OCCURRENCE OF AEOLIAN SEDIMENT TRANSPORT AND DATA SET

To be able to calculate annual aeolian sediment transport it needs to be known at how many hours per year aeolian sediment transport has been observed as well as a link of these times to weather data as wind speed, wind direction and precipitation. In this sub-section the identification of aeolian sediment transport occurrences as well as the weather data is explained.

Firstly, a year was chosen over which the annual aeolian sediment transport has been calculated. The year of choice was 2009, because no dune erosion took place. Dune erosion is assumed to take place if the water level reaches 250 cm +NAP or higher. To understand if 2009 was a year when no dune erosion took place, the water levels were analysed. The closest location to Egmond Beach with measured water level data available is IJmuiden. Figure 6 shows the locations Egmond Beach and IJmuiden, to give an impression of their distance. The measured water levels above 50 cm +NAP at IJmuiden can be seen in Figure 7. The highest water level of 201 cm +NAP has been obtained on November 23rd 2009. Given the fact that a year without dune erosion was chosen, the calculated annual aeolian sediment transport can be compared to the value found for the dune volume change in 2009.

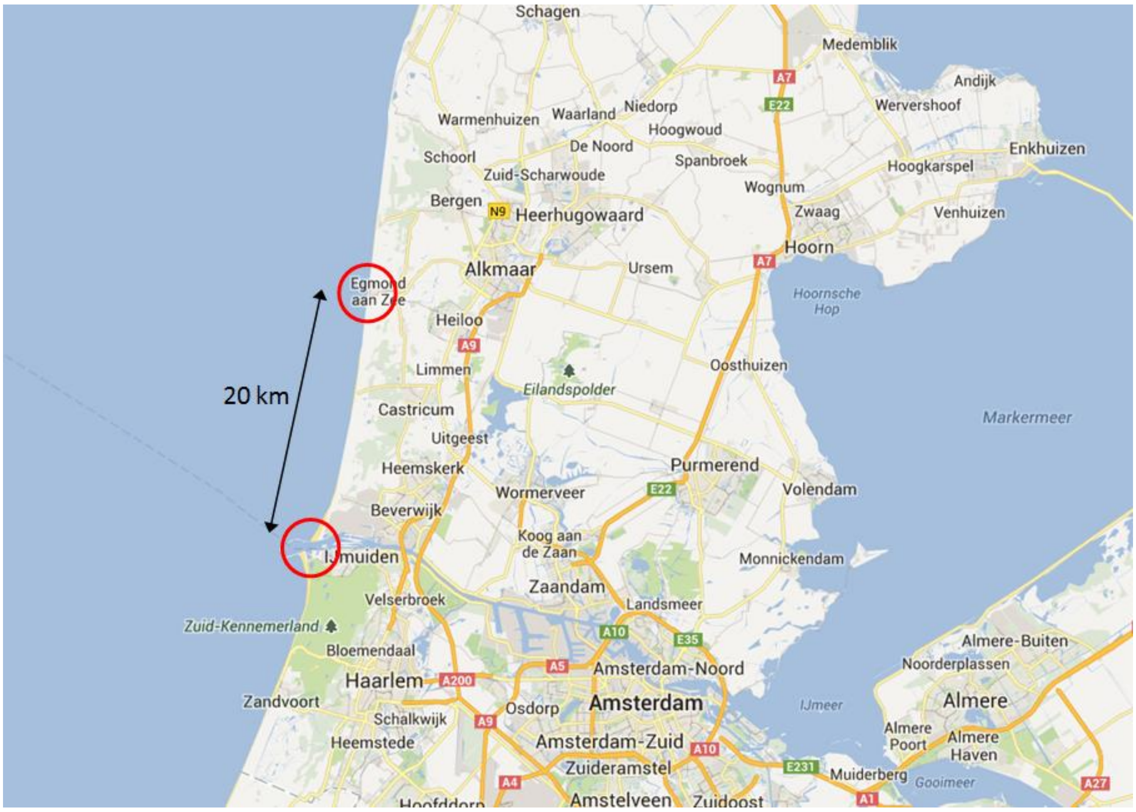

FIGURE 6: THE LOCATIONS EGMOND BEACH AND IJMUIDEN.

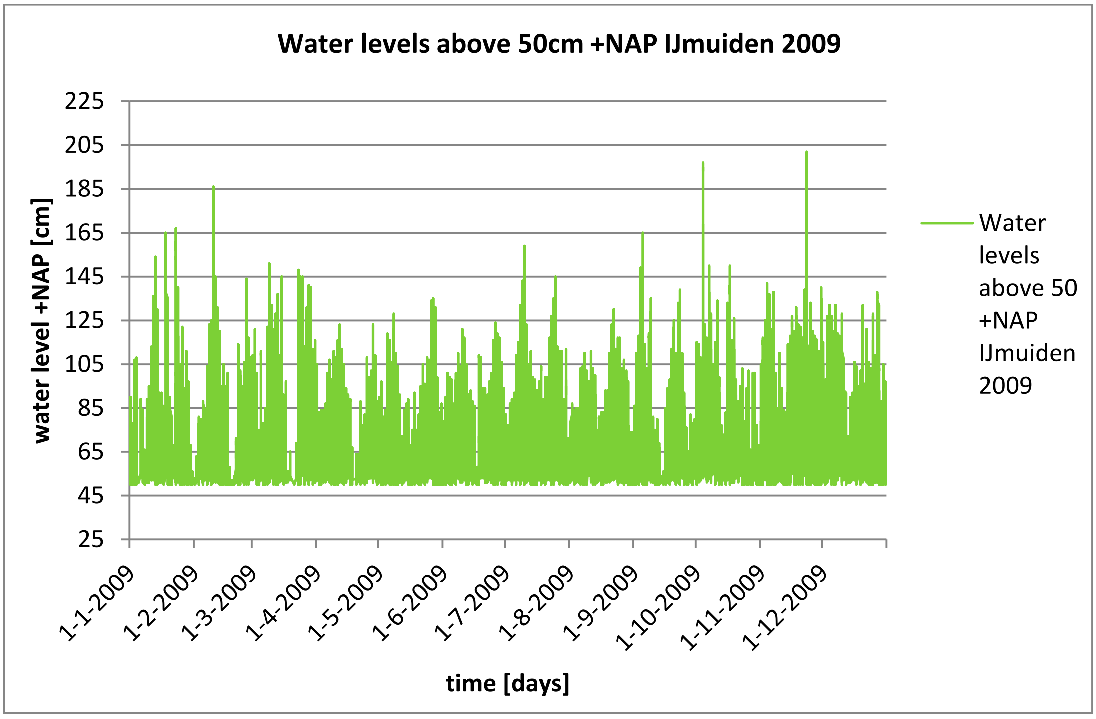

FIGURE 7: THE MEASURED WATER LEVELS ABOVE 50CM +NAP AT IJMUIDEN IN 2009 TO DETERMINE WHETHER THERE HAS BEEN DUNE EROSION AT EGMOND BEACH IN 2009.

The orientation of Egmond Beach is 7.13° North which means that all wind directions between 7.13° North and 187.13 ° North are considered as offshore wind directions. 277.13° North is perpendicular to Egmond Beach and has therefore the smallest possible beach width to get sediment into motion. For clarification, Figure 8 shows the wind directions at Egmond Beach.

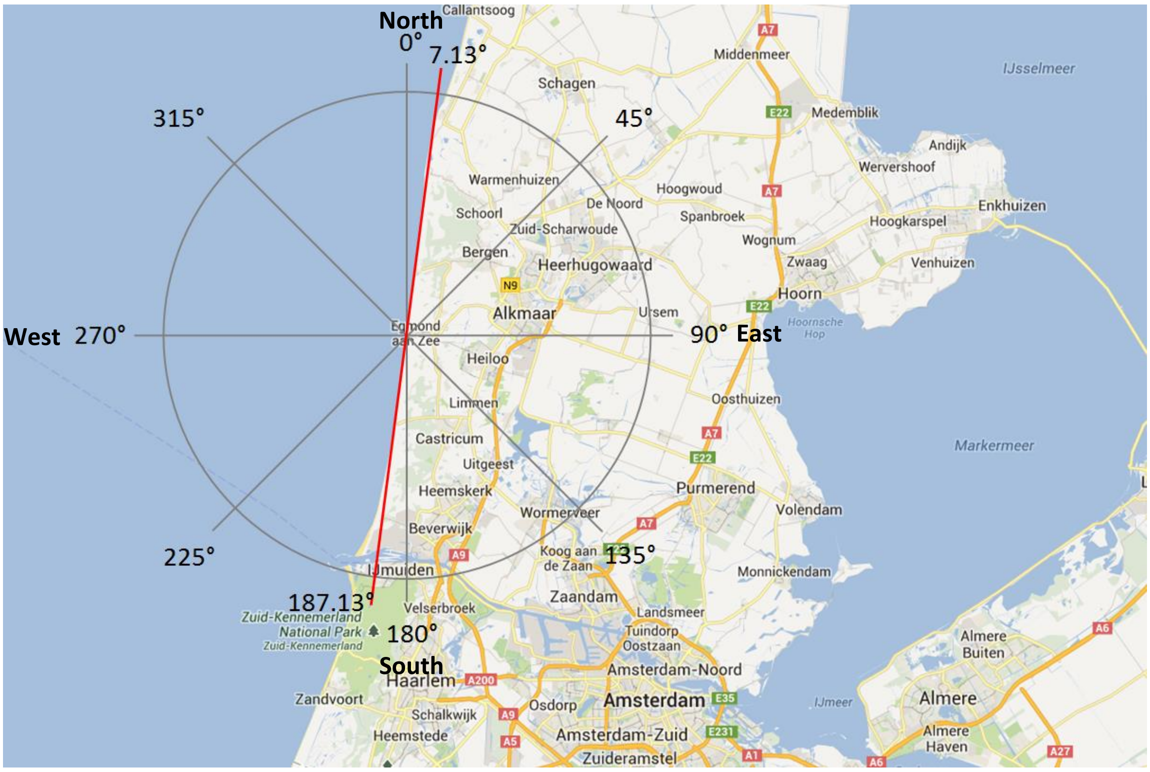

FIGURE 8: WIND DIRECTIONS AT THE DUTCH COASTLINE INCLUDING EGMOND BEACH AND THE ORIENTATION OF EGMOND BEACH (RED LINE).

3.2.1. Defining occurrence of aeolian sediment transport on ARGUS images

To study the link between the occurrence of aeolian sediment transport, wind speeds, wind directions and precipitation, a method to assess occurrence of aeolian sediment transport has been used. This method uses snapshot images from a long term image data base collected by an ARGUS video system located on Egmond Beach. ARGUS images are collected semi hourly during day-light hours and occurrence of aeolian sediment transport was determined visually.

During the winter months day-light hours are limited. Due to day-light limitations ARGUS images used for the identification of aeolian sediment transport occurrences were taken between 8.00 AM and 4.00 PM. This day-light restriction results in a period of 16 hours per day without possibility of observing aeolian sediment movement.

To be able to talk about aeolian sediment transport as such, the term aeolian sediment transport has been defined for this study. Aeolian sediment transport is the visible displacement of sediment. This displacement has to be visible between two consecutive ARGUS images. As aeolian sediment transport is defined as any movement of sediment in any direction on the beach, offshore wind directions have been considered during the process of observing aeolian sediment transport occurrences as well. While checking if aeolian sediment transport took place, attention has been paid to the fact that drying sand flattens out. This flattening of drying sand is not understood as aeolian sediment transport. An example of the flattening of drying sand can be found in Appendix 9.1 Figure 55.

Moments of aeolian sediment transport are defined as full hours, due to the hourly availability of wind and precipitation data. If the ARGUS images show a switch between no aeolian sediment to aeolian sediment transport on a half hour image the preceding full hour has been used for aeolian sediment transport analysis. In Appendix 9.1 examples of what is defined as aeolian sediment transport are given.

Two different ways to identify aeolian sediment transport occurrence have been used during this study. Firstly, a visual examination was done of all images for the occurrence of aeolian transport feature (bed forms, aeolian streamers). Switching back and forth between the different ARGUS images in a standard image viewer tool generally allowed for a really precise decision of whether or not such features moved, and hence whether aeolian sediment transport took place. In cases of doubt, additional analyses were done using a pixel intensity method on order to make a decision about transport occurrences. Hereafter these two methods will be explained in more detail.

As still some image remained for which there was uncertainty about aeolian sediment transport occurrences all images where marked in an overview according to how certain the occurrence of the aeolian sediment transport was. These totalled to 90% certain, 9% quite certain and 1% uncertain (also see Appendix 9.2.2)

Observing the occurrence of aeolian sediment transport on ARGUS images

Visually examining the ARGUS images for moving aeolian bed forms and aeolian streamers was one way to detect aeolian sediment transport occurrences. The movement was best identified when lighter coloured dry sand moved as bed forms or aeolian streamers over darker coloured, more moist, beach surface. Care was taken that local drying of sand, for instance on inactive aeolian bed forms, was not mistaken for aeolian transport (see Appendix 9.1 Figure 55). Also, it was checked whether movements were not caused by a slight movement of the camera, or shadows of clouds.

Defining aeolian sediment transport on ARGUS images using intensity plots in Matlab

If aeolian sediment transport could not be identified with enough certainty from the images directly, intensity plots in Matlab have been used to verify the decision made about the occurrence of aeolian sediment transport. These intensity plots illustrate the difference in pixel values of a certain point in the ARGUS image between two successive images. This method is based on the idea that the pixel intensity changes in an image at locations where movement takes place (Kim , et al., 2012).

To identify aeolian sediment transport occurrences, the pixel intensities along a single line on two consecutive images were extracted and plotted together (Figure 9, bottom panel). The line on which those intensities were measured should be positioned in a way that the line is more or less perpendicular to the crest of the aeolian features. For example: When it is suspected that sediment moves north-eastward, the line should be placed on the ridges as seen on the ARGUS images, with the end point of the line north-east from the start point of the line (Figure 9, upper left panel). In two consecutive images, pixel intensities along this line were extracted. Thus, it was possible to compare pixel intensities of both images through plotting both intensities in one graph. The horizontal axis of this plot represents the position along the line and the vertical axis represents the pixel intensity, relative to the average pixel intensity of the line. The relative intensity was used, rather than the absolute intensity, to take account of variations in brightness of the images. An intensity plot of one image looks somewhat like a rugged sine, where the peaks represent places on the line where dry sediment is present, and the lows represent those places with more moist sediment. Hence, sediment transport can be identified by comparing the positions of the peaks and lows of the graphs from both images. If these peaks and lows shift consistently in one direction, this is considered an indication that sediment is being transported. When peaks widen or direction of movement is less consistent this may also indicate drying of inactive bed forms occurred. To decide whether the changes on the pixel intensity pattern are related to drying or not, one has to re-examine the full ARGUS images again.

An example of this procedure can be seen in Figure 9. The ARGUS images used were taken on May 8th 2009 at 11.00 AM and 11.30 AM. The bottom panel of Figure 9 shows a black and a blue line. The black line refers to data from 11.00 AM and the blue one to 11:30 AM. It can be clearly seen that the blue line is in front of the black line in most of the cases. Therefore, it can be concluded that aeolian sediment transport took place between 11.00 AM and 11.30 AM on May 8th 2009.

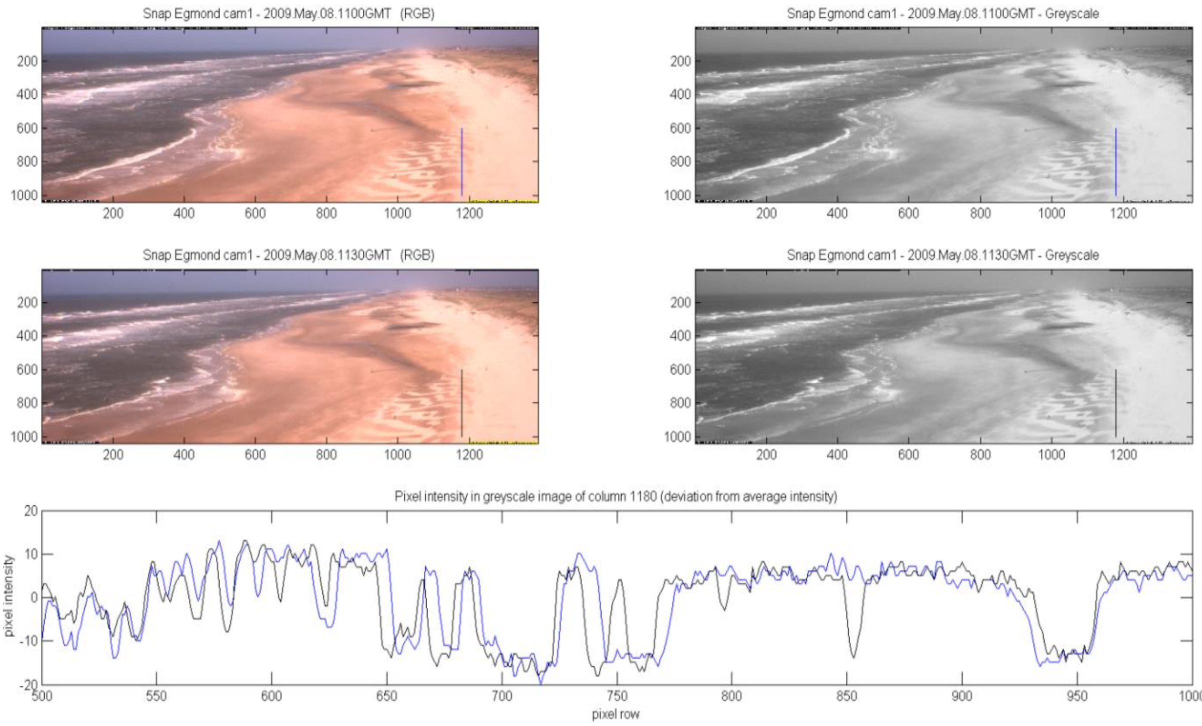

FIGURE 9: OBTAINING VISIBLE AEOLIAN SEDIMENT TRANSPORT USING PIXEL INTENSITY PLOTS OF TWO SUCCESSIVE ARGUS IMAGES IN MATLAB.

Another method used to identify aeolian sediment transport occurrences was an extension of the intensity plot method described above. This method greyscales all images of one day. Thereafter, one can manually define a line from which one wants to assess the occurrence of aeolian sediment transport. Once defined on one image, this line is adopted on all images of the regarding day. These pixel intensity plots of the same area in each image of the day are plotted next to each other. By doing so, one can directly see on the plot if sediment is moving. On the left hand side of Figure 10 the defined line over which the pixel intensities are analysed can be seen. In this case it is a vertical line. Nevertheless, the line can be drawn at any angle. On the right hand side of Figure 10 such a pixel intensity plot of a whole day is presented. Looking at the pink circle it can be seen that sediment moves rather quickly from 08:30 AM January 11th 2009 till 11:00 AM January 11th 2009 and thereafter continues moving more slowly.

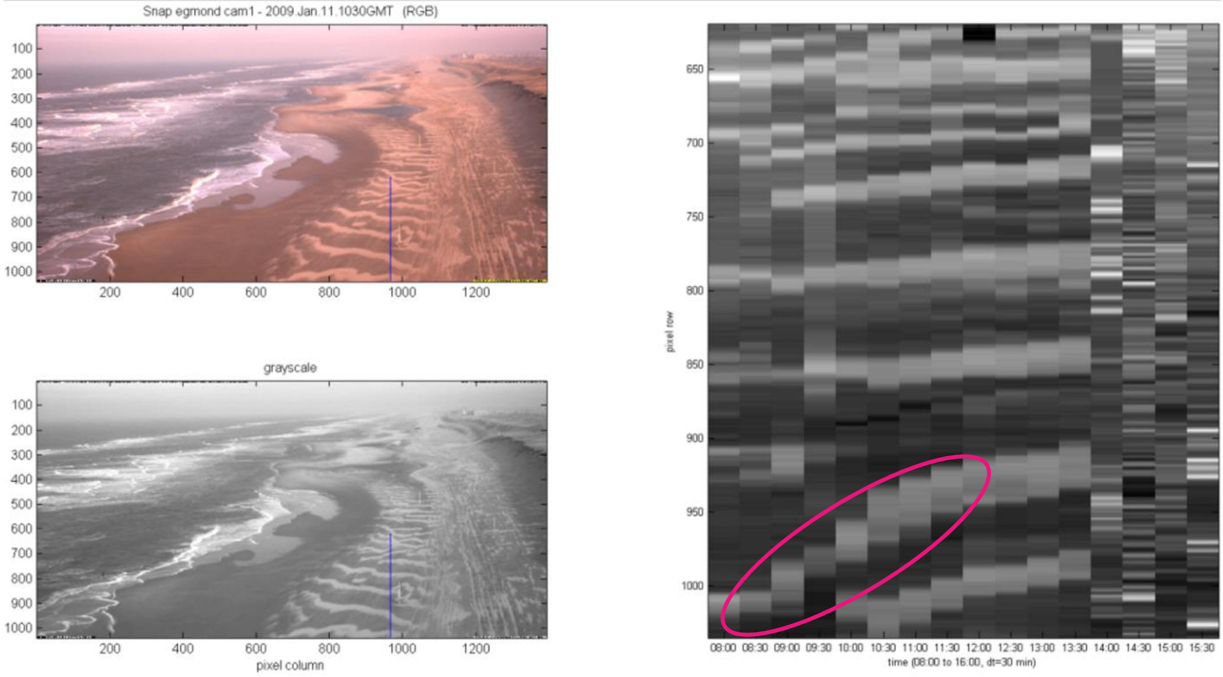

FIGURE 10: PIXEL INTENSITY PLOTS OF A WHOLE DAY TO DETECT VISIBLE AEOLIAN SEDIMENT TRANSPORT (JANUARY 11TH 2009).

3.2.2. WIND AND PRECIPITATION DATA

The wind station that provided the wind data for this study, including the hourly averaged wind speeds and hourly wind directions, is located in IJmuiden.

The weather stations closest to Egmond Beach and closest to the coast having precipitation data available are Petten and Wijk aan Zee. Petten is located to the North of Egmond Beach whereas Wijk aan Zee is located to the South of Egmond Beach. Figure 11 shows the locations of Petten and Wijk aan Zee with respect to Egmond Beach. Both weather stations represent the coast climate, which can be found at Egmond Beach.

Due to the fact that the data available at Petten is daily precipitation and the data provided from Wijk aan Zee is hourly precipitation, it has been decided to use the precipitation data from Wijk aan Zee. Thereafter, the hourly precipitation data of Wijk aan Zee was linked to the identified aeolian sediment transport occurrences, the hourly averaged wind speeds and the wind directions of IJmuiden. This has been done to create an overview and an understanding of the effect of precipitation on aeolian sediment transport.

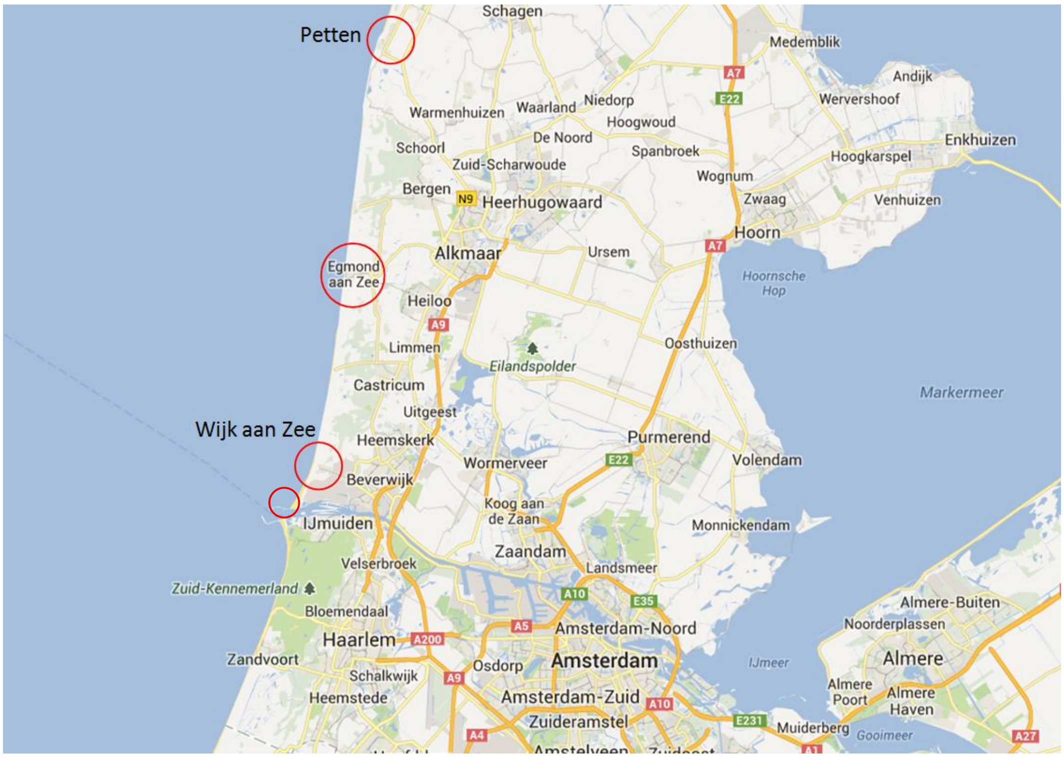

FIGURE 11: THE LOCATIONS OF PETTEN, WIJK AAN ZEE AND IJMUIDEN WITH RESPECT TO EGMOND BEACH.

3.2.3. DETERMINING THE FETCH DISTANCE

To calculate the aeolian sediment transport rate on Egmond Beach using the formula described in chapter 3.1, the fetch distances had to be determined. The ARGUS images were taken in a certain perspective as can be seen in Figure 12a. The pink line seems to be much shorter than the green line, because of the perspective of the figure. To be able to determine the fetch distances, the ARGUS images have to be projected on a horizontal plane as can be seen in Figure 12b, so that the two lines have the same length. This process is called rectification. Thereafter, the fetch distances have been determined using a program made in this study.

In sub-section 3.2.3.1 the rectification process is explained and in sub-section 3.2.3.2 a description of the definition of the fetch distances can be found.

a) **b)**

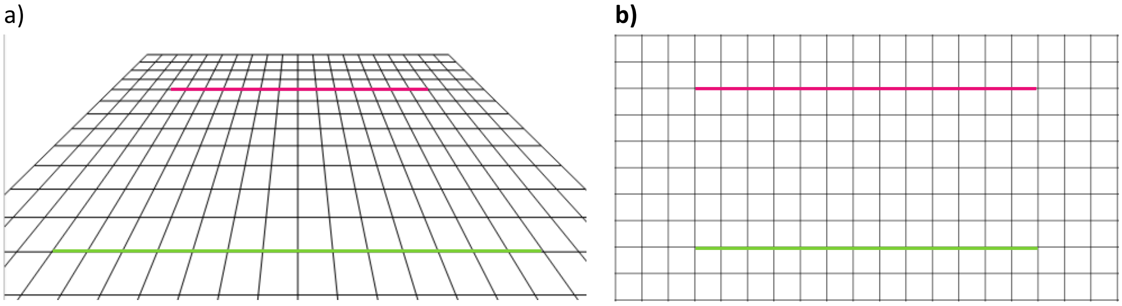

FIGURE 12: ON THE LEFT HAND SIDE THE PERSPECTIVE OF THE ARGUS IMAGES AS TAKEN AT EGMOND BEACH AND ON THE RIGHT HAND SIDE THE PROJECTED PERSPECTIVE OF AN ARGUS IMAGE ON A HORIZONTAL PLANE, CALLED A RECTIFIED IMAGE.

3.2.3.1. CONVERTING THE ARGUS IMAGES TO RECTIFIED IMAGES

To determine the fetch distance from the beach width, first of all the ARGUS images had to be rectified. The rectified images were created using a Matlab script provided by Deltares (ARE - Argus Runtime Environment). To project the ARGUS images on a horizontal plane, the Matlab script needs a corrected water level as projection plane. This water level can be different for every ARGUS image.

To correct the water level, data from the Rijkswaterstaat database was used (Rijkswaterstaat, 2009). This database contains, among other factors the following parameters that are essential to correct the water levels: the RMS wave height (Hrms), the offshore wave direction (Thm0) and the dominant wave period (Tpeak). For the year 2009, hourly data is available for the offshore wave period, the offshore wave direction, the wave height and the water level. For this specific year no values are available for the RMS wave height and the dominant wave period. Therefore, the RMS wave height was calculated using the wave height H_{m0} and following formula: $H_{rms} = \frac{H_{m0}}{\sqrt{2}}$ (Mangor, 2007). Thereafter, the dominant wave period was calculated using following formula: $T_p \sim 5.3 \cdot H_{m0}^{0.5}$ (Mangor, 2007). The RMS wave height and the dominant wave period have been calculated for all times that aeolian sediment transport occurrences were identified. By this means, all parameters are available to correct the water level and thereby create a projection plane. Subsequently, the water level has been corrected for all identified aeolian sediment transport occurrences, using the Matlab script provided by Deltares. Using these corrected water levels, the rectified images have been created.

Figure 13 shows such a rectified image. The x-axis represents the alongshore distance in meters and the y-axis the cross shore distance, in meter as well. At the bottom of the figure the sea water line can be seen. The pink circle frames a trough.

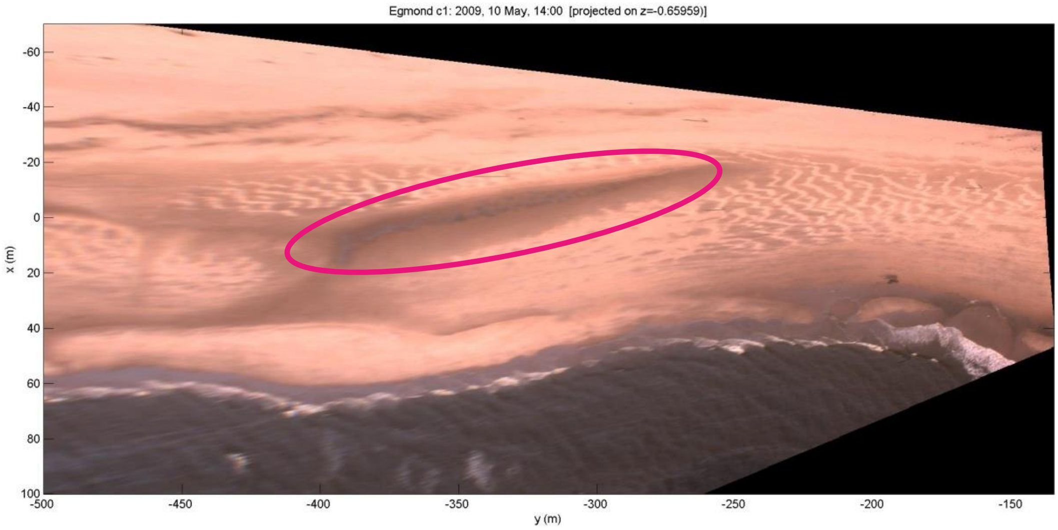

FIGURE 13: A RECTIFIED IMAGE OF EGMOND BEACH, ON THE X-AXIS THE ALONGSHORE DISTANCE AND ON THE Y-AXIS THE CROSS SHORE DISTANCE IN METER CAN BE SEEN.

3.2.3.2. DEFINING THE DIFFERENT FETCH DISTANCES

In this study two different groups of fetch distances have been considered. The first group considers varying fetch distances along the beach section that is visible in the rectified image. This variation takes place due to the varying shape of the water line and possible troughs on the beach. Therefore, these fetch distances consider the intertidal beach topography as complex and varying in alongshore direction. The fetch distances are measured at three different points along the beach. Those points are defined as -425m, -325m and -225m and are depicted in Figure 14. The fetch distances are always in the onshore direction behind possible troughs because it is known that troughs act as very efficient sediment transport interceptors. Sediment will not be transported across a trough (Anthony, et al., 2009).

The second group of fetch distances considers the intertidal beach topography as non-varying in alongshore direction. Therefore, the fetch distances are the same along the beach section that is visible in the rectified image. The fetch distance is always in the onshore direction behind possible troughs. This fetch distance is always equal to the shortest fetch distance of the first group.

To take the sensitivity of the measured fetch distance into account two cross shore measurement points have been chosen at -40m and -30m.

In Figure 14 it can be seen how the fetch distances have been defined in this study. The blue lines represent the fetch distances for a complex alongshore varying intertidal beach topography. The green lines outline the shortest fetch distance that is always chosen for the non-varying intertidal beach topography. All fetch distances start behind the trough that can be seen as light area in Figure 14. Further details about the determination process of the fetch distances can be found in Appendix 9.4**.**

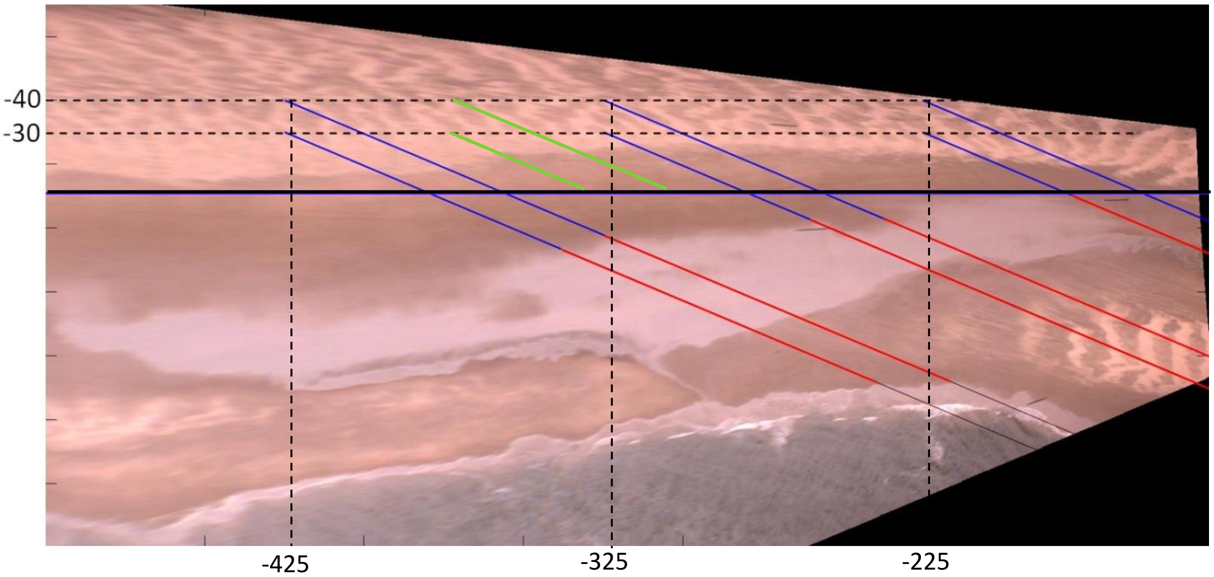

FIGURE 14: THE BLUE LINES SHOW THE FETCH DISTANCE. THE GREEN LINE SEPICTS THE SHORTEST FETCH DISTANCE THAT HAS ALWAYS BEEN CHOSEN FOR THE NON-VARYING INTERTIDAL BEACH TOPOGRAPHY. THE RED LINES SHOW AN ADDITION TO THE FETCH DISTANCE IF THE EFFECT OF THE TROUGHS IS NOT TAKEN INTO ACCOUNT.

3.3. Representative wind speed

The wind data needed for calculating the annual aeolian transport at Egmond Beach is measured at a wind station at IJmuiden, and averaged per hour. It appeared that the hourly averaged wind speed available from the long term wind monitoring at this location was not an appropriate input value, as it underestimated the occurrence of sediment transport. Many transport occurrences were identified on the images while the matching hourly averaged wind speeds were too low to get sediment into motion according to the transport equation used (see chapter 5.1 Figure 39). Instantaneous wind speeds can vary a lot during one hour (Tattelman, 1975). Due to the third power relationship between wind speed and transport, transport values increase rapidly as the wind speed increases. Using an hourly averaged wind speed value to calculate transport does not take into account the effects of the wind gusts on transport. Therefore, a 'representative wind speed' has been defined to be used as input for the aeolian sediment transport calculations taking into account the gustiness of the wind.

The development of a representative wind speed was done based on an analysis of high resolution time series for wind speed. The highest resolution time series for wind speed taken over several days was available from wind stations near Salt Lake City, United States of America (Mobbs, 2006; NCAR/EOL, 2011). The high resolution time series contain wind speeds measured per second for 2856 hours. The choice of using this wind data was done under the assumption that the behaviour of gustiness does not differ significantly at different locations.

In this chapter, the sediment transport formula described in section 3.1 is now defined as $f(U_Z)$:

$$f(U_Z) = K\frac{\rho_a}{g}\left(\frac{U_Z\kappa}{ln\left(\frac{z}{z_0}\right)} + A\left[(\rho_s/\rho_a)gd\left(1+K_gM\right)\right]^{\frac{1}{2}}\right)^2\left(\frac{U_Z\kappa}{ln\left(\frac{z}{z_0}\right)} - A\left[(\rho_s/\rho_a)gd\left(1+K_gM\right)\right]^{\frac{1}{2}}\right) \tag{10}$$

Where the output of *f* is the sediment transport rate in $kgm^{-1}s^{-1}$, and U_Z is the wind speed in ms^{-1} at measuring height *Z*. The values for the constants of this formula are stated in Appendix 9.1 Table 4. In this chapter, the fetch distance is not taken into account. The fetch distance is taken into account after the representative wind speed is calculated and filled out in the transport formula, see chapter 5.3 Table 3.

In the following three sub-sections the determination process of the representative wind speed is explained. Throughout the first sub-section it will be explained how high resolution time series are used to calculate hourly transport. In the second sub-section, it will be explained how a relationship between hourly averaged wind speed and hourly sediment transport is found. In the third sub-section, it will be explained how a representative wind speed is calculated based on an hourly transport rate.

Calculation of hourly sediment transport using high resolution time series

Firstly, the sediment transport per hour of the high resolution time series for wind speed was calculated. This was done by calculating sediment transport for every second during that hour using equation (10). Subsequently, the calculated sediment transports were summed up for the hour. $U_{z,t}$ is defined as the wind speed at height *Z* and second *t.* The calculation of the hourly transport using wind speed data per second can be expressed as following:

$$Q_{hour} = f\left(U_{Z,1}\right) + f\left(U_{Z,2}\right) + f\left(U_{Z,3}\right) + \cdots + f\left(U_{Z,3599}\right) + f\left(U_{Z,3600}\right) \tag{11}$$

Where *t=1* is the first second within the hour, *t=3600* is the last second within the hour, and Q_{hour} is the total transport during the hour considered.

RELATIONSHIP BETWEEN HOURLY AVERAGED WIND SPEED AND HOURLY SEDIMENT TRANSPORT

Next, a relationship between the hourly averaged wind speeds U_Z and hourly sediment transports Q_{hour} of the high resolution time series was determined. In order to determine this relationship, the hourly transport Q_{hour} and hourly averaged wind speed U_{Z,h_a} was calculated for every hour in the high resolution time series for wind speed. These results were plotted a scatter plot, with on the x-axis the hourly averaged wind speed and on the y-axis the hourly transport. Each point in the scatter plot represents the hourly transport for one hour. A curve is fitted through the scatter plot using the nonlinear least-square curve-fit module of Matlab. The scatter plot and fitted curve can be found in chapter 5.2 Figure 43.

The curve that is fitted through the scatter plot, has the following structure:

$$g(U_{z,h\_a}) = \frac{b(a + U_{z,h\_a})^3}{(1 + e^{-20(a+U_{z,h\_a})})^3} + \frac{c(d + U_{z,h\_a})}{1 + e^{-20(d+U_{z,h\_a})}} \tag{12}$$

For $b = 1, a = 0, c = 0\ and\ d < \infty$, this function has the following properties:

$$g(U_z) \approx \begin{cases} U_{z,h\_a}^3\ for\ U_{z,h\_a} > 0 \\ 0\ for\ U_{z,h\_a} \leq 0 \end{cases}$$

For $b = 0, a < \infty, c = 1\ and\ d = 0$, this function has the following properties:

$$g(U_z) \approx \begin{cases} U_{z,h\_a}\ for\ U_{z,h\_a} > 0 \\ 0\ for\ U_{z,h\_a} \leq 0 \end{cases}$$

a and *b* are used to move the third-power part of the graph along the x-axis and to influence the height, respectively. *c* and *d* are used to move the linear part of the graph along the x-axis and to influence the height, respectively. *a*, *b, c* and *d* are determined by the nonlinear least-square curve-fit module of Matlab, so that the curve fits the scatter plot best. The resulting fitting function (12) is called $g(U_{z,h\_a})$, which represents the hourly transport for the hourly averaged wind speed U_{Z,h_a}.

REPRESENTATIVE WIND SPEED USING HOURLY SEDIMENT TRANSPORT

The hourly transport $g(U_{z,h\_a})$ calculated in the previous step will *not* be the value that would be found if the hourly averaged wind speed itself would be used as input directly for the transport equation. In this final step it is explained how one can derive a single wind speed, the so-called representative wind speed that would provide this hourly transport value.

This will be done using the inverse of *f*, $f_{inverse}$, where $f_{inverse}\left(f(U_{z,h\_a})\right) = U_{z,h\_a}$.

$f_{inverse}$ gives a wind speed given a certain transport $f(U_z)$, based on formula (10). This way, it is possible to calculate the representative wind speed through the following expression:

$$U_{z,representative} = f_{inverse}\left(g(U_{z,h\_a})\right) \tag{13}$$

In this equation, U_{z,h_a} is the hourly averaged wind speed that needs to be converted to a representative wind speed. $g(U_{z,h\_a})$ is the formula that converts an hourly averaged wind speed to an hourly transport (see eq. 12). $f_{inverse}\left(g(U_{z,h\_a})\right)$ calculates the single hourly wind speed ($U_{z,representative}$) that should be filled out into $f(U_z)$ (eq. 10) in order to get the hourly transport taking wind gusts into account.

4. Field data analysis

In this chapter the results of the field data analysis will be presented. First of all the results of identification of the occurrence of aeolian sediment transport will be presented. Secondly, the results of the fetch distance determination will be presented.

4.1. Occurrence of aeolian sediment transport, wind speed and wind direction

Figure 15 gives the results of identified aeolian sediment transport for the year 2009 at Egmond Beach. Almost no aeolian sediment transport occurrences have been identified below hourly averaged wind speeds of 6 ms^{-1}. Wind directions played an important role in the occurrence of aeolian sediment transport. At 100° North and 140° North almost no aeolian sediment transport has been identified. Looking at the wind speeds between 210° and 330° North it can be seen that the threshold wind speed seems to be higher than for other wind directions. Having wind blowing alongshore (North and South) the phenomenon of high wind speeds and no aeolian sediment transport occurrences was rarely seen. Figure 15 depicts that no clear velocity threshold can be set that could be valid for all wind directions.

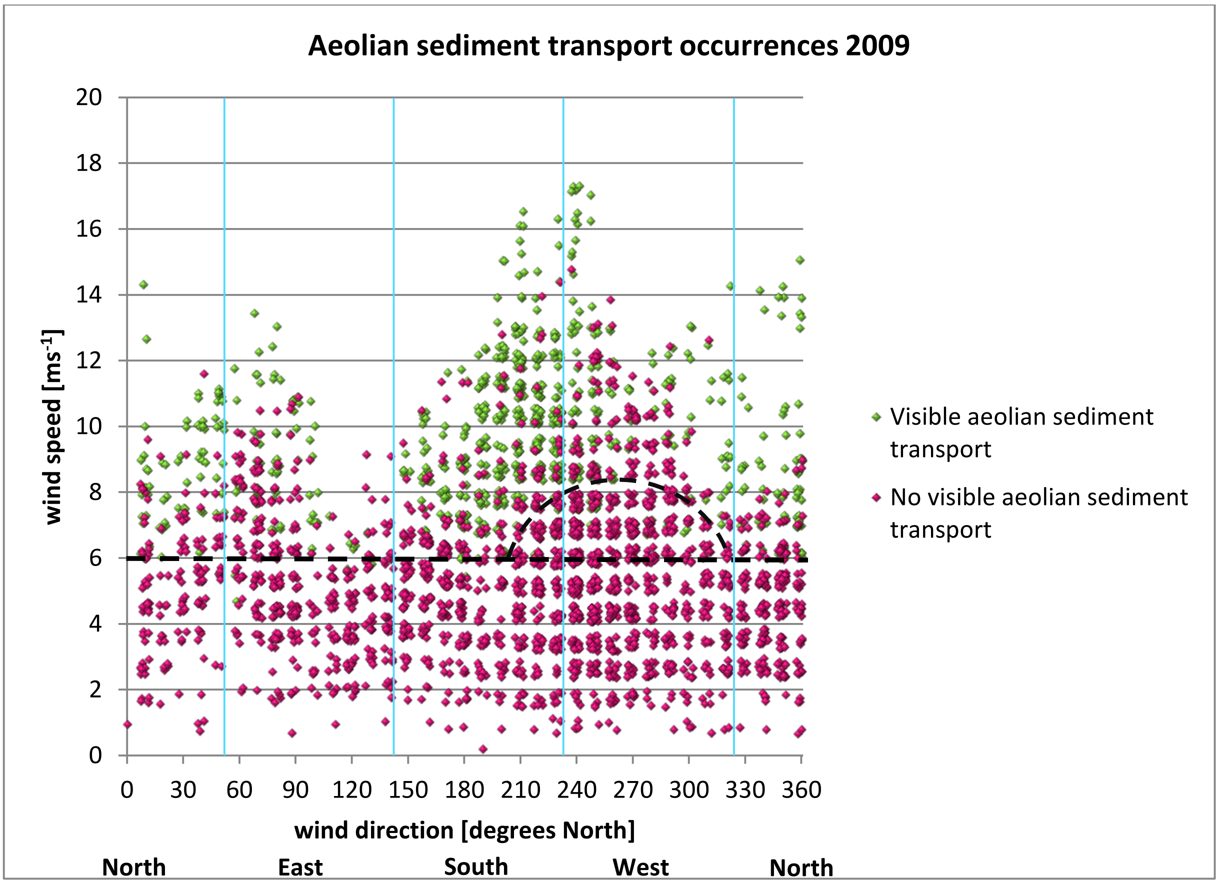

FIGURE 15: AEOLIAN SEDIMENT TRANSPORT OCCURRENCES IN 2009 AT EGMOND BEACH.

Figure 16 shows the aeolian sediment transport occurrences per onshore wind direction. It can be seen that most of the aeolian sediment occurrences were observed while the wind was blowing from between 190° and 250° and North and from 360° North. During the aeolian sediment transport occurrence all corresponding wind directions have a large alongshore component. For the times where almost no aeolian sediment transport has been identified, the wind was blowing mostly from the West.

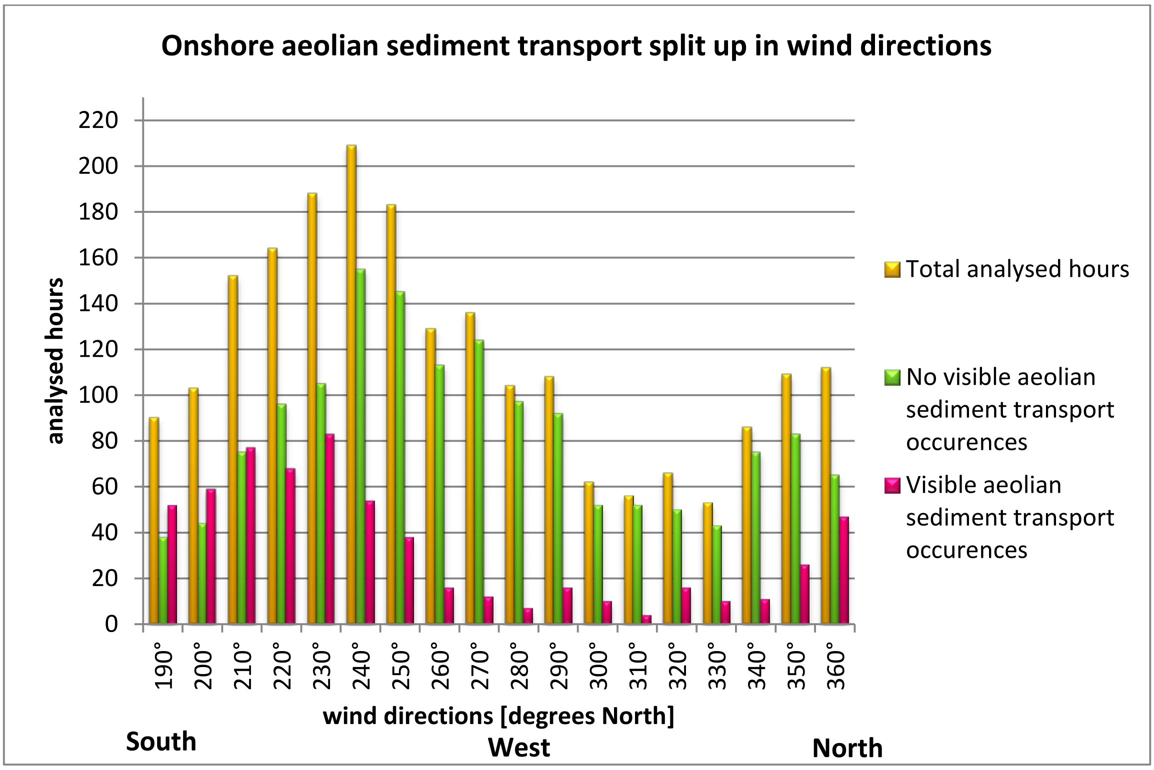

FIGURE 16: THE DISTRIBUTION OF AEOLIAN SEDIMENT TRANSPORT OCCURRENCES OF THE DIFFERENT ONSHORE WIND DIRECTIONS.

To get insight into the effect of the different wind speeds on aeolian sediment transport occurrences an overview was made that links the aeolian sediment transport occurrences to the different hourly averaged wind speeds. Figure 17 shows the distribution of aeolian sediment transport occurrences per wind speed. Figure 17 depicts that most aeolian sediment transport occurrences have been identified between wind speeds of 6 ms^{-1} and 12 ms^{-1}. Most aeolian sediment transport occurrences took place at 8 ms^{-1}, second most aeolian sediment transport occurrences has been observed at 7 ms^{-1}. No aeolian sediment transport was observed at wind speeds of less than 4 ms^{-1}.

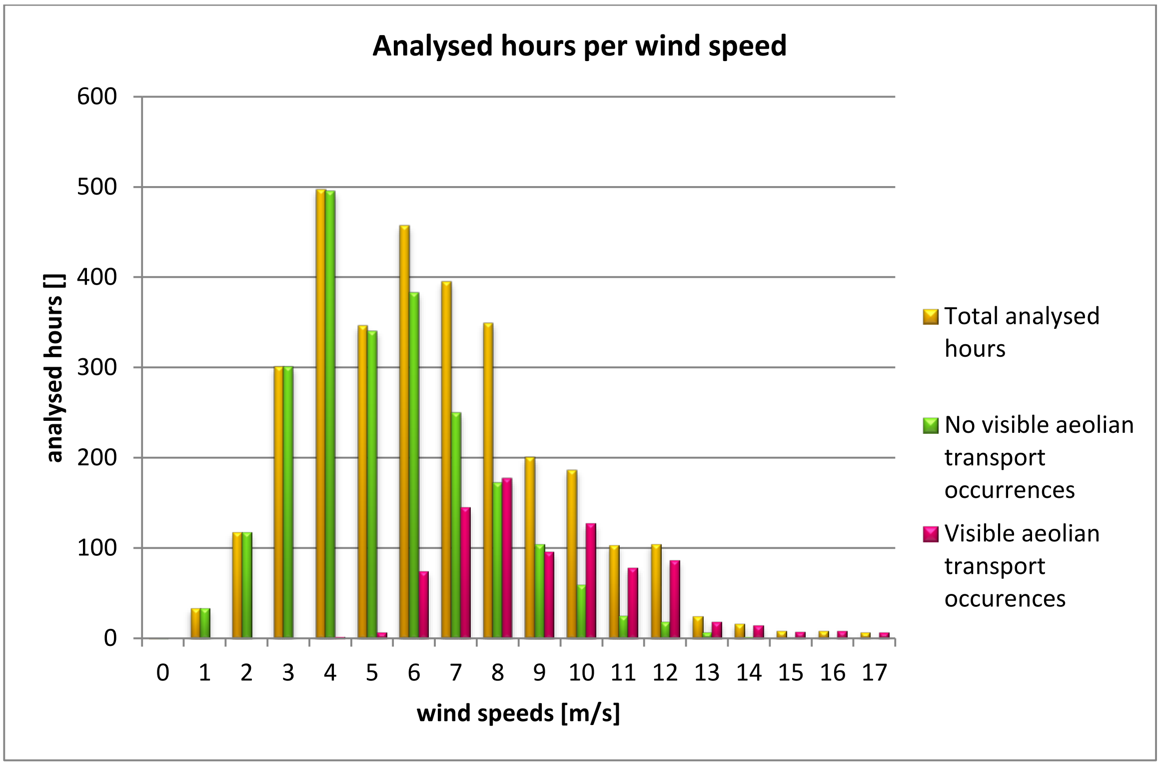

FIGURE 17: THE TOTAL ANALYSED HOURS BY AEOLIAN SEDIMENT TRANSPORT OCCURRENCES AND NO AEOLIAN SEDIMENT TRANSPORT OCCURRENCES PER HOURLY AVERAGED WIND SPEED.

For offshore wind directions clear aeolian sediment movement has been identified. For examples see Appendix 9.1. Because of the dune functioning as a wind limiting structure, offshore wind directions showed less aeolian sediment transport occurrences compared to the onshore wind directions.

The link between the ARGUS images and the hourly averaged wind speeds revealed that different wind speeds need different beach widths, and therefore fetch distances, to get sediment into motion. Occasionally high wind speeds have been detected and aeolian sediment transport occurrences were expected to be observed. However, because of the high tide, almost no intertidal beach was present and therefore no aeolian sediment transport could occur due to nearly no fetch distance. If there is almost no beach present is has been observed that only very high hourly averaged wind speeds, above 12 ms^{-1} can get sediment into motion. Such high wind speeds do not always get sediment into motion at all wind directions and beach conditions. An example of high wind speeds and a too short intertidal beach width to get sediment into motion can be seen in Figure 18.

FIGURE 18: EGMOND BEACH AT 10TH FEB 2009 AT 3:30 PM WITH HIGH WIND SPEEDS (10.7MS^{-1}) AND A WIND DIRECTION OF 330° NORTH BUT NO INTERTIDAL BEACH. THE TURQUOISE AREA IS THE INTERTIDAL BEACH, WHICH IS CURRENTLY FLOODED.

Figure 19 shows the distribution of the different hourly averaged wind speeds per wind direction at Egmond Beach for 2009. It can be seen that most of the winds, including the stronger ones, comes from the South-West, whereas almost no wind comes from the South-East. A lot of high hourly averaged wind speeds come from the South, South-West. The fact that most of the wind blows from the aforementioned directions, can as well be seen in Figure 15. The missing hourly averaged wind speeds from the South-East explain the gap of data points in Figure 15.

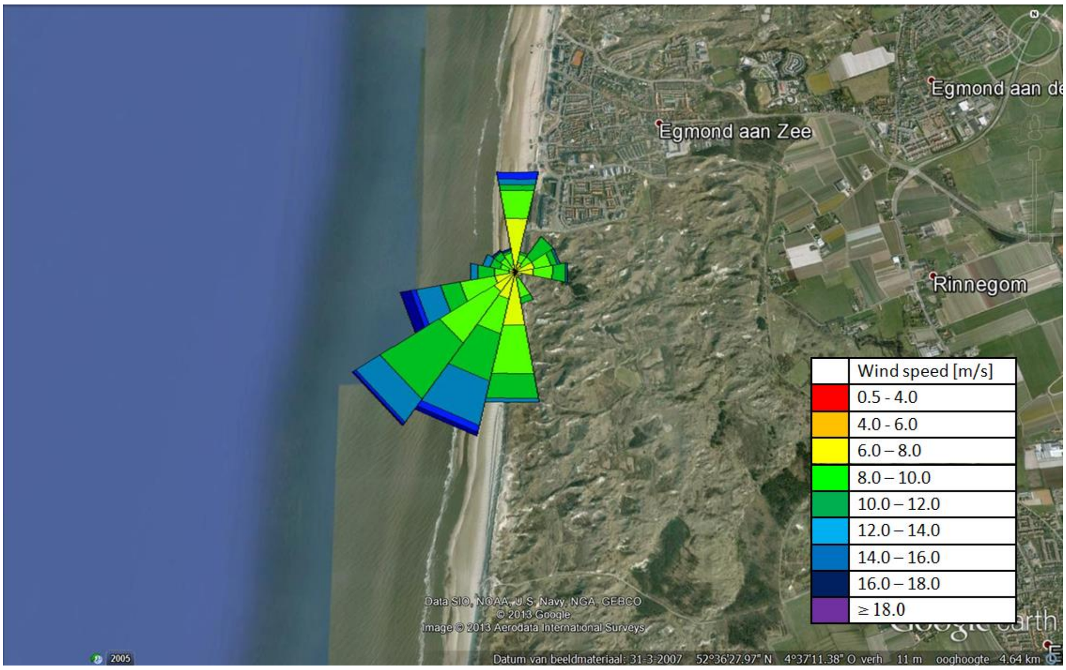

FIGURE 19: THE DISTRIBUTION OF THE HOURLY AVERAGED WIND SPEEDS PER WIND DIRECTION ON LOCATON EGMOND BEACH FOR 2009.

4.2. Occurrence of aeolian sediment transport, wind speed, wind direction and precipitation

The next step of gaining insight into the aeolian sediment transport occurrences at Egmond Beach was to analyse the relationship between aeolian sediment transport occurrences and measured precipitation.

In Figure 20 it can be seen that during precipitation almost no aeolian sediment transport occurred in offshore direction. During precipitation most aeolian sediment occurrences have been observed while wind was blowing almost alongshore from the South.

Figure 21 shows that for dry periods almost no aeolian sediment transport occurred while wind was blowing from the South-East. During the time when wind was blowing from offshore directions aeolian sediment transport occurrences have been identified.

It was assumed that high wind speeds are needed to get moist sand into motion. This assumption cannot be seen in Figure 20. In Figure 20 aeolian sediment transport occurred also at low wind speeds combined with precipitation.

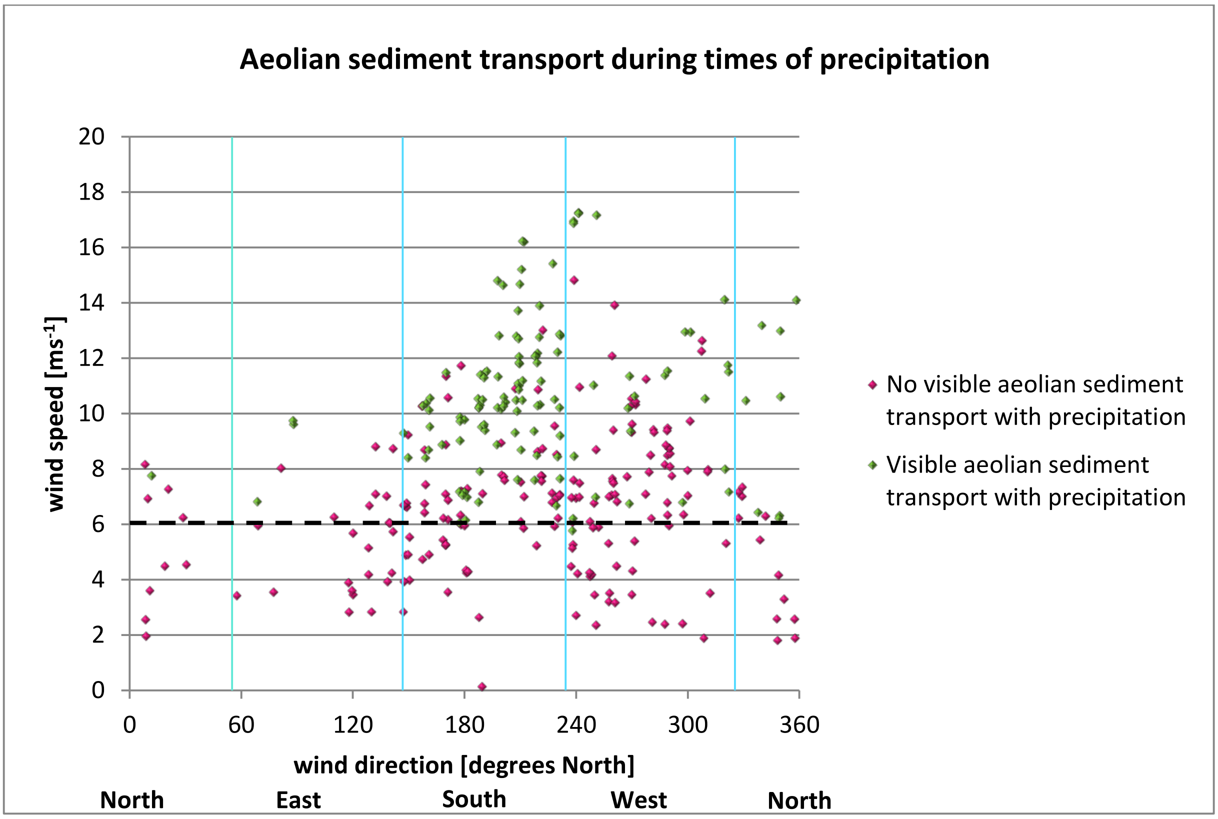

FIGURE 20: AEOLIAN SEDIMENT TRANSPORT DURING TIMES OF PRECIPITATION.

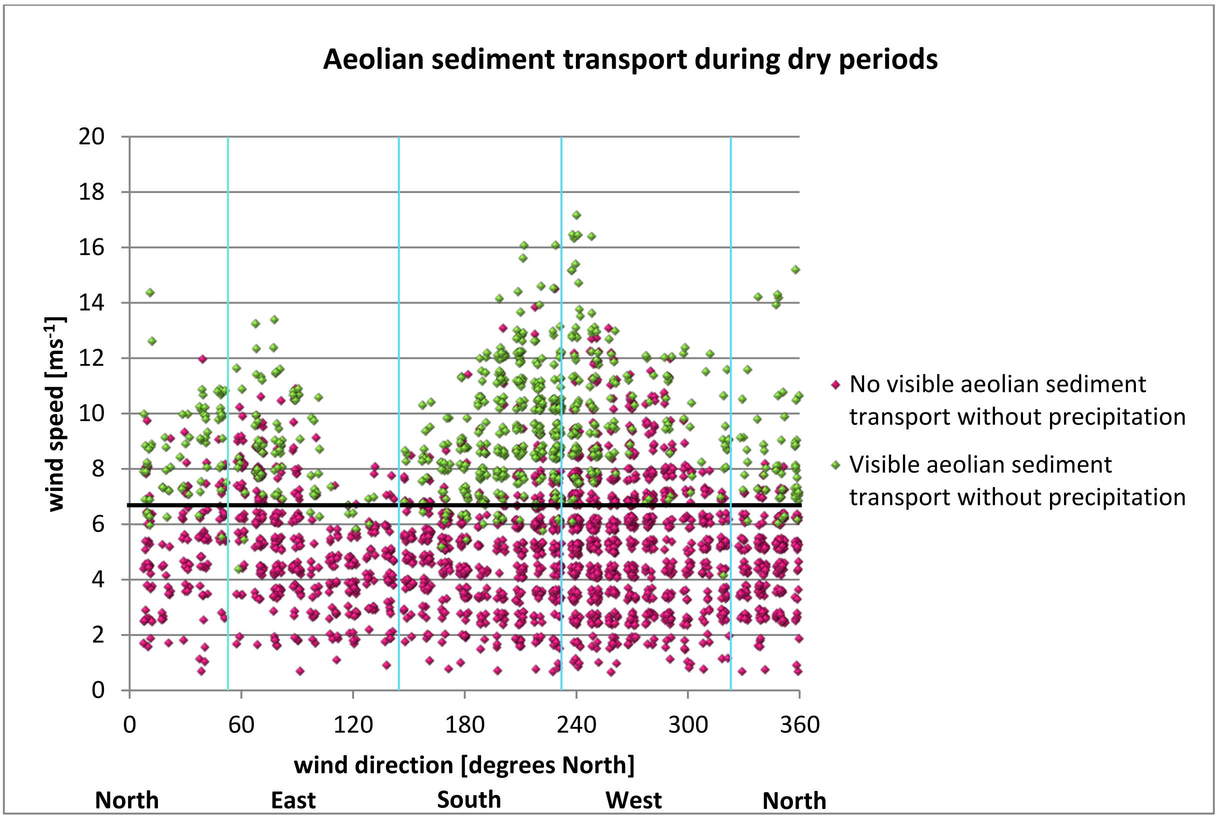

FIGURE 21: AEOLIAN SEDIMENT TRANSPORT IN NON-PRECIPITATTIONS CONDITIONS.

Having done this analysis the first research question concerning the occurrence of aeolian sediment transport has been answered:

In total 3260 hours of ARGUS images were available during daytime in 2009. 5475 hours of the year 2009 were hours overnight or too dark to observe aeolian sediment transport on the ARGUS images. Daytime precipitation occurred during 10% (326 hours). Of the 3260 ARGUS images taken during the daytime, 844 images (26% of the images) showed aeolian sediment transport. These occurrences were divided into offshore and onshore transport. From analysis, 603 occurrences of onshore aeolian sediment transport have been counted, which is 71% of the total aeolian sediment transport occurrences, covering 18% of the daytime hours for which ARGUS images were available. These results can as well be seen in Appendix 9.2.

No single velocity threshold could be set that is valid for all wind direction. Nevertheless, below an hourly averaged wind speed of 6 ms^{-1} almost no aeolian sediment transport occurrences have been identified, Figure 15. From Figure 15 it has been seen that during the hours when wind was blowing from the West (between 250° and 300° North) the velocity threshold that is needed to get sediment transport into motion seems to be higher than for wind from the alongshore wind directions. This may result from the fact that these wind directions are almost perpendicular to the coastline of Egmond Beach. Therefore, the fetch distance is smaller than for other wind directions which results in aeolian sediment transport that has not reached its maximum.

The velocity threshold for getting sediment transport into motion does not get higher during precipitation occurrences. Figure 20 shows that the velocity threshold below which no sediment movement is identified during precipitation is 6 ms^{-1}. During hours of precipitation almost no aeolian sediment transport occurrences have been identified in the offshore direction. Nevertheless, there were just a few precipitation hours during daytime compared to the large number of hours where no precipitation occurred. Therefore, no clear statement of the effect of precipitation on aeolian sediment transport occurrences can be made due to the limited amount of data.

4.3. Fetch distance determination

In this chapter the results of the fetch distance determination are presented. This chapter is divided into four sub-sections, one focussing on the fetch distance ignoring the alongshore varying intertidal beach topography, one taking the alongshore varying beach topography into account, one focussing on the theoretical critical fetch and one dealing with the effect of the changing intertidal beach topography on the aeolian sediment transport rate.

4.3.1. Ignoring the alongshore varying intertidal beach topography

The results of the fetch distance determination are plotted in a histogram to give an overview of the fetch distance occurrences (y-axis) per fetch distance length (x-axis). This way of presenting the results make is possible to directly compare the results of the fetch distances at the different locations at the beach, one at -30 m (Figure 22) and one at -40 m (Figure 23) cross shore the beach.

The theoretical maximum fetch distance that could have been seen at the beach intersection in the rectified images is 308 m. Therefore, all fetch distances above this threshold lie outside the beach intersection shown in the rectified image. These fetch distances were not taken into account analysing the results of the fetch distance determination.

Figure 22 and Figure 23 show the results of the fetch distance determination using the model developed, ignoring the varying intertidal beach topography at -30 m, respectively -40 m. In Figure 22 it can be seen that most fetch distances have a length between 0 m and 40 m. A maximum of almost 120 occurrences has been obtained at 30 m. In Figure 23 it can be seen that the maximum fetch distances are larger. Most fetch distances have been obtained between 30m and 60m, in which the maximum occurrences, 90, have been found at 40 m.

Comparing Figure 22 and Figure 23 shows that the maximum occurrence of Figure 22 is much higher than the maximum occurrences of Figure 23. The fetch distances of the occurrences of Figure 23 are more evenly distributed. In both figures it can be seen that the fetch distance occurrences drop smoothly after their maxima. Figure 22 shows this drop a little bit faster and has almost reached an equilibrium at 150 m which means that there are only a few fetch distance occurrences bigger than 150 m. Figure 23 shows the same behaviour a little bit slower. Here, the bars get smaller until a fetch distance of 190 m was reached. Thereafter, as well as in Figure 22, an equilibrium has almost been reached. Almost no fetch distance occurrences have been larger than 190 m. Fetch distances occurrences above 400 m and therefore not visible on the rectified images were summed up and form one bar at the end of each histogram.

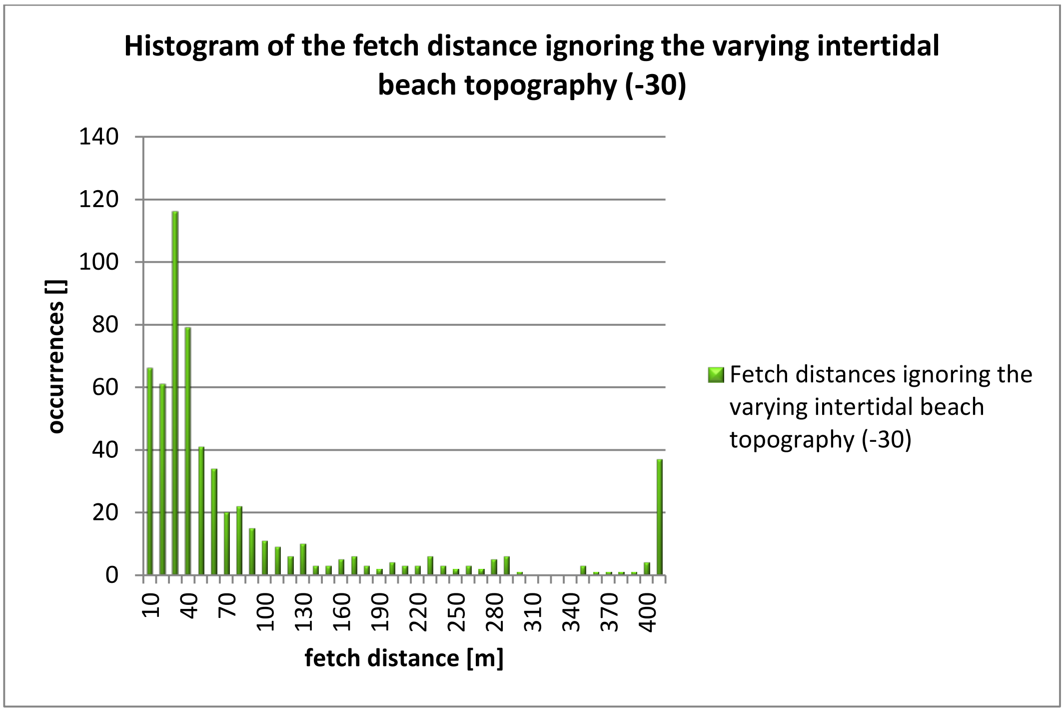

FIGURE 22: THE FETCH DISTANCES IGNORING THE VARYING INTERTIDAL BEACH TOPOGRAPHY AT -30 M.

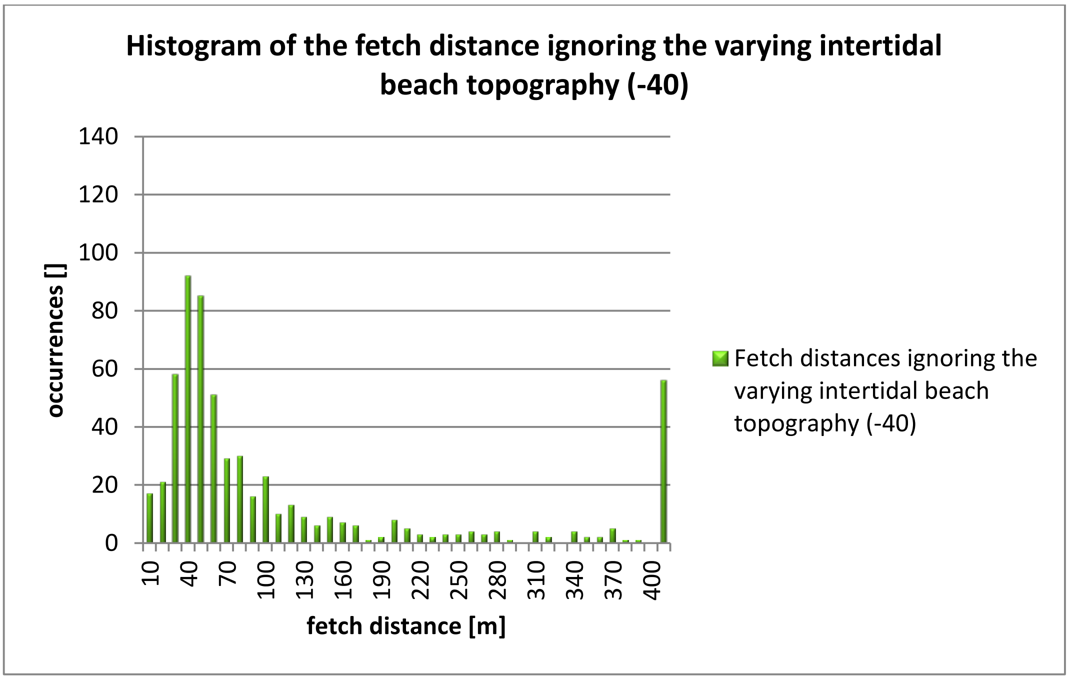

FIGURE 23: THE FETCH DISTANCES IGNORING THE VARYING INTERTIDAL BEACH TOPOGRAPHY AT -40 M.

4.3.2. TAKING INTO ACCOUNT THE ALONGSHORE VARYING INTERTIDAL BEACH TOPOGRAPHY

Figure 24, Figure 25 and Figure 26 show the results of the fetch distance determination taking into account the alongshore varying intertidal beach topography at -40 m. Again, all fetch distances above the calculated theoretical maximum fetch distance of 308 m are not taken into account when analysing the results. The y-axis shows the fetch distance occurrences and the x-axis depicts the fetch distance in meters.

Comparing the three figures it can be seen that on the left hand side of the rectified image (-425) maximum fetch distance occurrences lie at 60 m which is 10 m higher compared to the middle (-325) and the right hand side (-

225) of the rectified image. Nevertheless, more occurrences can be seen in the middle and on the right hand side of the beach, with a length of 50 m. The slope of the histogram from the left hand side of the beach is shallower compared to the slope of the histogram from middle and right hand side of the beach. Additionally, it can be seen that the equilibrium in meters of almost no fetch distance occurrences lies higher on the left hand side of the beach (230 m) compared to the middle (190 m) and the right hand side of the beach (200 m).

Taking a look at Figure 27, Figure 28 and Figure 29 it can be seen that the behaviour at -30 m differs from the behaviour obtained at -40 m. Overall, the fetch distance are smaller.

On the left hand sight of the beach (-425) the maximum fetch distance occurrences lie at 60 m which is 10 m higher compared to the middle (-325) and right hand side of the beach (-225). Most occurrences at one specific length can be seen in the middle (40 m) and on the right hand side (30 m) of the beach. The slope of the histogram from the left hand side of the beach is shallower compared to the slope of the histogram from middle and right hand side of the beach. The equilibrium in meters of almost no fetch distance occurrences lies higher on the left hand side of the beach (200 m) compared to the middle (170 m) and the right hand side of the beach (160 m).

As can be seen in 3.2.1 Figure 19, most of the wind blows from South-West. According to the fetch distance determination the wind blows from the right hand side of the image. Taking this fact into account the fetch distances at the left hand side of the image (-425) have to be larger than the fetch distances in the middle or on the right hand side. This explains the shallower slope on the right hand side of the maximum at -425 as well as the higher maximum of occurrences.

Fetch distances occurrences above 400 m and therefore not visible on the rectified images were summed up and formed one bar at the end of each histogram.

Overall, it has been seen that the fetch distance measured varies dependent on the measurement point (-40 m or -30 m). It has been observed that the measurement point of -30 m is covered in water during tide. Therefore, it has been chosen to calculate the annual onshore aeolian sediment transport using the fetch distances measured at -40 m.

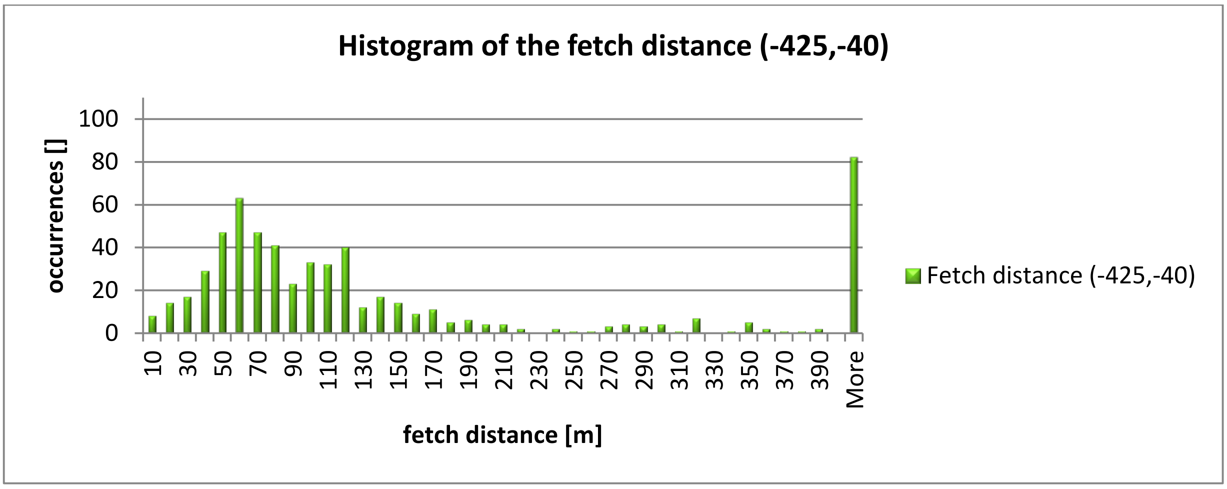

FIGURE 24: THE FETCH DISTANCE TAKING THE VARYING INTERTIDAL BEACH TOPOGRAPHY INTO ACCOUNT AT (-425,-40).

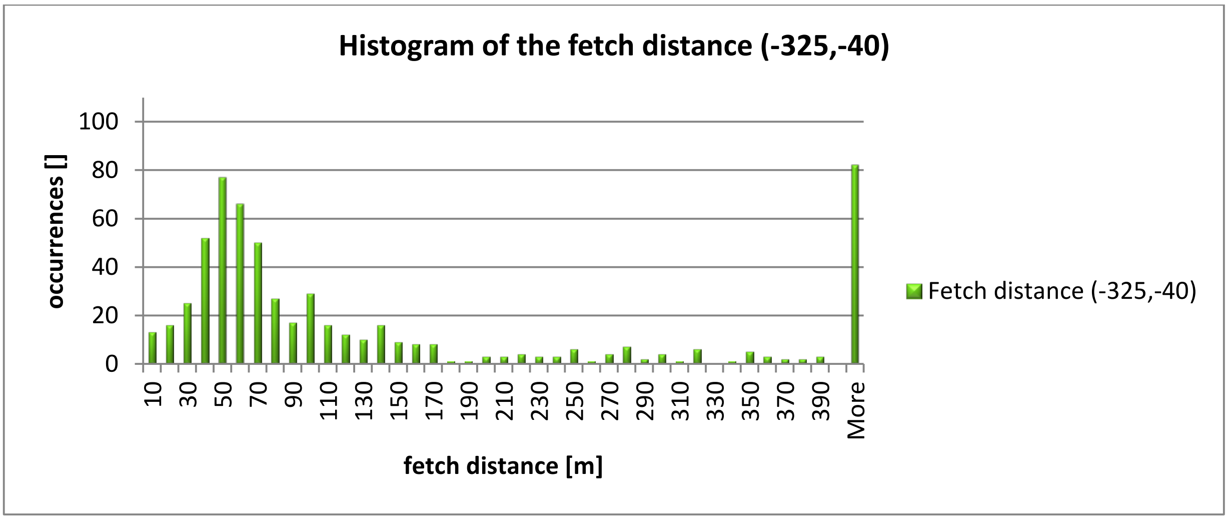

FIGURE 25: THE FETCH DISTANCE TAKING THE VARYING INTERTIDAL BEACH TOPOGRAPHY INTO ACCOUNT AT (-325,-40).

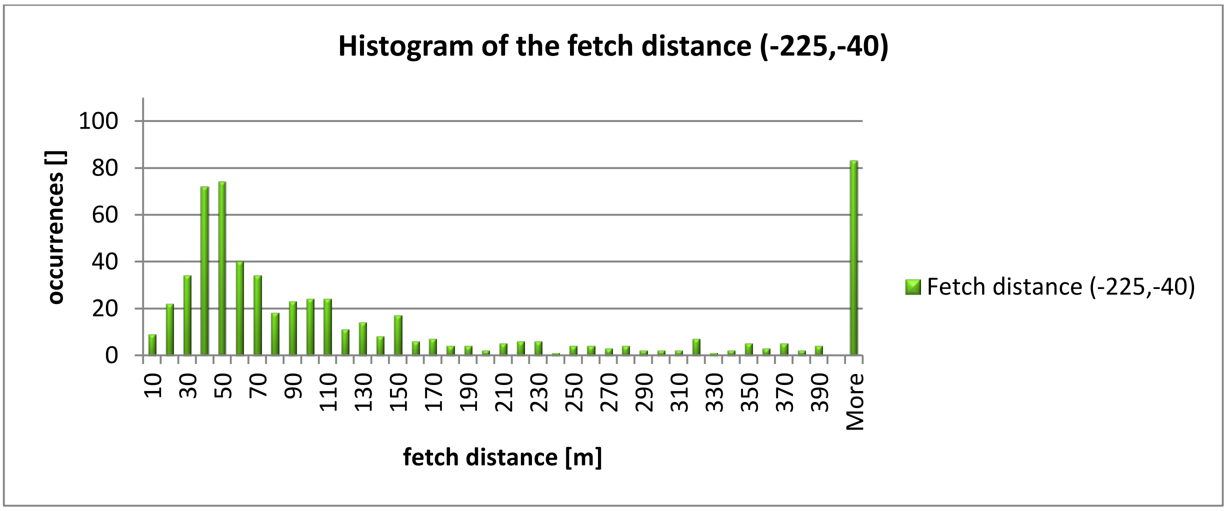

FIGURE 26: THE FETCH DISTANCE TAKING THE VARYING INTERTIDAL BEACH TOPOGRAPHY INTO ACCOUNT AT (-225,-40).

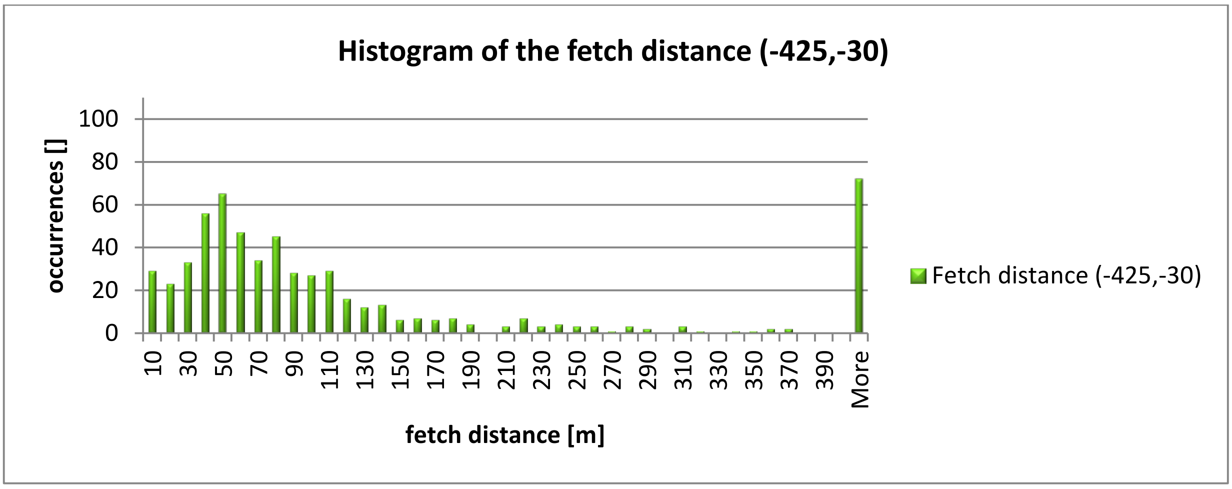

FIGURE 27: THE FETCH DISTANCE TAKING THE VARYING INTERTIDAL BEACH TOPOGRAPHY INTO ACCOUNT AT (-425,-30).

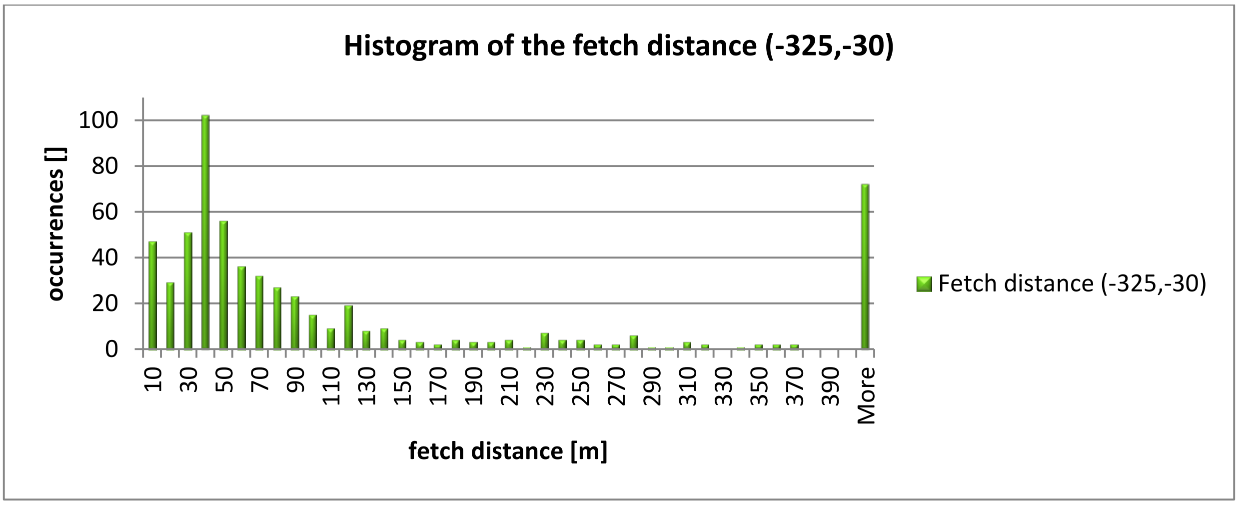

FIGURE 28: THE FETCH DISTANCE TAKING THE VARYING INTERTIDAL BEACH TOPOGRAPHY INTO ACCOUNT AT (-325,-30).

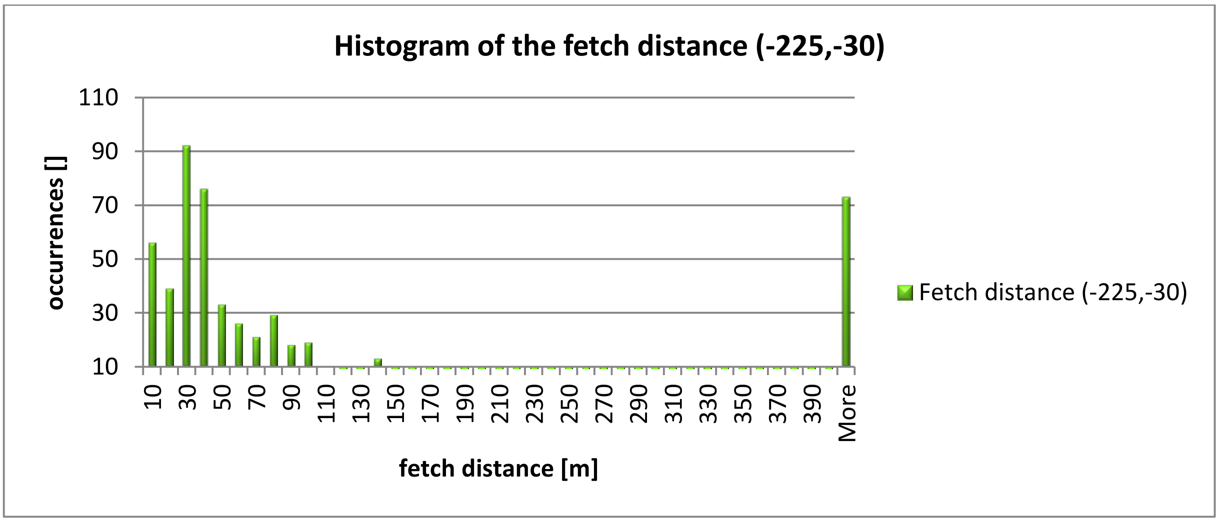

FIGURE 29: THE FETCH DISTANCE TAKING THE VARYING INTERTIDAL BEACH TOPOGRAPHY INTO ACCOUNT AT (-225,-30).

4.3.3. THEORETICAL CRITICAL FETCH DISTANCE

Figure 30 shows the calculated critical fetch distance for all identified aeolian sediment transport occurrences. To calculate the critical fetch distance following formula was used:

$$F_c = b \cdot (U_* + U_{*tm}) \tag{5}$$

With *b=9* (van Dijk, 1996), U_* the shear velocity and U_{*tm} the threshold shear velocity of moistened sand. The shear velocity and threshold shear velocity have been calculated for every aeolian sediment transport occurrence, as explained in chapter 3.1. Figure 30 shows that the critical fetch distances calculated vary between 5.6 m and 10 m.

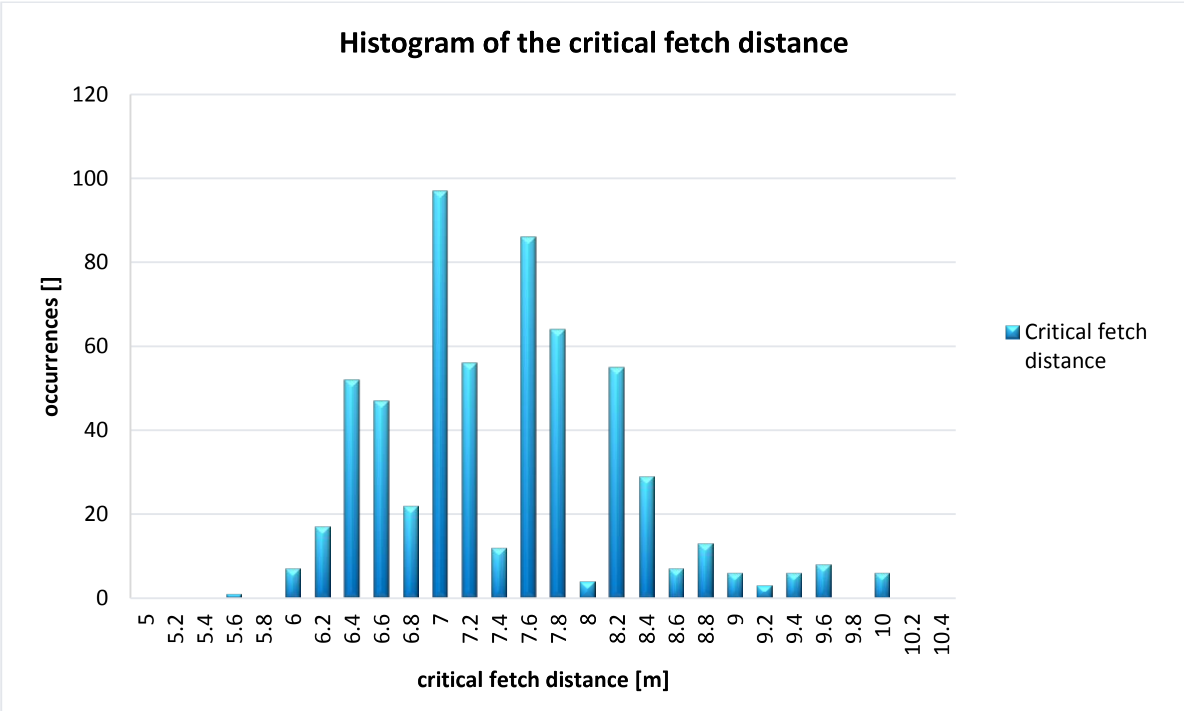

FIGURE 30: THE CRITICAL FETCH DISTANCE CALCULATED FOR ALL IDENTIFIED AEOLIAN SEDIMENT TRANSPORT OCCURRENCES IN 2009.

4.3.4. SATURATED AND NON-SATURATED SEDIMENT TRANSPORT

Comparing the results of the actual fetch distance determination to the results of the theoretical critical fetch distance determination, it can be seen that the theoretical critical fetch distance is almost always smaller than the determined fetch distance (95%). If the critical fetch distance is smaller than the actual fetch distance, the sediment transport rate has reached a so called equilibrium, and the fetch distance is no longer of influence on the sediment transport rate. Due to this result, the aeolian sediment transport reaches almost always theoretical saturation.

The low proportion of calculated critical fetch distances exceeding the measured fetch distances can be seen in Figure 31 for an alongshore non-varying fetch length and in Figure 32 for an alongshore varying fetch length. In both cases no more than 5% of the calculated critical fetch distances exceed the related measured fetch distance.

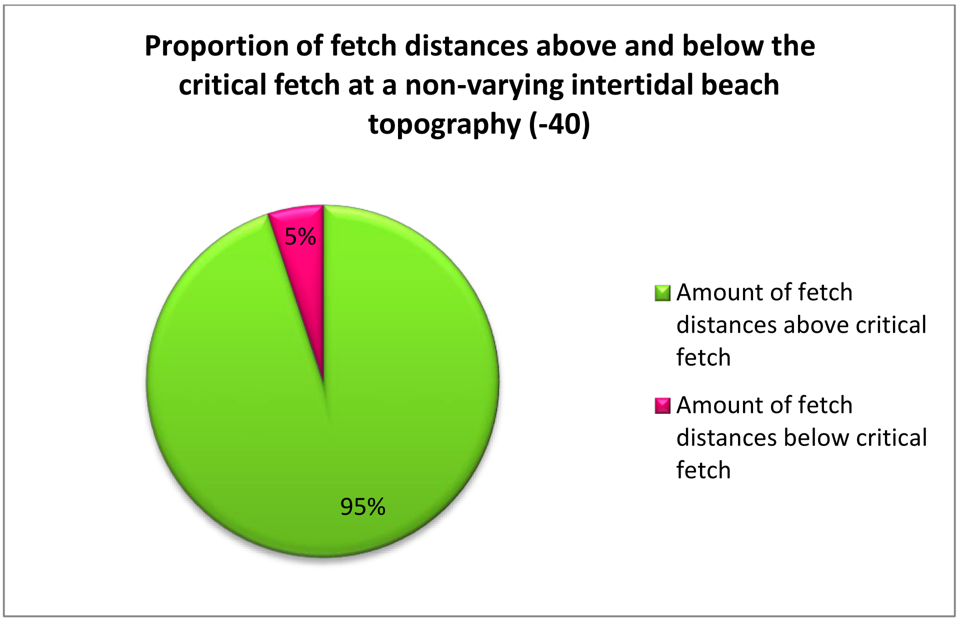

FIGURE 31: THE PROPORTION OF FETCH DISTANCES ABOVE AND BELOW THE CRITICAL FETCH AT A NON-VARYING INTERTIDAL BEACH TOPOGRAPHY (-40).

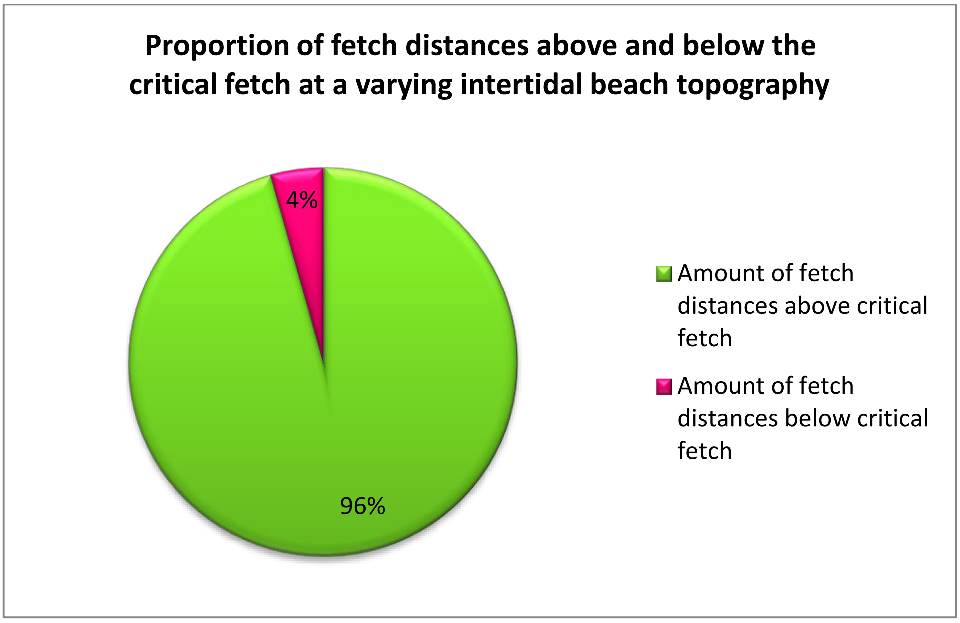

FIGURE 32: THE PROPORTION OF FETCH DISTANCES ABOVE AND BELOW THE CRITICAL FETCH AT A VARYING INTERTIDAL BEACH TOPOGRAPHY (-40) AVERAGED OVER THE THREE LOCATIONS (-225,-40), (-325,-40), (-425,-40).

As a results of this analysis the first part of the second research question concerning the effect of the fetch distance on aeolian sediment transport has been answered:

Comparing values of the calculated critical fetch distance to the values obtained during the measurement of the actual fetch distance, it can be concluded that there are only a few times when the critical fetch distance has been larger than the actual measured fetch distance. This is the case for both the alongshore non-varying intertidal beach topography and the alongshore varying intertidal beach topography, as can be seen in Figure 31 and Figure 32.

5. AEOLIAN SEDIMENT TRANSPORT CALCULATIONS

In this chapter the sensitivity analysis will be presented as well as the developed representative wind speed and the calculated annual aeolian sediment transport.

5.1. SENSITIVITY ANALYSIS

In this sub-section the sensitivity of the aeolian sediment transport formula on the different variables and parameters used throughout this study is assessed.

The values chosen for the different parameters (grain diameter *d*, density for sediment ρ_s, Kawamura's constant *K*, correlational factor according to grain size K_g, surface roughness length z_0, moisture content *M*, proportionality constant *A*) follow from a profound literature study (Sherman, et al., 1998; Bauer, et al., 2009; Davidson-Arnott, et al., 2008; Nordstorm, et al., 1992; Yang, et al., 2005; Dong, et al., 2002; Dong, et al., 2003). The choice of these parameters is explained in chapter 3.1. The values used for these parameters and all constants can be found in Appendix 9.1 Table 4. The variables tested during the sensitivity analysis are the moisture content (*M*), the wind speed at height z (U_z) the roughness length of the surface (z_0), the proportionality coefficient (*A*), the correlational factor according to grain size (K_g), the threshold shear velocity of moistened sand (U_{*tm}), the shear velocity (U_*) the grain diameter (*d*), the fetch distance (*F*) and the critical fetch (*Fc*). The results for the fetch distance and the critical fetch can be found in the Appendix 9.1. The dashed line in the figures of the sensitivity analysis gives the value used in this study. In this study the sensitivity analysis has been done using the One-at-a-time (OAT) method, changing one factor at a time and seeing what effect this procedures on the output. (Czitrom, 1999). One input variable is changed and the others are kept at their nominal values, so that any observed changes can be reduced to this single variable. Having done this for one variable, this variable has been brought back to its nominal value and the procedure was done for another variable. By changing one variable at a time the comparability of the results will be guaranteed.

If the moisture content increases the aeolian sediment transport rate decreases. Moist sand is more difficult to get into motion, therefore the higher the surface moisture content gets the lower the aeolian sediment rate gets per time. The moisture content used in this study is equal to 0.25% (Yang, et al., 2005). The relationship between the aeolian sediment transport rate and the surface moisture content is depicted in Figure 33.

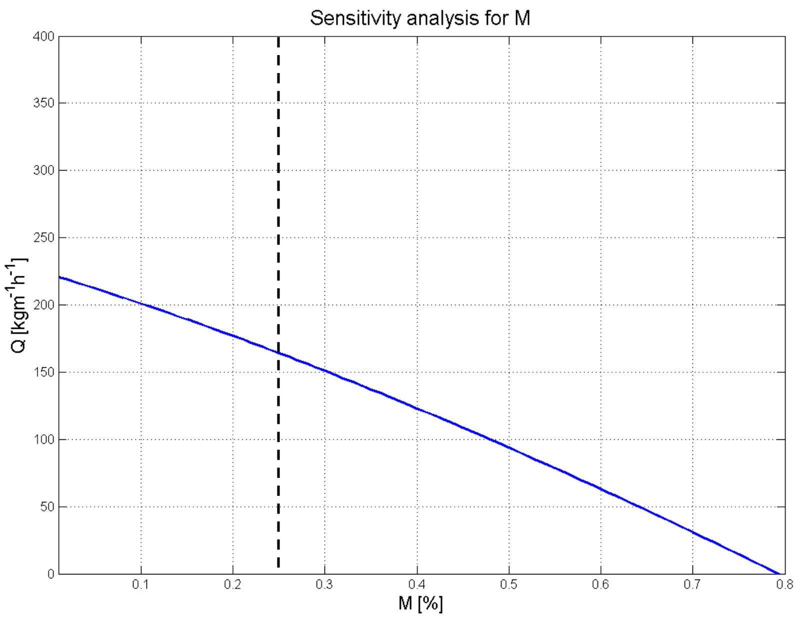

FIGURE 33: THE RELATIONSHIP BETWEEN THE AEOLIAN SEDIMENT TRANSPORT RATE AND THE SURFACE MOSITURE CONTENT.

The moisture content directly affects the threshold shear velocity. An increasing moisture content results in an increasing threshold shear velocity. Figure 34 shows the relationship between aeolian sediment transport rate and the threshold shear velocity. While the threshold shear velocity is increasing the aeolian sediment transport rate is decreasing significantly.

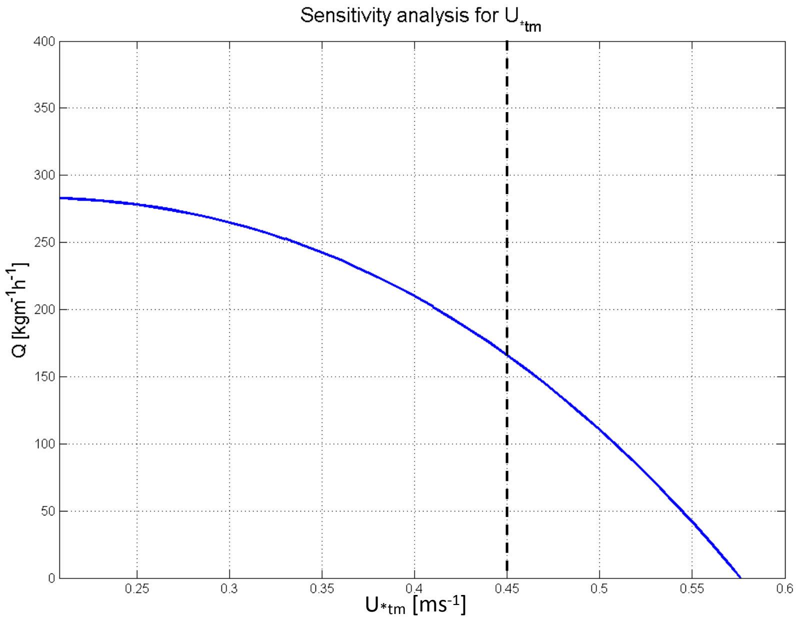

FIGURE 34: THE RELATIONSHIP BETWEEN AEOLIAN SEDIMENT TRANSPORT AND THE THRESHOLD SHEAR VELOCITY.

If the grain diameter increases the sediment transport rate decreases. A larger grain diameter results is a larger threshold shear velocity. The larger the threshold shear velocity the lower the aeolian sediment transport as is depicted in Figure 34. Figure 35 shows that if the grain diameter reaches a certain size the transport rate turns zero. Larger grains have a higher threshold shear velocity and can become too large to be moved by wind. The range of the grain diameter is chosen considering the grain diameters available at the beach (Han, et al., 2009). The relationship between the aeolian sediment transport rate and the grain size diameter can be seen Figure 35.

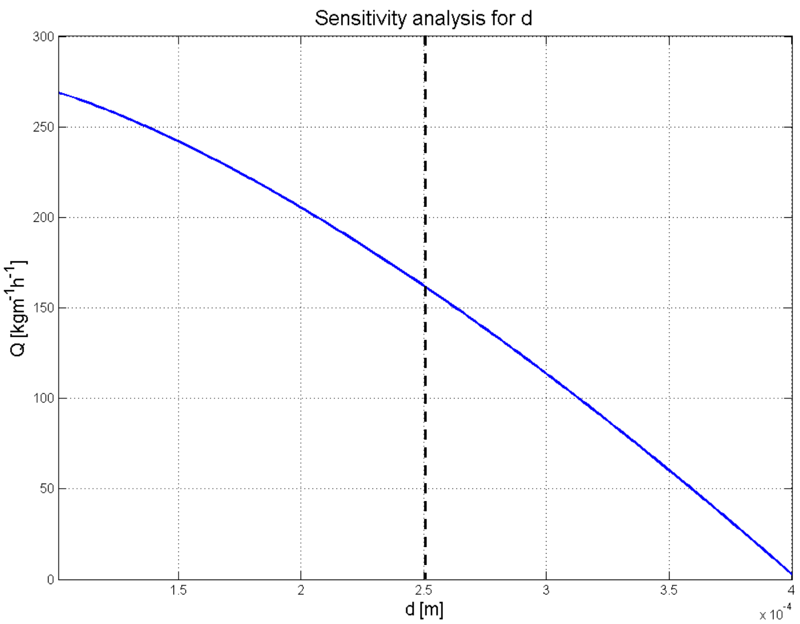

FIGURE 35: THE RELATIONSHIP BETWEEN THE AEOLIAN SEDIMENT TRANSPORT RATE AND THE GRAIN SIZE DIAMETER.

An increasing proportionality constant leads to a decreasing aeolian sediment transport. If the proportionality constant increases the threshold shear velocity increases as well. This results, as has been seen in Figure 35, in a decrease of aeolian sediment transport. The range chosen for *A* depends on the Reynolds number per grain size (Han, et al., 2009). The relationship between the aeolian sediment transport and the proportionality constant *A* is depicted in Figure 36.

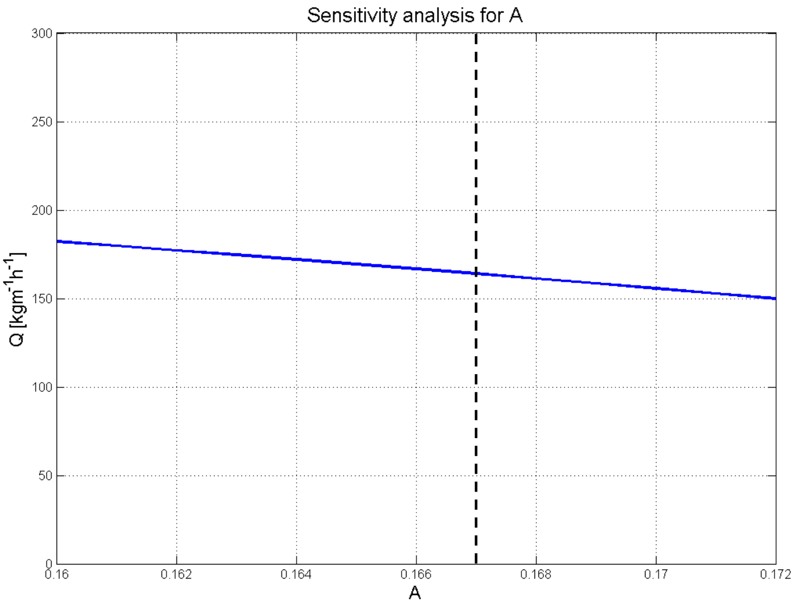

FIGURE 36: THE RELATIONSHIP BETWEEN THE AEOLIAN SEDIMENT TRANSPORT RATE AND THE PROPORTIONALITY CONSTANT A.

The relationship between the aeolian sediment transport rate and the correlational factor according to grain size K_g can be described as negative linear. An increasing value of K_g results in an increasing values of the threshold shear velocity. An increasing threshold shear velocity results in a decreasing sediment transport rate given in Figure 34. The effect of this factor is lower compared to the effect of Kawamura's constant *K*. The range of K_g depends in the grain size (Dong, et al., 2002). The relationship between the aeolian sediment transport rate and the correlational factor is depicted in Figure 37.

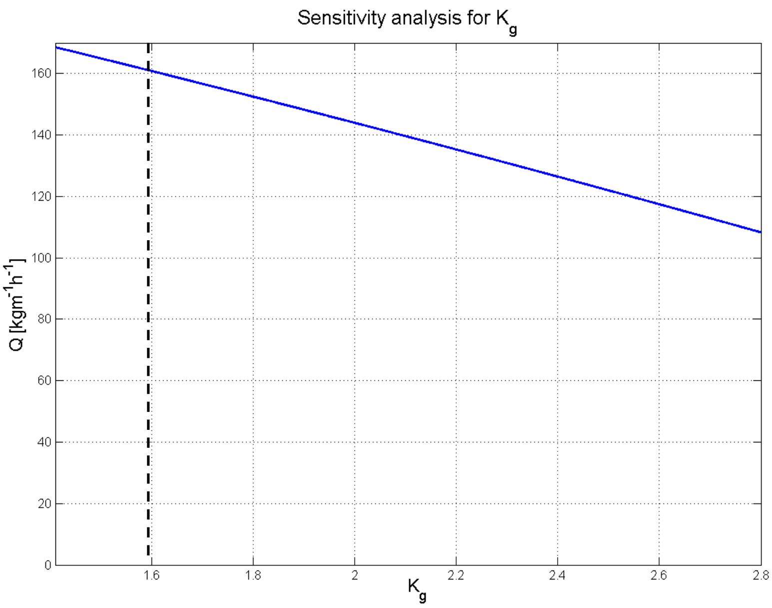

FIGURE 37: THE RELATIONSHIP BETWEEN AEOLIAN SEDIMENT TRANSPORT AND THE CORRELATIONSHIPAL FACTOR ACCORDING TO GRAIN SIZE DEFINED BIJ DONG ET AL. (2003).

Figure 38 depicts the relationship between the aeolian sediment transport rate and the shear velocity. An increasing shear velocity results in an increasing aeolian sediment transport rate.

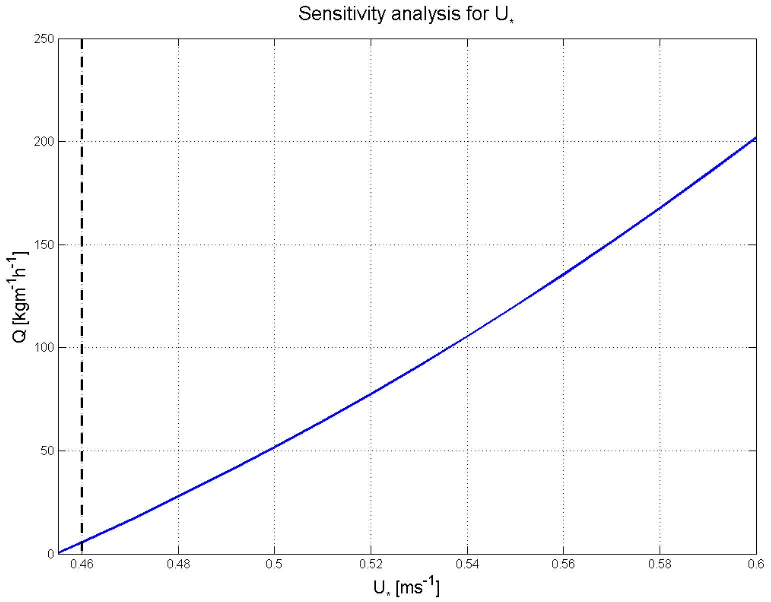

FIGURE 38: THE RELATIONSHIP BETWEEN AEOLIAN SEDIMENT TRANSPORT RATE AND SHEAR VELOCITY.

Above a wind speed of 12 ms^{-1} a positive relationship between wind speed at height *z* and the aeolian sediment transport rate has been found. If the wind speed at height *z* increases, the aeolian sediment transport rate increases as well. The relationship between the aeolian sediment transport rate and the wind speed is given in Figure 39.

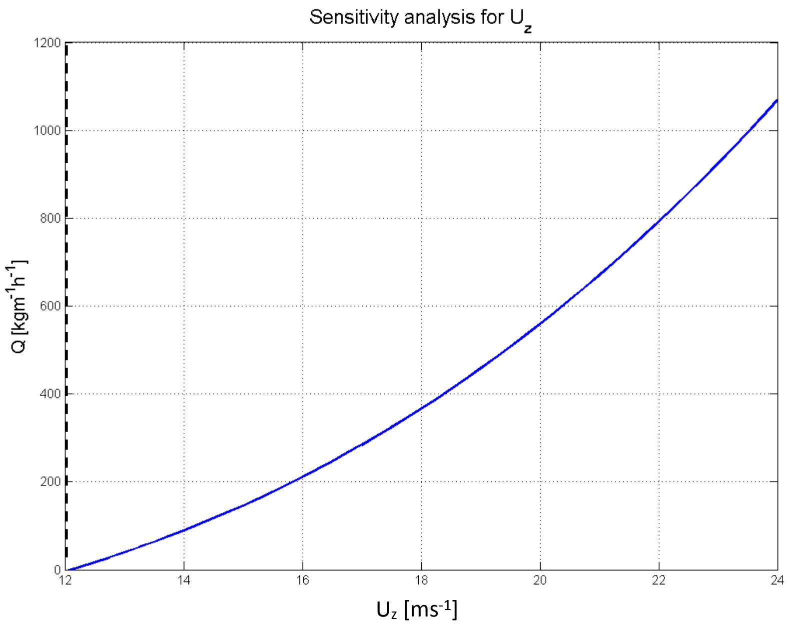

FIGURE 39: THE RELATIONSHIP BETWEEN THE AEOLIAN SEDIMENT TRANSPORT RATE AND THE WIND SPEED AT HEIGHT Z=10M.

The relationship between the surface roughness length (z_0) and the aeolian sediment rate can be described as square root relationship. A smaller surface roughness length results in a smoother surface which results in a decrease of the shear velocity. The range of z_0 is based on literature study (Hsu, 1971; Hansen, 1993; Nordstorm, et al., 1992; Sherman, et al., 1990; Sherman, et al., 1998). Many different values for the surface roughness length can be found in literature (Hansen, 1993, Hsu, 1971 and Sherman, et al., 1990). These values can differ up to 0.03 m. These variations result in aeolian sediment transport rate changes of up to 0.3 m^{3}m^{-1}h^{-1}. These large changes are especially found between 0.0001 m and 0.0006 m. Thereafter the aeolian sediment rate increases more slowly. The relationship between the aeolian sediment transport rate and the roughness length of the surface is given in Figure 40.

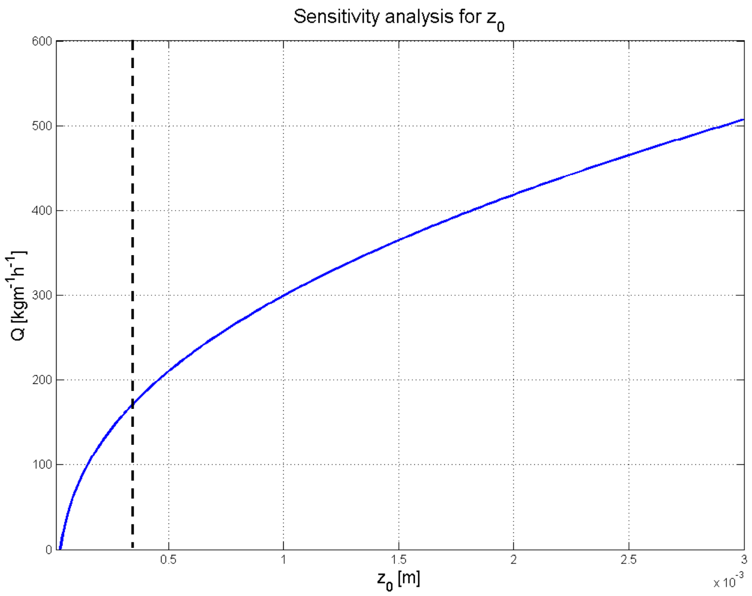

FIGURE 40: THE RELATIONSHIP BETWEEN THE AEOLIAN SEDIMENT TRANSPORT RATE AND THE ROUGHNESS LENGTH OF TE SURFACE.

The whole transport equation is multiplied with Kawamura's empirical constant *K*. Therefore, the aeolian sediment transport rate increases linear with the increasing value of *K*. The range of *K* depends on the different values that have been found in literature (Belly, 1962; Kadib, 1965). In this study *K* is equal to 2.78 as found by Kawmura (1951) for a grain diameter of 0.25 mm. This relationship is given in Figure 41. Small changes of this constant will lead to a moderate change of aeolian sediment transport.

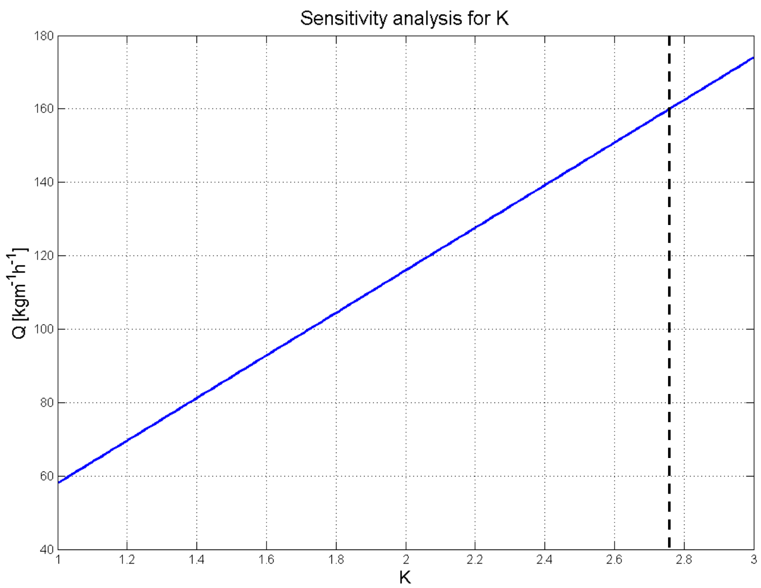

FIGURE 41: THE RELATIONSHIP BETWEEN AEOLIAN SEDIMENT TRANSPORT AND KAWAMURA'S CONSTANT K DEPENDING ON THE GRAIN SIZE.

The relationship between the critical fetch distance and the moisture content is given in Figure 42. It can be seen that an increasing moisture content results in an increasing theoretical critical fetch distance. The range of the moisture content has been chosen as in Figure 33.

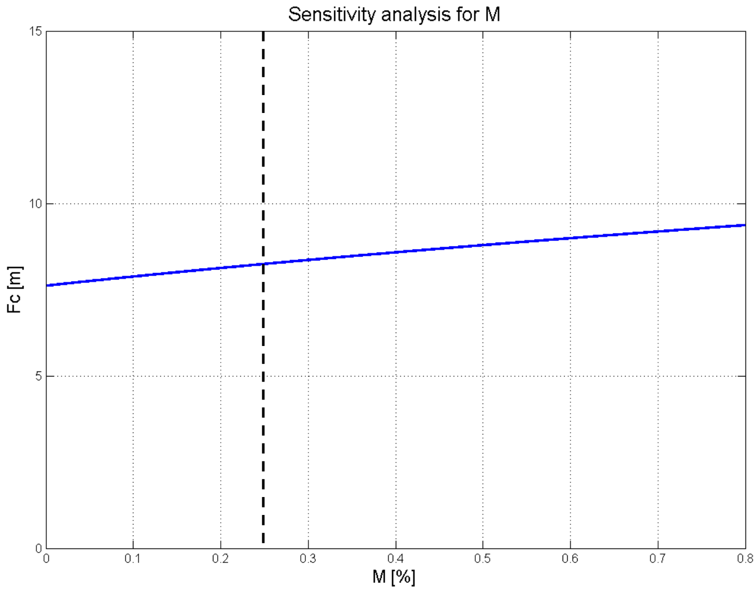

FIGURE 42: SENSITIVITY ANALYSIS FOR THE MOSITURE CONTENT ON THE CRITICAL FETCH DISTANCE.

Using the constants as described and explained in Appendix 9.1 Table 4, only wind speeds above 12 ms^{-1} at 10 m height can be considered. For wind speed values below 12 ms^{-1} the aeolian sediment transport formula used is not applicable.

The roughness surface length is assessed to have considerable effect on the calculated aeolian sediment transport. Literature differs much about the value of this parameter. These facts have to be taken into account while analysing annual aeolian sediment transport (Hsu, 1971; Hansen, 1993; Nordstorm, et al., 1992; Sherman, et al., 1990; Sherman, et al., 1998).

Overall, it can be said that the choice of the parameters is essential for the resulting calculated aeolian sediment transport. Therefore, all parameter values have been chosen carefully considering numerous scientific papers dealing with the choice and determination of these parameters (Bauer, et al., 2009; Darke, et al., 2009; Delgado-Fernandez, 2010; Dong, et al., 2002; Dong, et al., 2003; Hansen, 1993; Hsu, 1971; Kawamura, 1951; Rice, 1990; Yang, et al., 2005; van Dijk, 1996; von Kármán, 1930). Having gained this insight into the magnitude of influence that different parameters have on aeolian sediment transport, the variability of the parameters on the annual aeolian sediment transport calculations can be assessed.

5.2. REPRESENTATIVE WIND SPEED

In this sub-section the results of the representative wind speed determination are presented.

Figure 43 gives the aeolian sediment rate calculated for each hour using the higher resolution wind data over the different wind speeds including a fitted line. The figure depicts that the aeolian transport rate increases with increasing wind speed. Furthermore, the higher the hourly averaged wind speed the higher the difference in wind speed. The highest wind speeds are on the right hand side of the figure. These high wind speeds only occurred occasionally which means that there are not as many data points as in the middle or on the left hand side of the figure. The aeolian sediment transport rises moderately until a wind speed of 12.5 ms^{-1}. Thereafter, the aeolian sediment transport rises very quickly. The curve fitted through Figure 43 is defined as:

$$Q = 0.408 \cdot \left(\frac{(U_z - 7.08)^3}{\left(1 + e^{177.01 - 25 \cdot U_z}\right)^3}\right) + 0.259 \cdot \left(\frac{U_z - 6.00}{1 + e^{150.04 - 25 \cdot U_z}}\right), R^2 = 0.96.$$

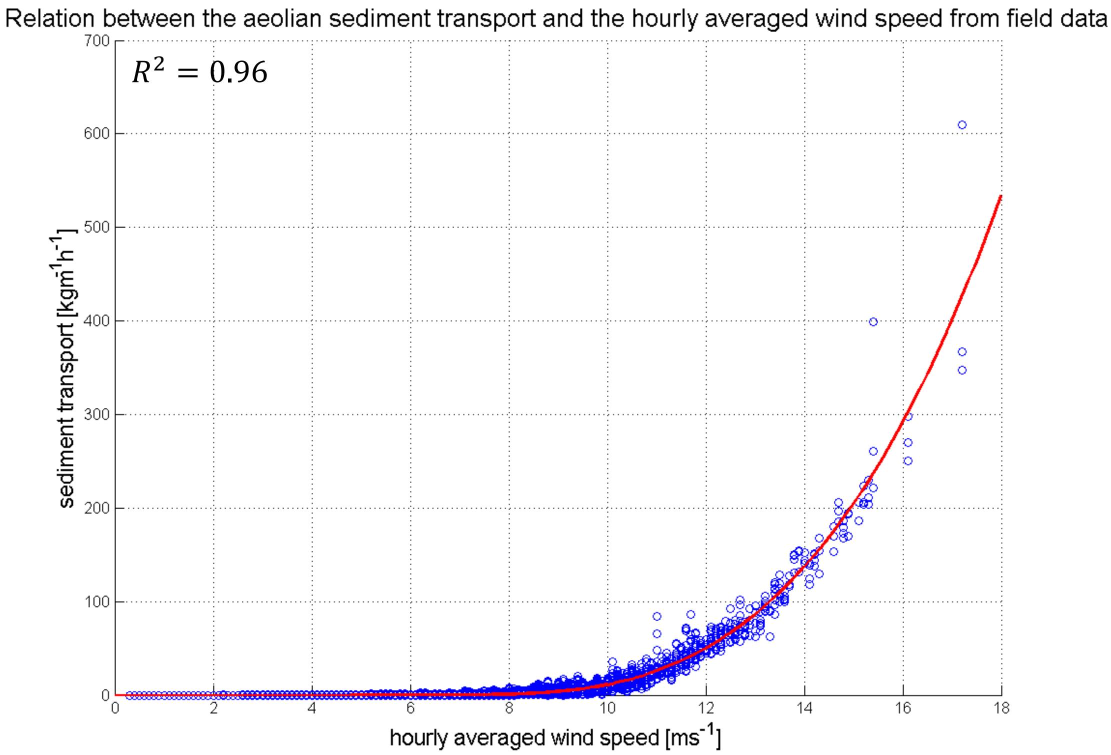

FIGURE 43: THE AEOLIAN SEDIMENT TRANSPORT OVER THE HOURLY AVERAGED WIND SPEEDS AS DERIVED FROM FIELD INCLUDING A FITTED CURVE.

Figure 44 shows the relationship between the representative and the hourly averaged wind speeds. It can be seen that the representative wind speeds are always higher than the hourly averaged ones. Nonetheless, a difference can be seen in how much the representative and hourly averaged wind speeds differ. Figure 44 depicts that the least difference in wind speeds has been found at a wind speed of 14 ms^{-1}.

Until an averaged wind speed of 6 ms^{-1} the representative wind speed is constant. This means no aeolian sediment transport can be calculated. The sensitivity analysis, chapter 5.1, showed that beyond wind speeds of 12 ms^{-1} the transport formula used is not applicable. Nevertheless, due to the gustiness of the wind, higher peaks than 12 ms^{-1} can be found at an hourly averaged wind speed of 6 ms^{-1}. Beginning at a wind speed of 6 ms^{-1} the hourly averaged wind speed is translated to a representative wind speed. Figure 44 gives a near linear relationship between representative wind speed and hourly averaged wind speed starting at an hourly averaged wind speed of 15 ms^{-1}. As can be seen, the difference between the corrected wind speed and the line y=x (blue line) is linear from 15 ms^{-1} on, which means that from 15 ms^{-1} on, the wind speed gets corrected linearly.

It cannot be seen that the wind speed correction starts from 6 ms^{-1} from Figure 44, but when zoomed in on the hourly average wind speed of 6 ms^{-1}, it can be seen that there is a slight correction from 6 ms^{-1} on, see Figure 45.

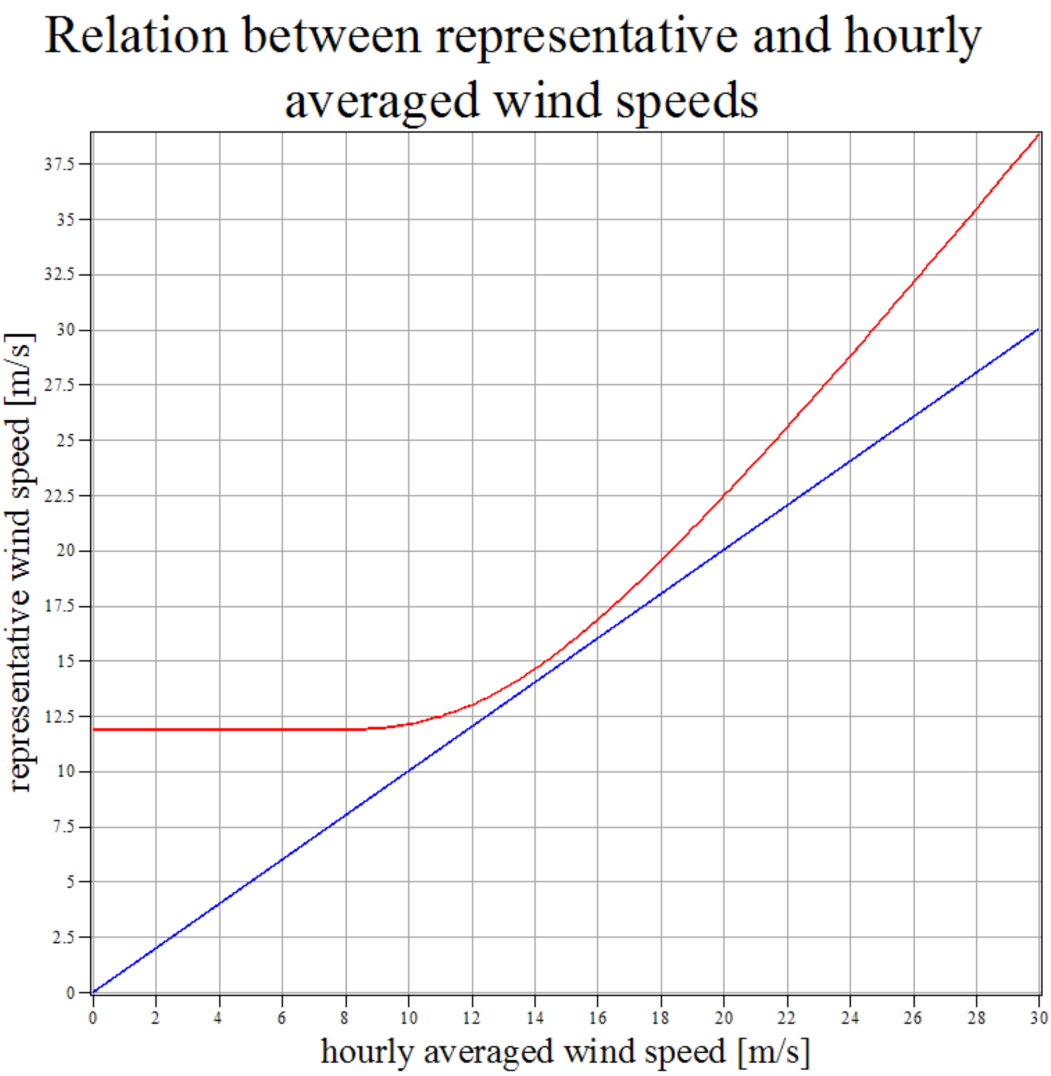

FIGURE 44: THE RELATIONSHIP BETWEEN THE REPRESENTATIVE AND THE HOURLY AVERAGED WIND SPEED.

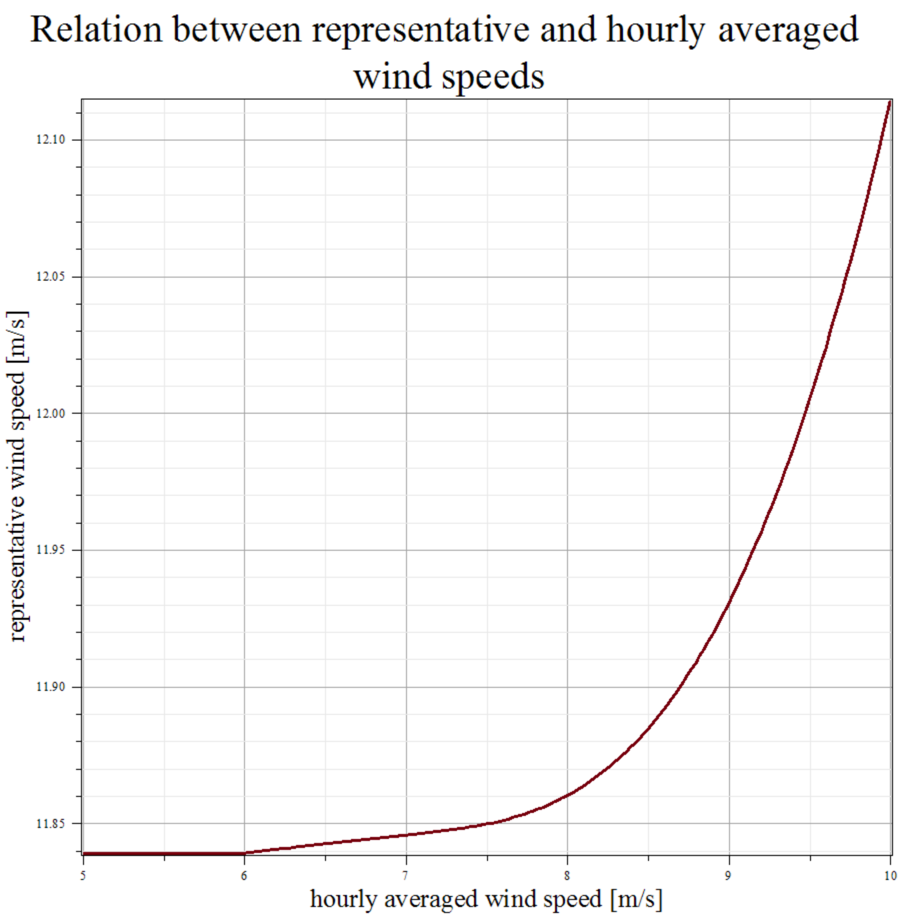

FIGURE 45: THE RELATIONSHIP BETWEEN THE REPRESENTATIVE AND THE HOURLY AVERAGED WIND SPEED ZOOMED IN.

Overall, higher resolution time series of wind speeds made it possible to account for the gustiness of the wind. Furthermore, the third power relationship between sediment transport and wind speed has been kept while fitting the curve to the scatter plot.

5.3. ANNUAL ONSHORE AEOLIAN SEDIMENT TRANSPORT CALCULATIONS

In this sub-section the results of the annual onshore aeolian sediment transport calculations are presented.

Figure 46 characterizes the aeolian transport conditions as hourly averaged wind speeds and fetch availability at the times where no aeolian sediment transport was identified on the ARGUS images. The hourly averaged wind speeds have been divided into below and above 6 ms^{-1}. The threshold velocity of 6 ms^{-1} has been chosen due to the fact that below 6 ms^{-1} almost no aeolian sediment transport has been identified on the ARGUS images. The hourly averaged wind speeds above 6 ms^{-1} are again divided into having and not having (or not identified) an intertidal beach at the ARGUS images. When an intertidal beach was present the fetch distance was assumed to be larger than the theoretical critical fetch. No intertidal beach, resulting from very high water levels and the sea covering the intertidal beach, means the fetch distance is equal to zero and the aeolian sediment transport rate being zero. 45% of all hours where no aeolian sediment transport occurrences have been identified had hourly averaged wind speeds above 6 ms^{-1}. In 11% of the cases almost no intertidal beach was visible on the ARGUS images and therefore the aeolian sediment transport rate is zero.

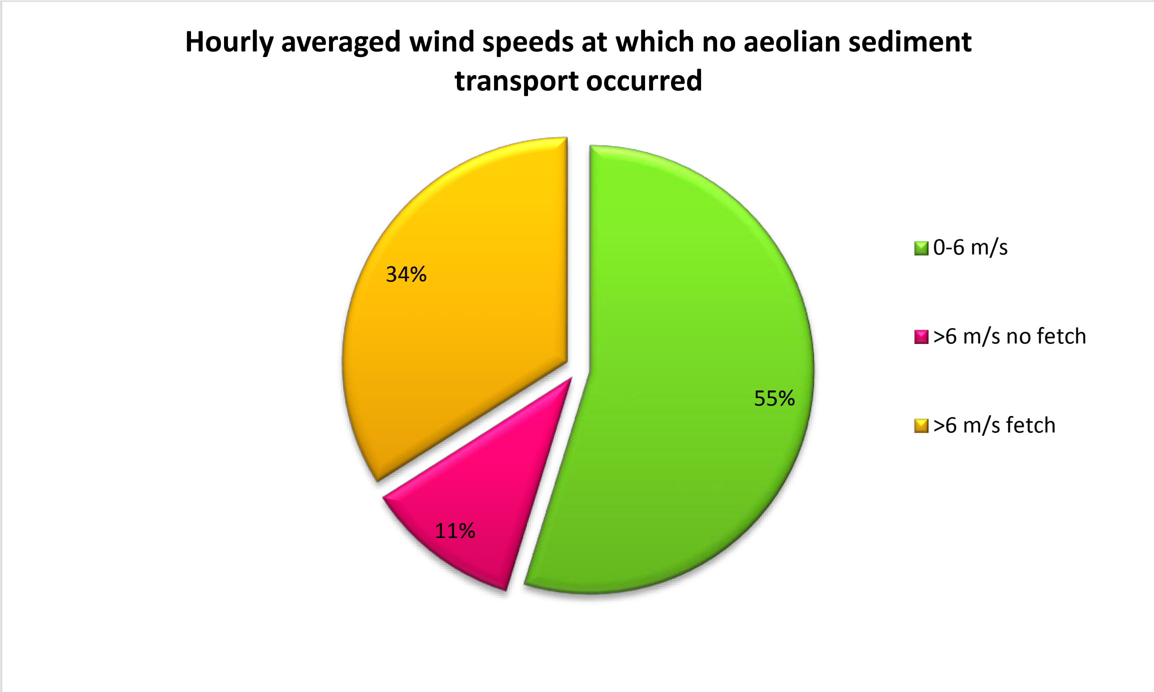

FIGURE 46: HOURLY AVERAGED WIND SPEEDS MEASURED AT NO AEOLAIN SEDIMENT TRANSPORT OCCURRENCES.

Table 3 shows the results of the annual aeolian sediment transport calculations for the difference in beach widths considering only the cross shore component. An explanation about the determination of the cross shore component of the aeolian sediment transport can be found in Appendix 9.5. To assess the effect of aeolian sediment transport when it is not identified on the video images, the times where no sediment transport was identified on the ARGUS images were analysed. Table 3 gives that the annual onshore aeolian transport rate calculated for the alongshore varying fetch distances is always larger than the rate calculated for the non-varying fetch distances.

The observed annual onshore aeolian sediment transport is calculated to be equal to 6.89 $m^3m^{-1}y^{-1}$. The annual aeolian sediment transport that can be calculated for the times where no aeolian sediment transport has been observed but wind speeds were high enough to get sediment into motion and a fetch distance was present, is equal to 2.51 $m^3m^{-1}y^{-1}$. Both of these values have been extrapolated from daytime hours to night-time hours. The explanation the extrapolation can be found in Appendix 9.6.

Cross shore component of the aeolian sediment transport	Non-varying fetch distance	Varying fetch distance
Observed aeolian sediment transport [$kgm^{-1}y^{-1}$]	10,151	11,031
Observed aeolian sediment transport [$m^3m^{-1}y^{-1}$]	6.34	6.89
No observed aeolian sediment transport [$kgm^{-1}y^{-1}$]	4,015	-
No observed aeolian sediment transport [$m^3m^{-1}y^{-1}$]	2.51	-
Total aeolian sediment transport [$m^3m^{-1}y^{-1}$]	-	9.4

TABLE 3: THE RESULTS OF THE ANNUAL ONSHORE AEOLIAN SEDIMENT TRANSPORT CALCULATIONS FOR A FIXED AND VARIABLE BEACH WIDTH IN 2009 FOR EGMOND BEACH.

Having done these calculations the second research question concerning the amount of annual aeolian sediment transport has been answered:

Overall, the total calculated annual aeolian sediment transport is 9.4 $m^3m^{-1}y^{-1}$ which is almost the same amount as found by Arens (2010), who measured the dune volume change per year at Egmond Beach to be 10 $m^3m^{-1}y^{-1}$ (Arens, 2010).

The calculated annual aeolian sediment transport for the alongshore varying fetch distances is 8% higher than the value calculated for the non-varying fetch distance. The annual aeolian sediment transport that has been calculated for the cases where no transport has been observed but a fetch distance was available, is 2.51 $kgm^{-1}y^{-1}$. This means that 25% of the total annual aeolian sediment transport results from cases where no sediment transport has been observed, but a fetch distance was available.

6. DISCUSSION

The sensitivity analysis in chapter 5.1 reveals that the equation used to calculate the aeolian sediment transport is most sensitive to the change in surface roughness length. The suitable surface roughness length was very carefully chosen. Nevertheless, many different values for the surface roughness length can be found in literature (Hansen, 1993, Hsu, 1971 and Sherman, et al., 1990). These values can differ up to 0.03 m. These variations result in aeolian sediment transport rate changes of up to 0.3 $m^3m^{-1}h^{-1}$. These large changes are especially found between 0.0001 m and 0.0006 m thereafter the the aeolian sediment rate increases more slowly.

In this study the moisture content was assumed to be constant over the whole beach. Chapter 5.1, Figure 33, shows that the sediment transport rate increases when the moisture content decreases. In this relationship it was shown that changes in surface moisture content can result in a difference in sediment transport of up to almost 120 $kgm^{-1}h^{-1}$. Different studies show variations in surface moisture content varying from 0% to 15% (Edwards, et al., 2012; Oblinger, et al., 2008; Atherton, et al., 2001; Yang, et al., 2005). Using the formula stated in 3.1 it can be seen that for a surface moisture content higher than 0.8% (depending on wind speeds and parameters defined in Appendix 9.1 Table 4) no aeolian sediment transport can be calculated, Figure 33.

Measuring the beach surface moisture content is complex and no method is verified yet to represent the actual beach surface moisture content. Only the moisture content at the top layer of the beach surface is of importance for the aeolian sediment transport calculations. This top layer is assumed to be no thicker than about 1 mm. Wind blowing over the beach surface is assumed to dry this thin top layer and make sediment available for movement. Therefore, it is chosen to use a smaller surface moisture content than generally stated. Due to the thin and quickly drying top surface layer and the observations from the ARGUS images, that at relatively small hourly averaged wind speeds (6 ms^{-1}) aeolian sediment transport occurrences have been observed, it is chosen to use the surface moisture content as suggested by Yang et al. (2005). The surface moisture content in this study is therefore assumed to be 0.25% for the intertidal area (Yang, et al., 2005). However, the moisture content changes along and across the intertidal beach area. Therefore, assuming the moisture content to be constant is a crude schematization.

The effect of the moisture content on the critical fetch distance shows that the critical fetch will vary between 7.5 m for dry sand to 8.5 m for the maximum moisture content, chapter 5.1 Figure 42. Therefore, if the moisture content varies, the effect on the critical fetch will be quite small according to existing theory. Field studies reported much higher fetch distances (Davidson-Arnott, et al., 1996; Davidson-Arnott, et al., 2008). These high critical fetch distances might have been obtained due to the fact of sand availability. Sand has to be available for transportation meaning sand has to be dry enough to be picked up by wind (de Vries, 2013).

In this study offshore aeolian sediment transport is assumed to be insignificant compared to onshore aeolian sediment transport. Nevertheless, it has been found that 29% of the identified aeolian sediment transport instances have been offshore, see Appendix 9.2.3. These identified aeolian sediment transport occurrences showed aeolian sediment transport from the intertidal beach seawards. Therefore it is assumed that the offshore identified aeolian sediment transport will not contribute to the increase in dune volume. However, literature assumes that offshore wind directions contribute to dune volume increase due to secondary airflow effects (Lynch, et al., 2008; Jackson, et al., 2013). This difference in observation may result from the fact that in this study attention was paid to the intertidal beach and the studies of Jackson (2013) and Lynch (2008) focused on the fore dune.

During the hours that transport was identified in the ARGUS images, 75% of the calculated annual aeolian sediment transport took place. During the hours that no transport was identified in the ARGUS images, 25% of the calculated annual aeolian sediment transport took place. Both values are based on daytime hours, and extrapolated to night-time hours. It has to be kept in mind that the ratio between identified (75%) and not identified (25%) annual aeolian sediment transport is site specific and can vary due to climate, the set-up of ARGUS video image installation or the image capturing frequency.

7. Conclusion

The study was set out to explore the annual amount of sediment that the wind can transport from the intertidal beach to the upper beach. It was also sought to find the effect of the varying alongshore fetch distances on the onshore annual aeolian sediment transport. The study aimed at answering the main question of how much sediment can leave the intertidal beach by wind in the onshore direction on an annual basis by answering two sub questions:

1. ***How often and under which conditions does aeolian sediment transport occur (wind speeds, precipitation)?***

In total 3260 hours of ARGUS images were available during daytime in 2009. 5475 hours of the year 2009 were hours overnight or too dark to observe aeolian sediment transport on the ARGUS images. Daytime precipitation occurred during 10% (326 hours). Of the 3260 ARGUS images taken during the daytime, 844 images (26% of the images) showed aeolian sediment transport. These occurrences were divided into offshore and onshore transport. From analysis, 603 occurrences of onshore aeolian sediment transport have been counted, which is 71% of the total aeolian sediment transport occurrences, covering 18% of the daytime hours for which ARGUS images were available. This results can as well be seen in Appendix 9.2.

The most aeolian sediment transport occurrences have been identified while wind was blowing alongshore or nearly alongshore the beach. Wind directions from North-West resulted in the observation of most aeolian sediment transport occurrences. Almost no aeolian sediment transport occurrences have been identified with wind blowing from the South-East, see chapter 4.1 Figure 16.

No single velocity threshold for aeolian sediment transport occurrences was found. For winds blowing mainly in the alongshore direction, transport occurrences were identified at lower wind speeds than for cross shore wind directions. Below an hourly averaged wind speed of 6 ms^{-1} almost no aeolian sediment transport occurrences were identified, see chapter 4.1 Figure 15.

Due to precipitation aeolian sediment transport was assumed to get hindered. The sediment on the top layer of the beach gets wet and therefore less sediment is supposed to be available for transportation. This top layer needs to dry first. Nevertheless, this assumption could not be confirmed during the data analysis, Figure 20 and Figure 21.

2. ***How much aeolian sediment transport can occur in theory under these conditions and has the varying intertidal beach topography effect on this result?***

The total theoretical amount of annual onshore aeolian sediment transport was calculated to be 9.4 $m^3m^{-1}y^{-1}$ in 2009 at Egmond Beach, assuming transport occurrences at night (not captured by ARGUS video images) to be proportional to transport occurrence during daytime. The total theoretical annual onshore aeolian sediment transport rate includes the observed transport occurrences as well as the not observed transport occurrences with fetch. Comparing the calculated annual onshore aeolian sediment transport rate to the amount of annual dune volume change (10.0 $m^3m^{-1}y^{-1}$) reposted by Arens (2010), it can be seen that these values are almost the same.

Due to the varying fetch distances, the varying complex intertidal beach topography was expected to have significant effect on the aeolian sediment transport. However, only in 5% of the aeolian sediment transport occurrences, the fetch distance was smaller than the theoretically predicted critical fetch. The difference in transport rate between a non-varying fetch distance and an alongshore varying fetch distance is 0.88 $m^3m^{-1}y^{-1}$, chapter 5.3 Table 3. This is 8% of the total annual onshore aeolian sediment transport. It can be concluded that the small amount of cases, for which the fetch distance is smaller than the critical fetch, can result in a non-negligible difference in annual onshore aeolian sediment transport between non-varying fetch distances and alongshore varying fetch distances.

In some of the hours where no transport was observed, the beach width of the intertidal area was very small or not present and hence no fetch was available. For all other times without visual signs of aeolian transport (which was 82% of the time), a contribution of the annual aeolian sediment transport was calculated of 2.51 $m^3m^{-1}y^{-1}$ in total. This is 25% of the total amount of annual aeolian sediment transport that was calculated for the times that sediment transport occurrences were identified.

Studying onshore annual aeolian sediment transport resulted in two main conclusions:

- Firstly, it can be concluded that given the aeolian sediment transport formula used in this study, it is possible to calculate annual aeolian sediment transport within a realistic order of magnitude, if representative wind speeds are used, in order to account for gustiness, instead of hourly averaged wind speeds. However, the formula used is most sensitive to changes in surface roughness length. Therefore, the surface roughness length is one of the key parameters of onshore annual aeolian sediment transport calculations. In existing studies the moisture content has been found to be an influential parameter for calculating aeolian sediment transport (Atherton, et al., 2001; Bauer, et al., 2009; Davidson-Arnott, et al., 2008; Davidson-Arnott, et al., 2005). This significance has also been seen in this study, as the moisture content can influence the aeolian sediment transport with half as much impact as the surface roughness length (chapter 5.1, Figure 33 and Figure 40).
- Secondly, during the hours that transport was identified in the ARGUS images, 75% of the calculated annual aeolian sediment transport took place. During the hours that no transport was identified in the ARGUS images, 25% of the annual aeolian sediment transport was calculated. Both values are based on daytime hours, and extrapolated for night-time hours. Therefore, it can be concluded that the identification of sediment transport occurrences on ARGUS images is an important part of the annual aeolian sediment transport calculation method.

8. RECOMMENDATIONS

To obtain a better understanding of onshore aeolian transport from the intertidal beach, further research is required. Throughout this study, several assumptions had to be made. These assumptions are a crude schematization of the conditions at the beach.
In this chapter, the most important or most influential assumptions are discussed in the sub-sections and a recommendation for further research is given.

ROUGHNESS SURFACE LENGTH

Assumption: The roughness surface length is assumed to be 0.0003 and not is temporally and spatially varying.
Recommendation: Determine the roughness surface length at the beach and its variability.
Impact: high
Explanation: The aeolian sediment transport formula used is most sensitive on the surface roughness length. Many different values for the surface roughness length at the beach can be found in literature. These values vary up to 0.03 m. These variations result in aeolian sediment transport rate changes of up to 0.3 $m^3m^{-1}h^{-1}$. These large changes are especially found between 0.0001 m and 0.0006 m thereafter the the aeolian sediment rate increases more slowly. The surface roughness length is varying on temporal an spatial scale. Due to the sensitivity of the aeolian sediment transport formula on this parameter, the temporal and spatial variations should be quantified and included in the sediment transport calculations.

MOISTURE CONTENT

Assumption: The moisture content is constant over the whole beach.
Recommendation: Adjust the existing equation to take variable moisture content over the beach into account.
Impact: moderate to high
Explanation: The aeolian sediment transport formula used takes into account the moisture content. Nevertheless, it is not known if the formula which is a combination of existing theory reflects the reality. Therefore, future research should address the relationship between moisture content and threshold velocity in the aeolian sediment transport process. The assumption that the moisture content is a constant over the whole does not match the reality. Therefore, it is recommended to adjust the existing equation or more likely to derive a different equation that takes the moisture content as a variable into account.

9. APPENDIX

9.1. PICTURES SHOWING WHAT IS MEANT BY VISIBLE AEOLIAN SEDIMENT TRANSPORT FOR THIS STUDY

NORTH

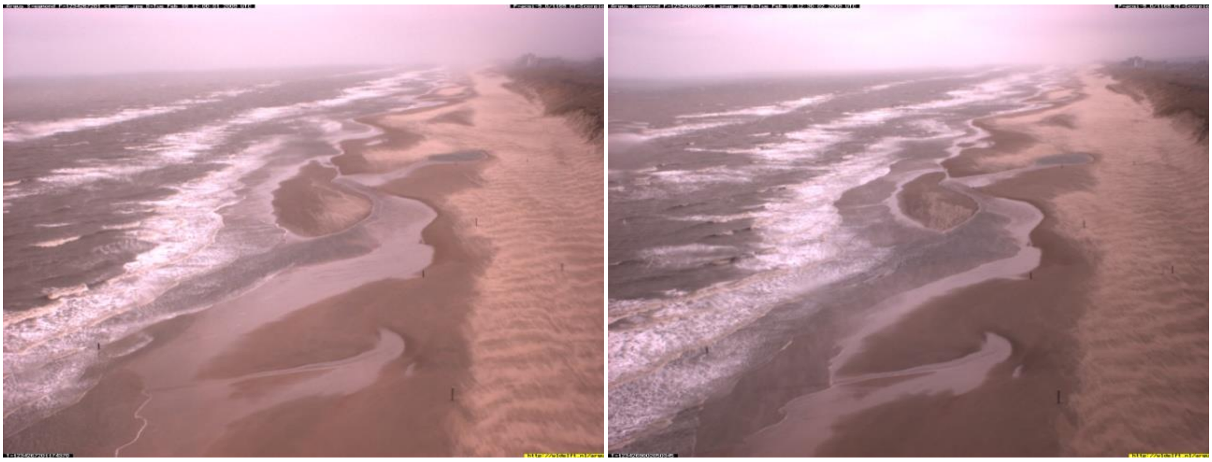

FIGURE 47: VISIBLE AEOLIAN SEDIMENT TRANSPORT. WIND DIRECTION: NORTH. (FEB 10TH 12.00 AM AND 12.30 AM)

NORTH-EAST

FIGURE 48: VISIBLE AEOLIAN SEDIMENT TRANSPORT. WIND DIRECTION: NORTH-EAST. (MAY 12TH 9.00 AM AND MAY 12TH 9.30 PM)

EAST

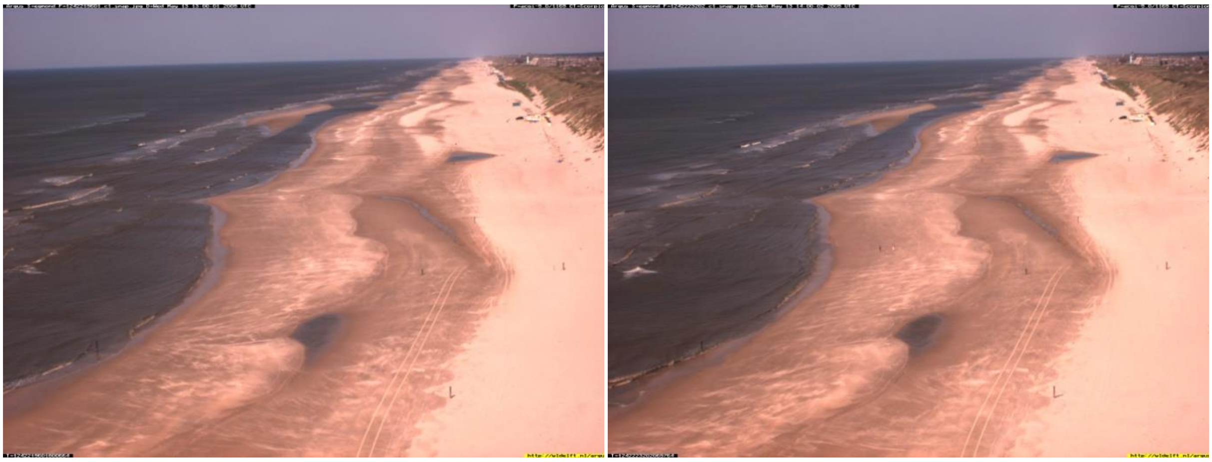

FIGURE 49: VISIBLE AEOLIAN SEDIMENT TRANSPORT. WIND DIRECTION: EAST. (MAY 13TH 1.00 PM AND MAY 13TH 2.00 PM)

SOUTH-EAST

FIGURE 50: VISIBLE AEOLIAN SEDIMENT TRANSPORT. WIND DIRECTION: SOUTH-EAST.

SOUTH

FIGURE 51: VISIBLE AEOLIAN SEDIMENT TRANSPORT. WIND DIRECTION: SOUTH. (JAN 17TH 12.00 AM AND 12.30 AM)

SOUTH-WEST

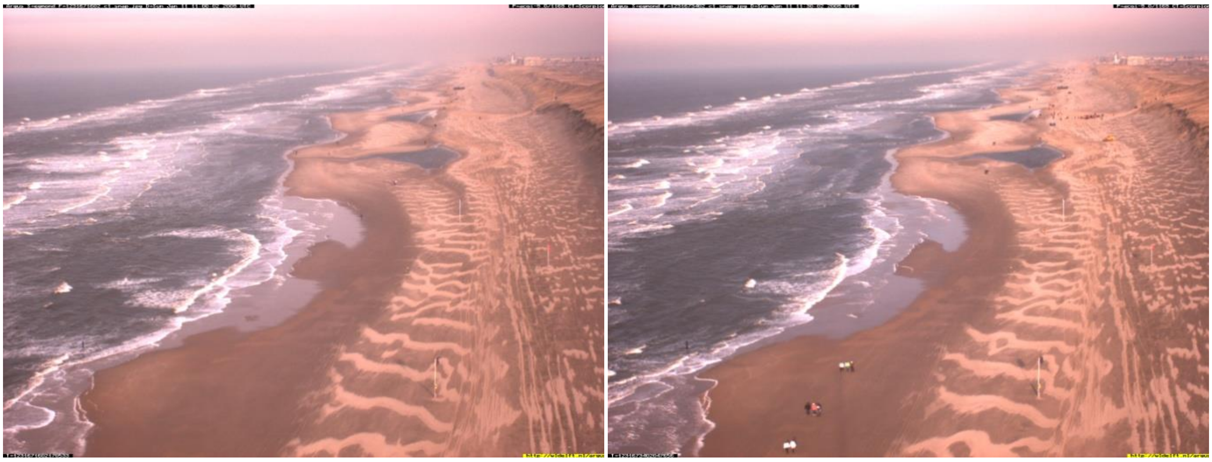

FIGURE 52: VISIBLE AEOLIAN SEDIMENT TRANSPORT. WIND DIRECTION: SOUTH-WEST. (JAN 11 11.00 AM AND 11.30 AM)

NORTH-WEST

FIGURE 53: VISIBLE AEOLIAN SEDIMENT TRANSPORT. WIND DIRECTION: NORTH-WEST. (FEB 10TH 12.00 AM AND 1.00 PM)

VISIBLE AEOLIAN SEDIMENT TRANSPORT WITH BERY LITTLE WIND 4.6 ms^{-1} 60 DEGREES NORTH

FIGURE 54: OBTAINED VISIBLE AEOLIAN SEDIMENT TRANSPORT DESPITE VERY LITTLE WIND SPEED. (MAY 20TH 2:30 PM AND 3:00 PM)

Figure 55 depicts the flattening of sand bars during the drying process. Due to the widening of the bars this process could be identified as aeolian sediment transport occurrence. Nevertheless, the flatting sand is not defined as aeolian sediment transport.

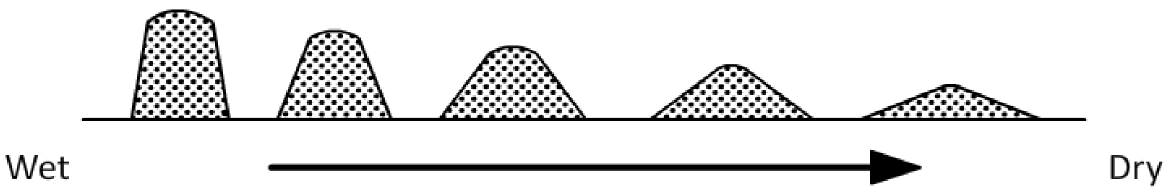

FIGURE 55: FLATTENING OF SAND BARS DURING THE DRYING PROCESS.

9.2. USABILITY OF THE DATA

To analyse the visible aeolian sediment transport a large amount of data was needed. Data consists of ARGUS images, wind speeds, wind direction, precipitation and water levels. For some time intervals no data was available, e.g. ARGUS images at night. This chapter gives an overview of the amount of data available and the amount a data actually used during this study. As said before ARGUS images were only available during the day which in this study was defined as the time interval between 8.00 AM and 4.00 PM. Figure 56 shows the proportion of daytime when ARGUS were available. About 37% of the images were taken between 8.00 AM and 4.00 PM. These 37% of the images were used in this study. The other 63% could not be used because there were no ARGUS images or the images were taken in the dark.

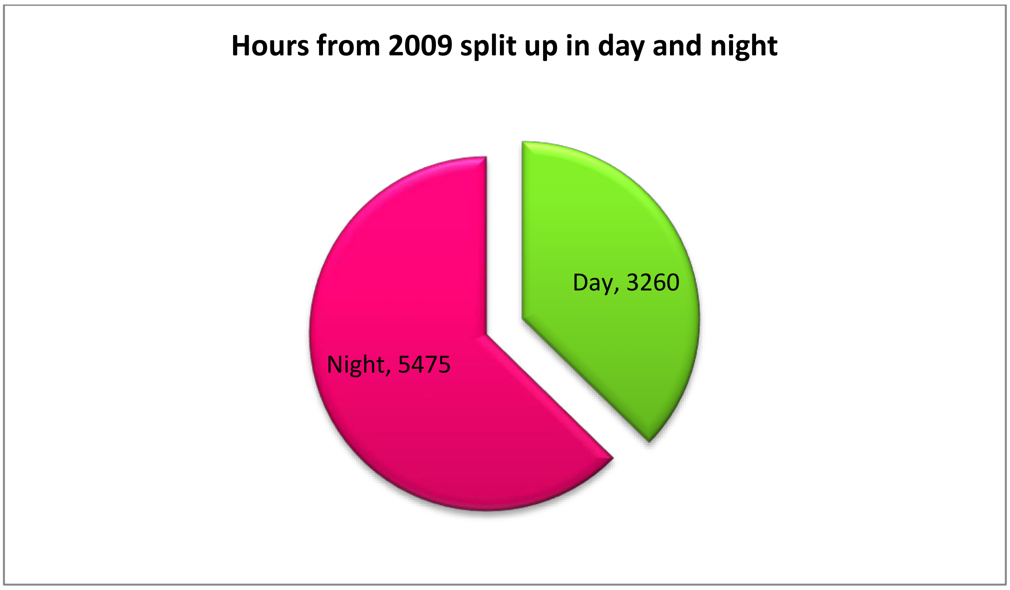

FIGURE 56: THE PROPORTION OF TIME FOR WHICH ARGUS IMAGES WERE AVAILABLE IN 2009 BY DAY AND NIGHT.

Not all ARGUS images that were taken during the daytime were usable for further analysis. Figure 57 shows one of those not usable days were no beach can be seen because of fog. If the wind speeds of such a day were very low it has been assumed that no aeolian sediment transport took place. If the wind speeds were in a range where usually visible aeolian sediment could have been obtained these days were not used in this study because it is not yet known if the moisture of the fog has any effect on aeolian sediment transport or not.

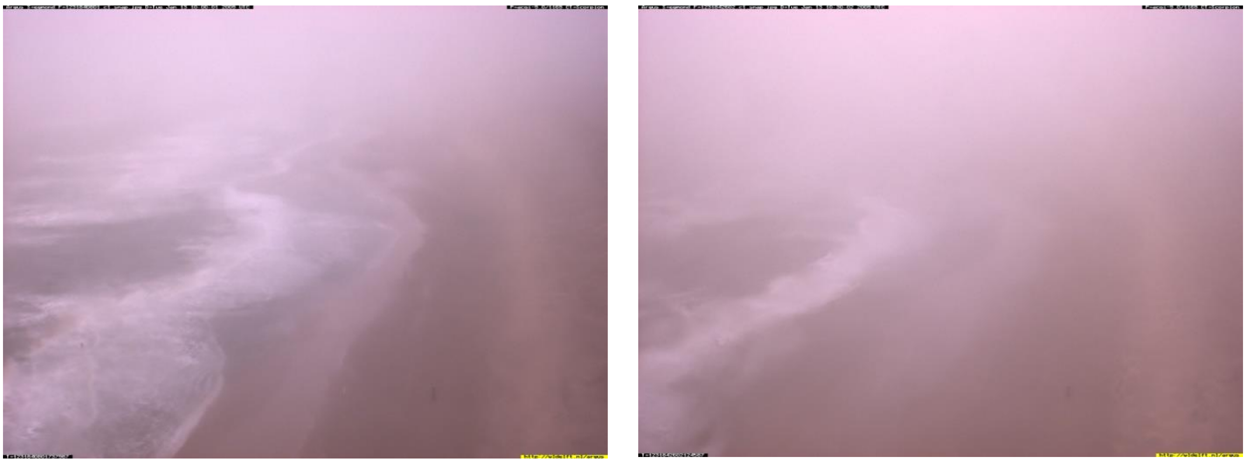

FIGURE 57: ARGUS IMAGES FROM JANUARY 13TH 2009 10.00 AM AND 10:30 AM.

Another visible aeolian transport limiting factor was snow. During the winter month several days long the beach was covered in snow. If the beach was covered in snow no visible aeolian sediment could have taken place no matter how high the wind speeds were. These days have not been used in this study. An example of these days is given in Figure 58. In Figure 58 it can be clearly seen that a large amount of the beach is covered in snow and therefore is not usable to obtain visible aeolian sediment transport.

FIGURE 58: ARGUS IMAGES FROM DECEMBER 31ST 2009 2.00 PM AND JANUARY 1ST 2009 8.00 AM.

Figure 59 show the proportion of the ARGUS image day hours that were usable and unusable as described above. Only 3% of all the day ARGUS images were not usable. This means of the total ARGUS image data 36% has been used during this study.

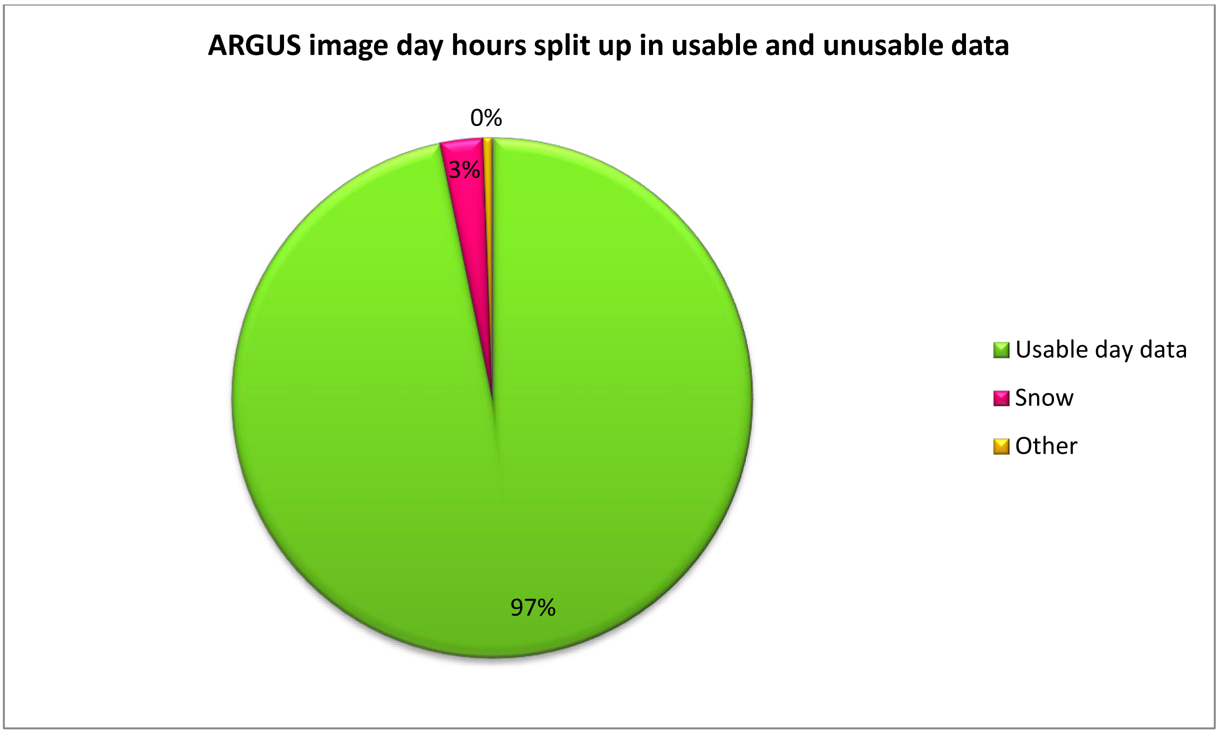

FIGURE 59: THE PROPORTION OF THE REMAINING ARGUS IMAGE DAY HOURS IN USABLE AND UNUSABLE DATA.

9.2.1. Precipitation

To get an indication of the distribution of rainy and dry days during which the ARGUS image data was considered, the year is divided into rainy and dry days. This distribution can be seen in Figure 60. Most of the times have been dry, just 10% of all data used during this study was during precipitation.

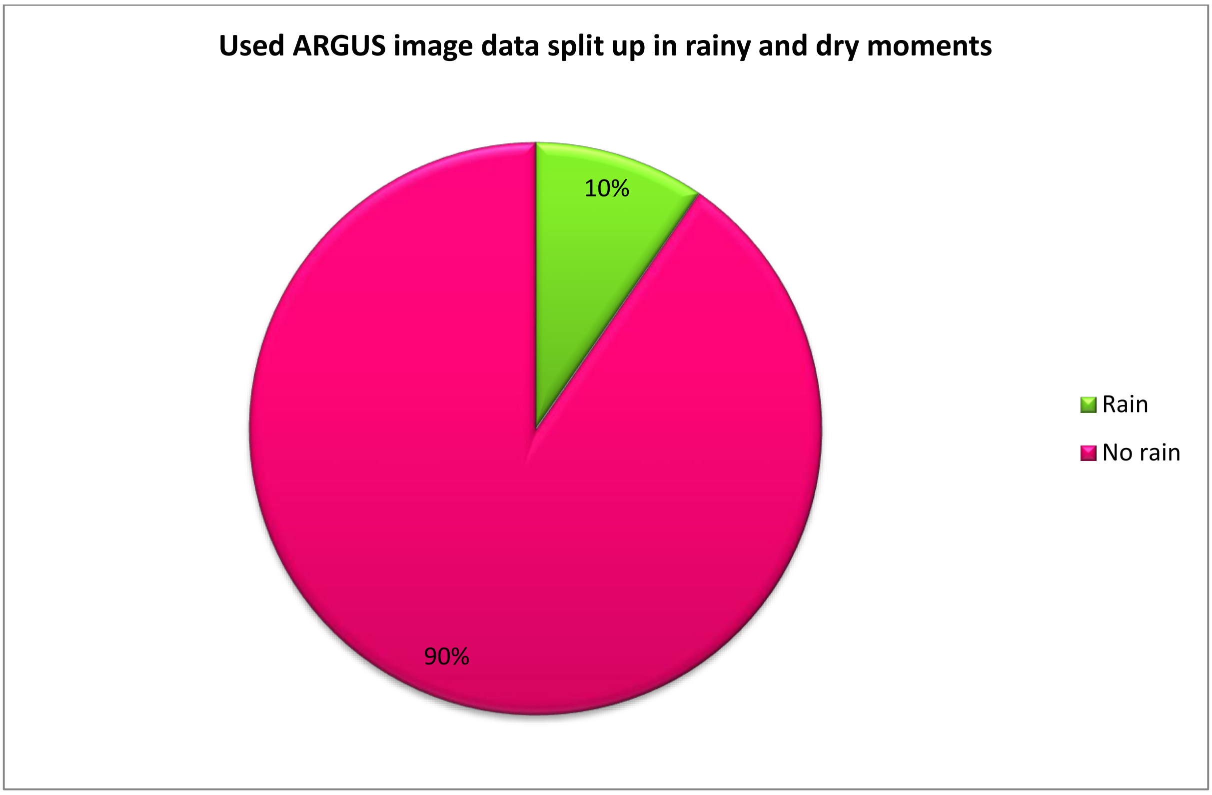

FIGURE 60: THE PROPORTION OF DRY AND RAINY DAYS IN THE ARGUS IMAGE DATA USED.

9.2.2. Uncertainties obtaining visible aeolian sediment transport

While looking for visible aeolian sediment transport using the different methods described above there were still times where it was more certain that visible aeolian sediment transport took place than at other times. Therefore the measure of uncertainty is added to the overview made and every observation has an uncertainty number, 1 not certain, 2 quite certain, 3 certain, which indicates the uncertainty of the decision made about whether there is visible aeolian sediment transport or not. Figure 61 is an overview of the amount of data which is categorized as certain, quite certain and not certain. Only about 10% of the data considered is categorized as quite certain and not certain which is 3.7% of the total data. Figure 62 presents the obtained visible aeolian sediment transport without the observations that have been marked as quite certain and not certain. Figure 63 only shows the observations that have been marked as uncertain, compared to the total amount of observations in Figure 62. It can be seen that the proportion of uncertain data is quite small. Most uncertainties can be found in onshore direction. Nevertheless, most of these uncertainties are in the quite certain category. Wind directions 220-220° shows the most uncertainty without having precipitation. A very small amount shows uncertainty during precipitation periods. It can be concluded because of the almost equal distribution of uncertain data over wind speeds and wind directions that the uncertainties found will not significantly influence the result of this study.

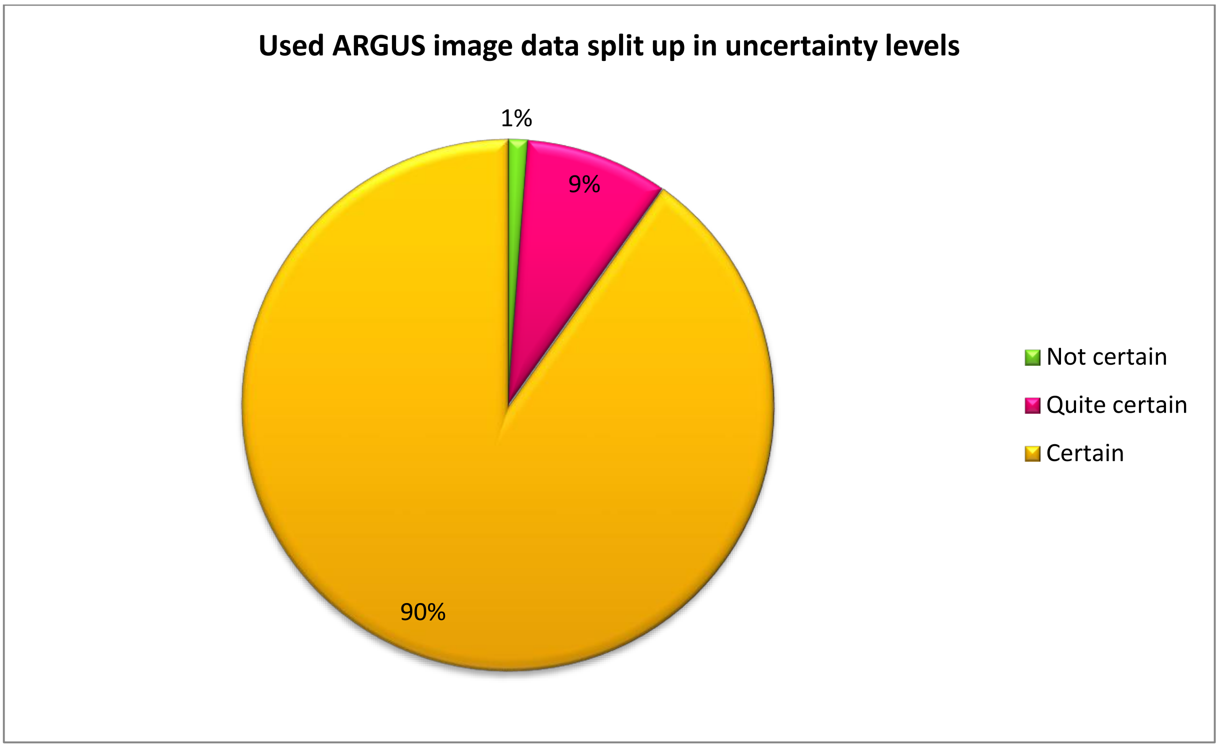

FIGURE 61: THE USED ARGUS IMAGE DATA BY UNCERTAINTY LEVELS.

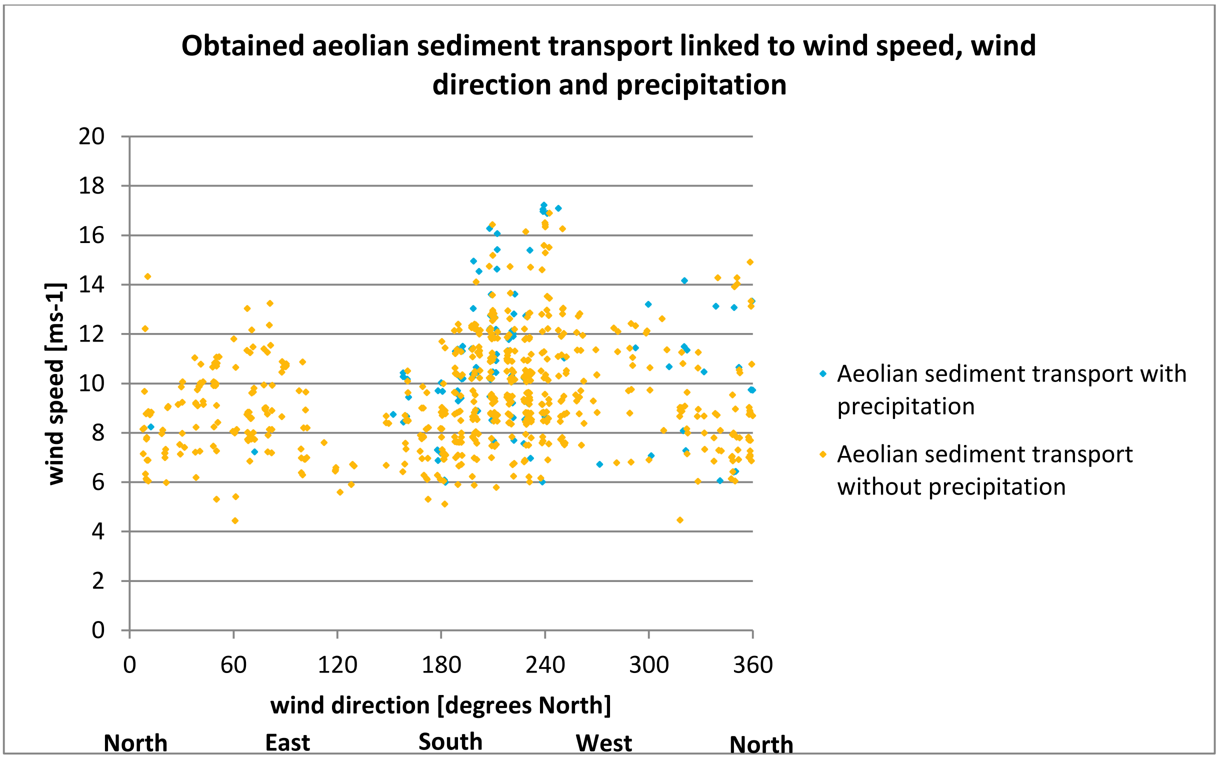

FIGURE 62: THE OBTAINED VISIBLE AEOLIAN SEDIMENT TRANSPORT LINKED TO WIND SPEED, WIND DIRECTION AND PRECIPITATION CONSIDERING ONLY THE OBSERVATIONS THAT HAVE SHOWN CERTAIN VISIBLE AEOLIAN SEDIMENT TRANSPORT.

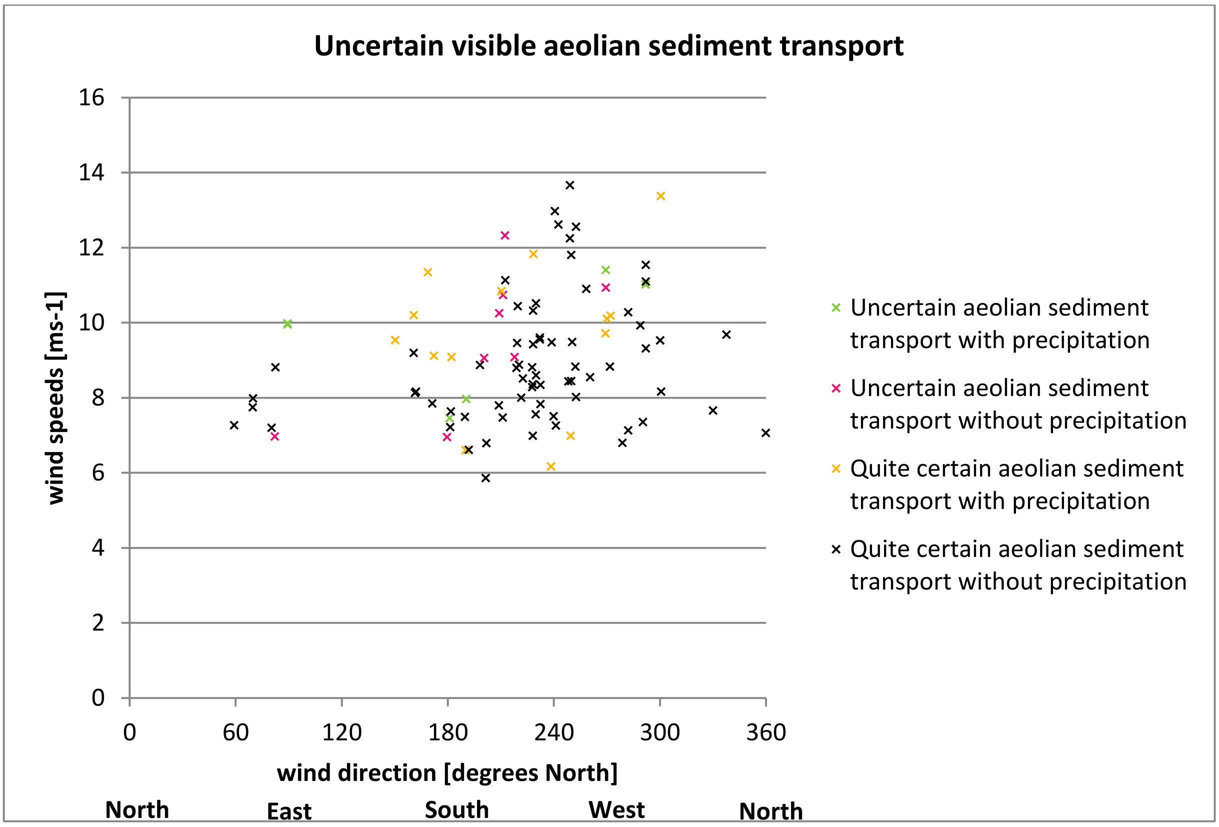

FIGURE 63: THE UNCERTAIN VISIBLE AEOLIAN SEDIMENT TRANSPORT.

9.2.3. Offshore and onshore data

Gaining insight in the process of aeolian sediment transport processes requires gaining insight into wind processes. To do so the wind directions were analysed. First of all the distribution of onshore and offshore winds needs to be known. The goal of this study is to get an indication of the amount of sediment transported towards the dune. Therefore, the onshore winds are important for this study. As can be seen in Figure 64 72% of the visible aeolian sediment transport took place in the onshore direction, the other 28% of the visible aeolian sediment transport took place in the offshore direction.

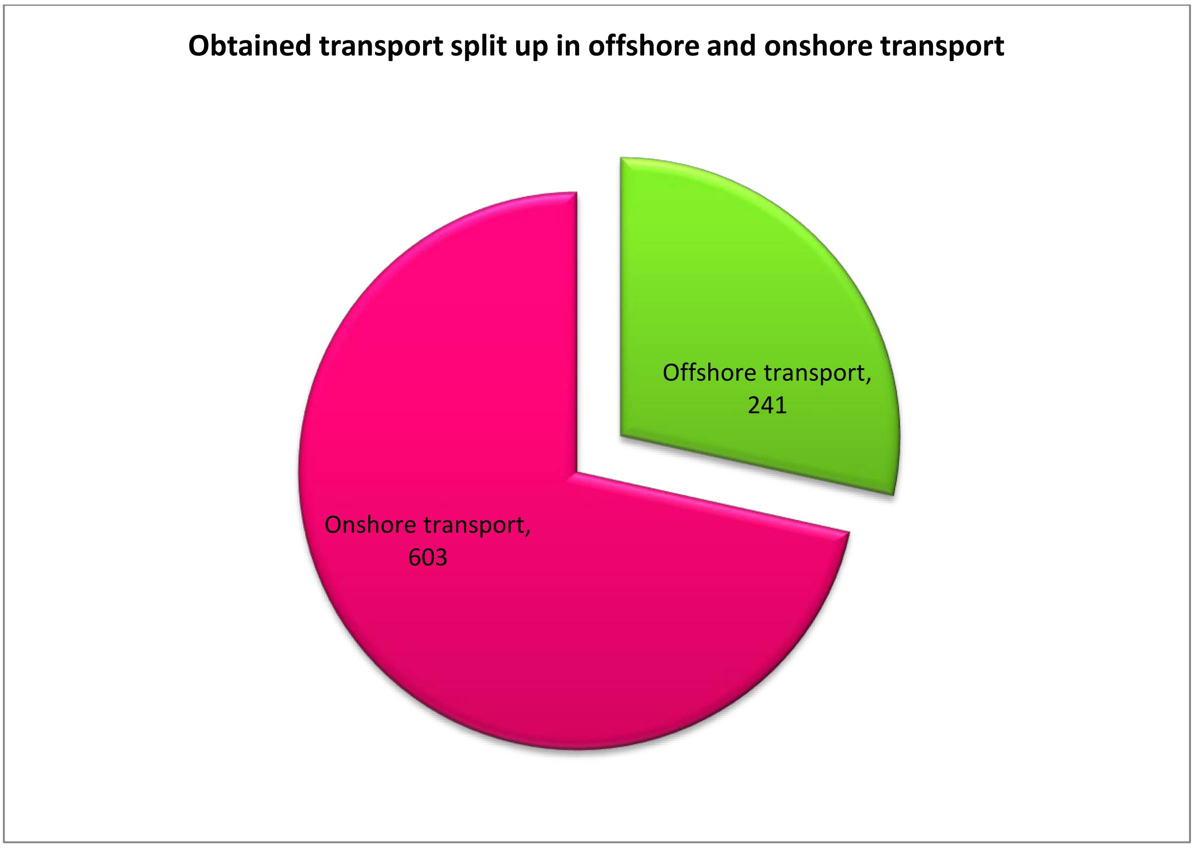

FIGURE 64: THE DISTRIBUTION OF OFFSHORE AND ONSHORE WIND DURING VISIBLE AEOLIAN SEDIMENT OCCURRENCES.

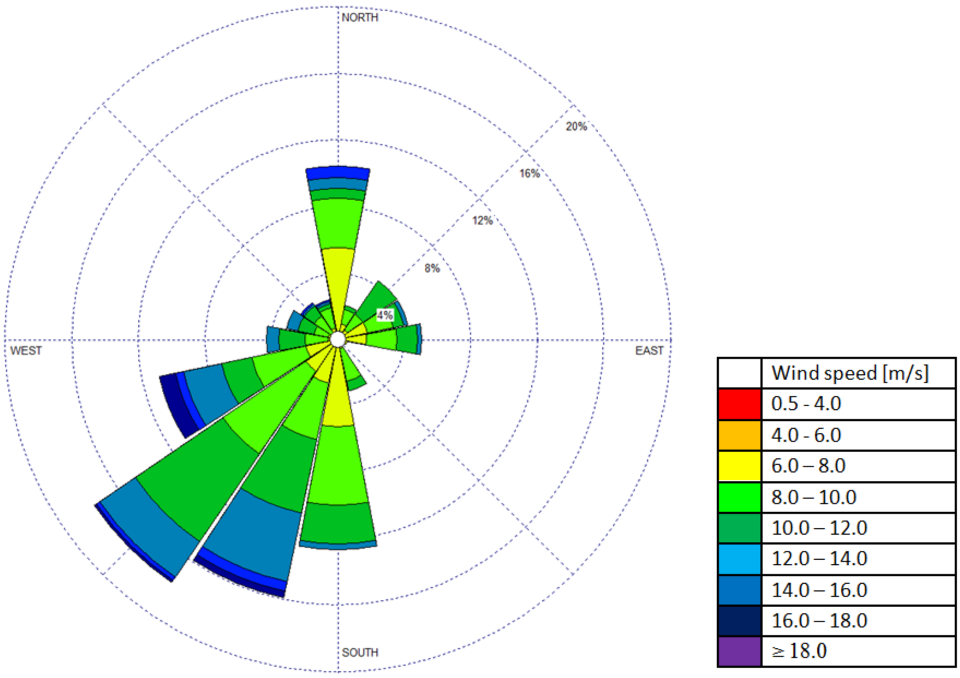

FIGURE 65: THE DIFFERENT WIND SPEEDS BY WIND DIRECTIONS.

9.3. SENSITIVITY ANALYSIS

Parameters	Values	Description
d	0.00025	Grain diameter [m]
A	0.167	Proportionality coefficient depending on the grain diameter; decreases linearly with the square root of the particle friction Reynolds number $A = 0.172 - 0.0046 Re_{*t}^{0.05} = 0.167$ for $d \geq 0.1 \cdot 10^{-3} m$ (Dong, et al., 2002)
k	0.4	Von Kármán constant
K	2.78	Kawamura's constant for grain sizes of 0.00025m
b	9	Coefficient according to van Dijk (1996)
g	9.81	Gravitational acceleration constant [ms^{-2}]
$\boldsymbol{\rho_a}$	1.225	Density of air at sea level at 15 °C [kgm^{-3}]
$\boldsymbol{\rho_s}$	2650	Density of pure crystalline quartz [kgm^{-3}]
$\mathbf{K_g}$	1.59	Correlational factor according to grain size of 0.000225 m defined by Dong (2002)
$\mathbf{z_0}$	0.0003	Surface roughness length [m] (Sherman, et al., 1998)
z	10	Height of measured wind speeds [m]
$\mathbf{U_z}$	12 (assumed)	Hourly averaged wind speed at height z [ms^{-1}]
M	0.25	Moisture content [%] according to Yang & Davidson-Arnott (2005)
F	5 (assumed)	Fetch distance [m]
$\mathbf{U_*}$	$U_z \frac{k}{\ln z/z_0} = 0.46$	Friction velocity "law of the wall" (von Kármán, 1930) [ms^{-1}]
$\mathbf{U_{*tm}}$	$A\left(\left(\frac{\rho_s}{\rho_a}\right) gd(1 + K_g \cdot M)\right)^{0.5} = 0.45$	Threshold friction velocity of moistened sand [ms^{-1}] Dong 2003
$\mathbf{F_c}$	$b \cdot (U_* + U_{*tm}) = 9.28$	Critical fetch [m] (Kawamura, 1951; van Dijk, 1996; Dong, et al., 2002)
$\mathbf{Q_m}$	$K\left(\frac{\rho_a}{g}\right)(U_* + U_{*tm})(U_* - U_{*tm})^2 = 161.23$	Maximum potential transport [$kgm^{-1}h^{-1}$]
Q	$Q_m \left(\frac{2}{\pi}\right) \sin^{-1} \frac{F}{F_c} = 58.42$	Visible aeolian sediment transport rate [$kgm^{-1}h^{-1}$]

TABLE 4: NOMINAL VALUES FOR THE PARAMETERS USED DURING THIS STUDY. THE WIND SPEED AND FETCH DISTANCE ARE THE ONLY VARIABLE INPUT PARAMETERS.

The fetch distance and the aeolian sediment transport rate showed of positive exponential relationship until the fetch distance reaches 10m at which the aeolian sediment transport rate increased exponential to 165 $kgm^{-1}h^{-1}$. Thereafter an equilibrium state is reached and the aeolian sediment transport did not increase any more as the fetch distance increased. The relationship between the aeolian sediment transport rate and the fetch distance can be seen in Figure 66.

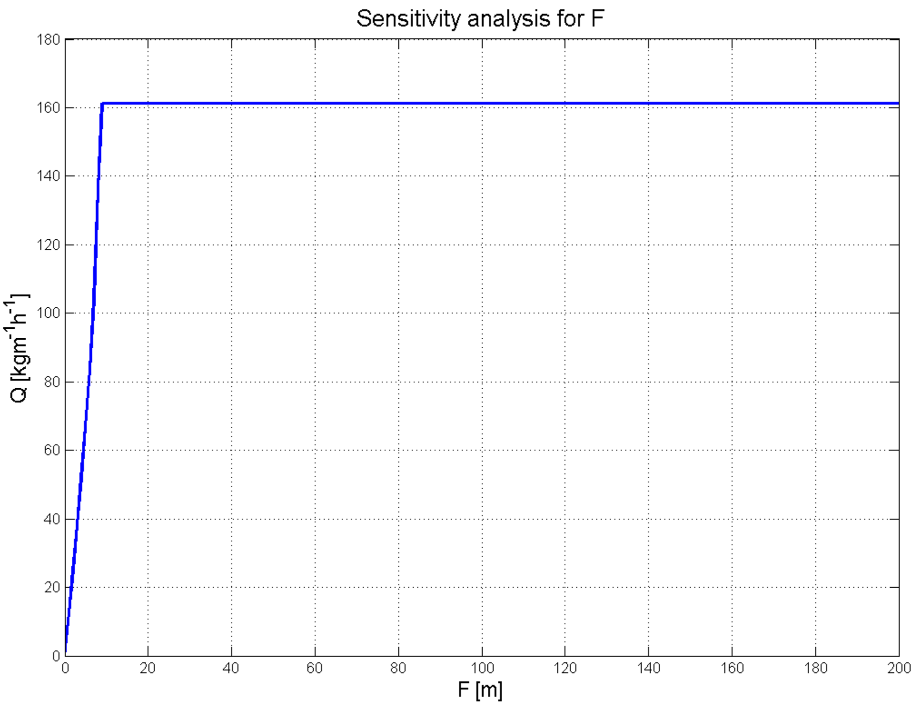

FIGURE 66: THE RELATIONSHIP BETWEEN THE AEOLIAN SEDIMENT TRANSPORT RATE AND THE FETCH DISTANCE.

Until the critical fetch distance reached a value of 50m the calculated aeolian sediment transport stayed constant. After this point the calculated aeolian sediment transport decreases exponentially. Eventually the point is reached where the critical fetch is not smaller than the fetch. Therefore, the useful part of this figure is the part where the calculated aeolian sediment transport decreased exponentially. The relationship between the aeolian sediment transport rate and the critical fetch distance can be seen in Figure 67.

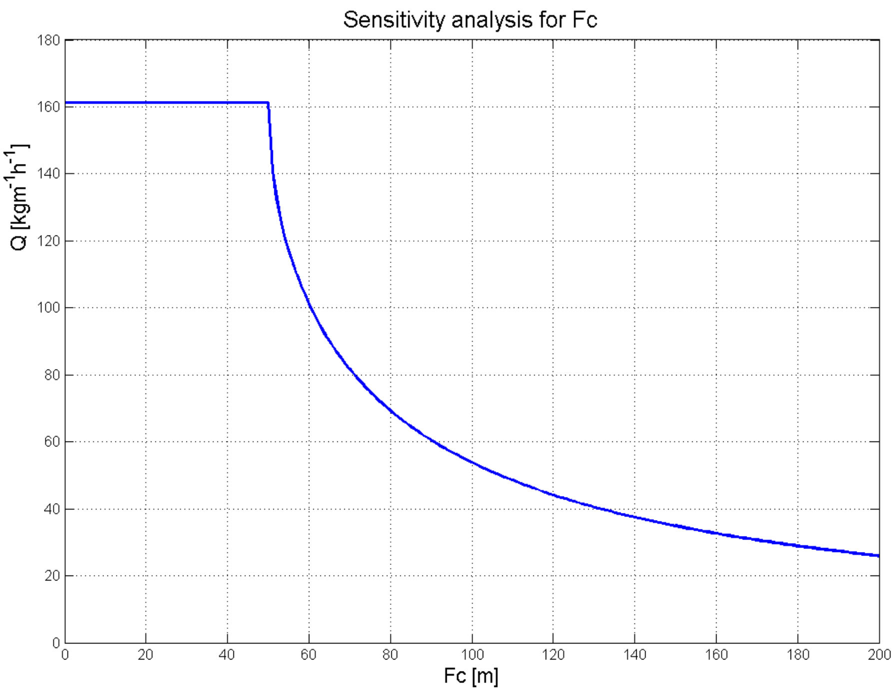

FIGURE 67: THE RELATIONSHIP BETWEEN THE AEOLIAN SEDIMENT TRANSPORT RATE AND THE CRITICAL FETCH DISTANCE.

Figure 68 shows the relationship between aeolian sediment rate, moisture content and wind speed at height z for the formula (10). The linear relationship between the sediment transport rate and the moisture content is clearly visible as well as the parabolic relationship between the aeolian sediment transport rate and the wind speed.

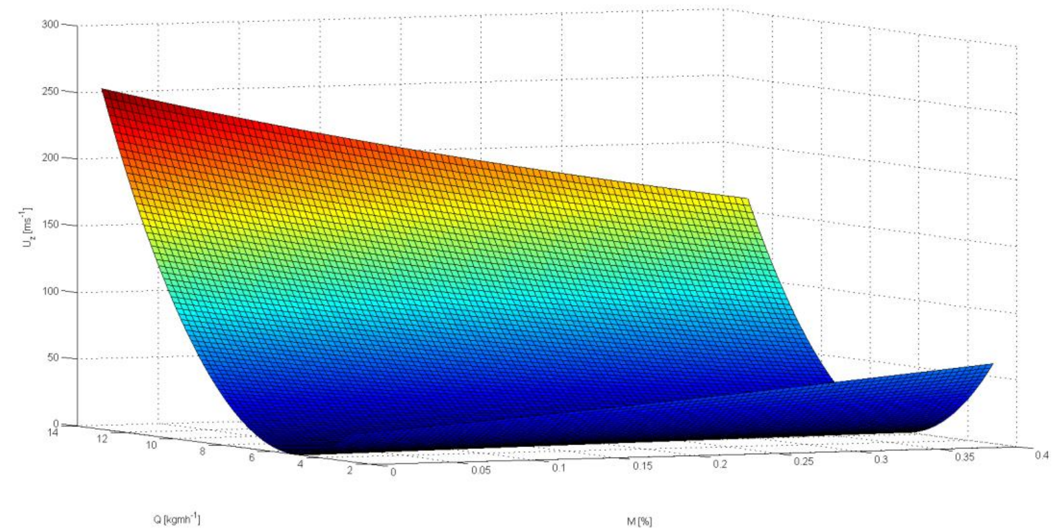

FIGURE 68: THE RELATIONSHIP BETWEEN TRANSPORT RATE, WIND SPEED AND MOISTURE CONTENT.

9.4. DETERMINATION OF THE FETCH DISTANCES

To be able to determine the fetch distances, a database was created linking all rectified images showing aeolian sediment transport to the wind direction, the hourly averaged wind speed measured at 10m above NAP, the corrected water level and the calculated critical fetch. For the calculation of the critical fetch see equation 5 in chapter 3.1. Each image in the database got a unique id. The program created using JavaScript uses the database to get all the information needed to determine the fetch distances.

The JavaScript model loads a rectified image and predetermines six lines in black at the angle of the wind direction starting at -40m or -30m cross shore. The three predetermines lines at one height (-40m or -30m) are 100m apart , as can be seen in Figure 69. The first line starts at (-425,-40) the second one starts at (-325,-40), the third one at (-225,-40), the fourth one at (-425,-30), the fifth one at (-325,-30) and the sixth one at (-225,-30). These generated lines have no determined length yet.

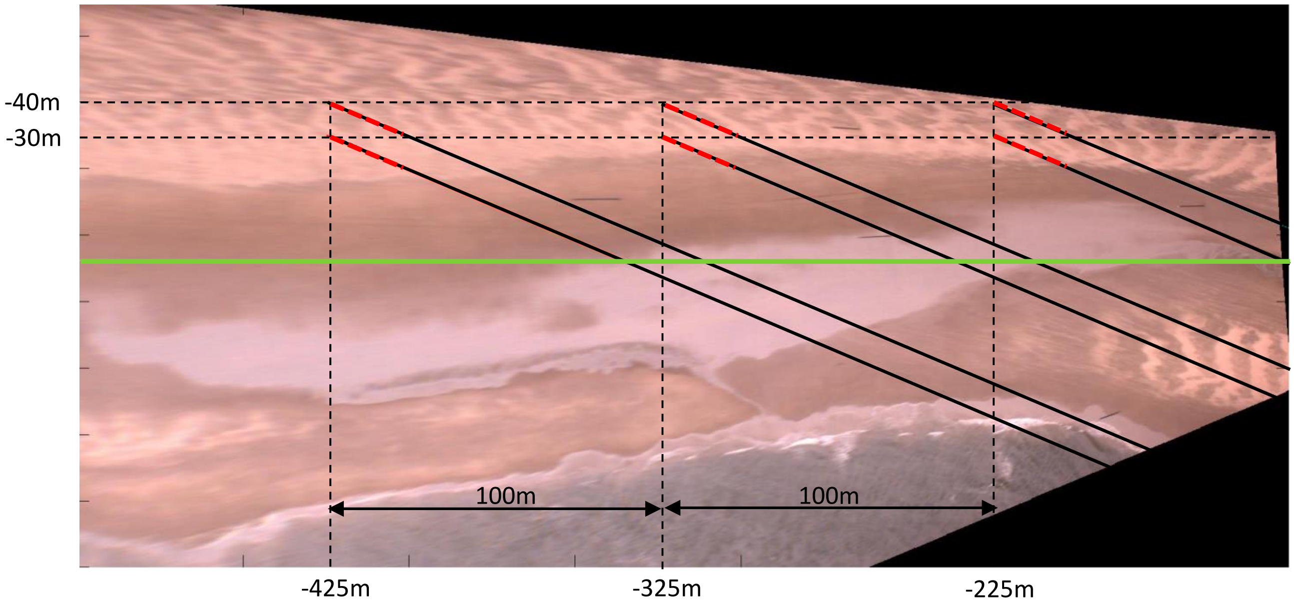

FIGURE 69: A LOADED RECTIFIED IMAGE INTO THE JAVASCRIPT PROGRAM. THE SIX PREDETERMINED LINES REPRODUCING THE WIND DIRECTION (BLACK), THE GREY LINE REPRESENTS THE MOUSE CURSOR TO DEFINE THE LENGTH OF EACH BLACK LINE, THE SIX DASHED RED LINES ARE SHOWING THE CALCULATED CRITICAL FETCH.

Every line can get an individual length by clicking with the mouse at the point on the rectified image until which the fetch distance should be calculated. By moving the mouse cursor the green line moves up or down. While determining one fetch distance for the whole beach intersection one has to pick the shortest fetch distance that can be seen in the image. Due to the fact of the green line covering the whole picture one can see very quickly where the shortest fetch distance is located.

By clicking at a point in the image the length of the fetch distance is defined and saved in the database. After having defined a fetch distance the line turns blue, as can be seen in Figure 70.

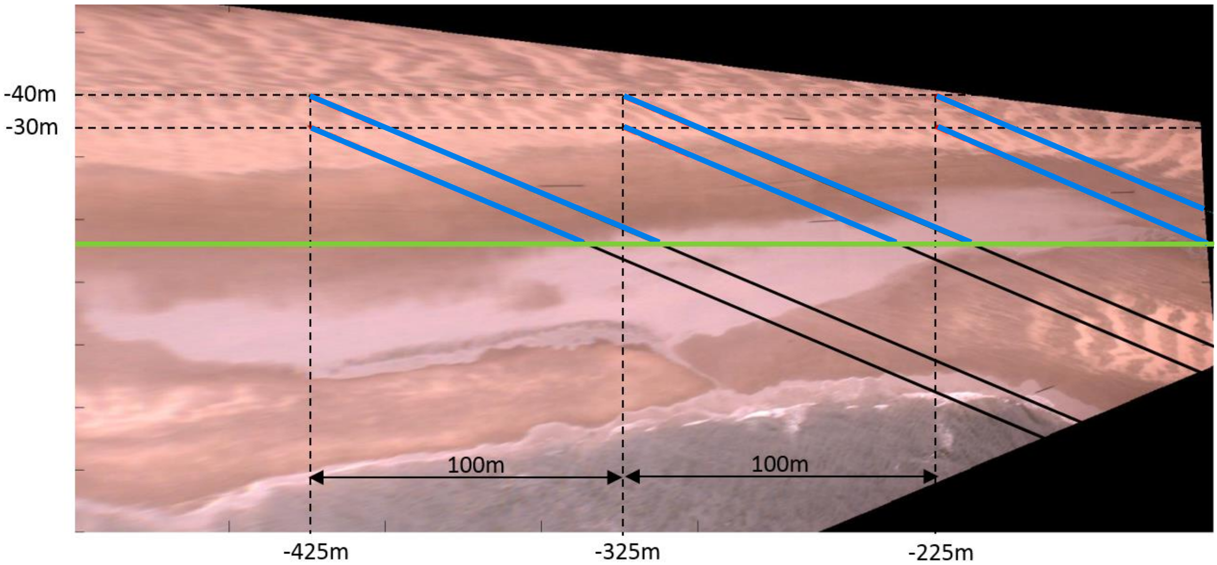

FIGURE 70: A LOADED RECTIFIED IMAGE INTO THE JAVASCRIPT MODEL. ALL DEFINED FETCH DISTANCES TURNED BLUE AFTER HAVING BEEN DEFINED.

After having made a choice for all six fetch distances for the varying intertidal topography one fetch distance for the whole non-varying beach intersection has to be determined.

The mouse cursor has to be moved in onshore direction behind the trough so that the shortest fetch distance can be determined. The determination process for the non-varying fetch distance can be seen in Figure 71.

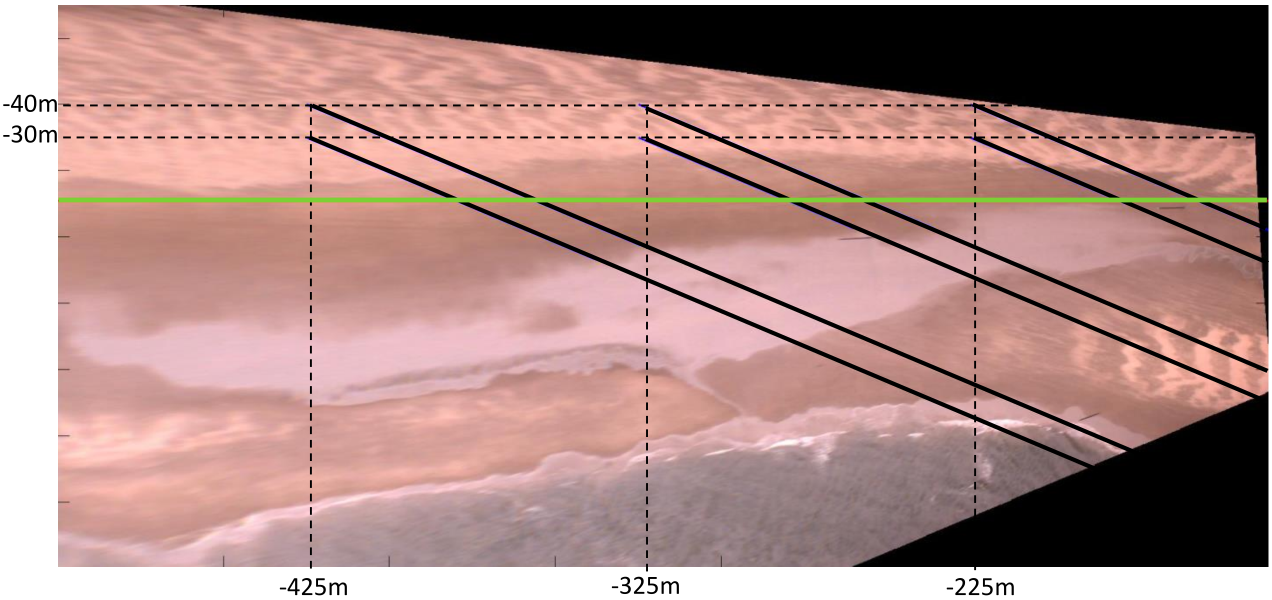

FIGURE 71: A LOADED RECTIFIED IMAGE INTO THE JAVASCRIPT MODEL. DETERMINATION OF THE LAST FETCH DISTANCE THAT DOES NOT TAKE THE VARYING INTERTIDAL BEACH TOPOGRAPHY INTO ACCOUNT BY MOVING THE MOUSE CURSOR ONSHORE BEHIND THE TROUGH.

All fetch distance which would end not visible in the image are not taken into account while analysing the fetch distance results.

The maximum fetch distance that could theoretically be seen in the images is 308.6m. The green lines that can be seen in Figure 72 show the maximum theoretical fetch distance.

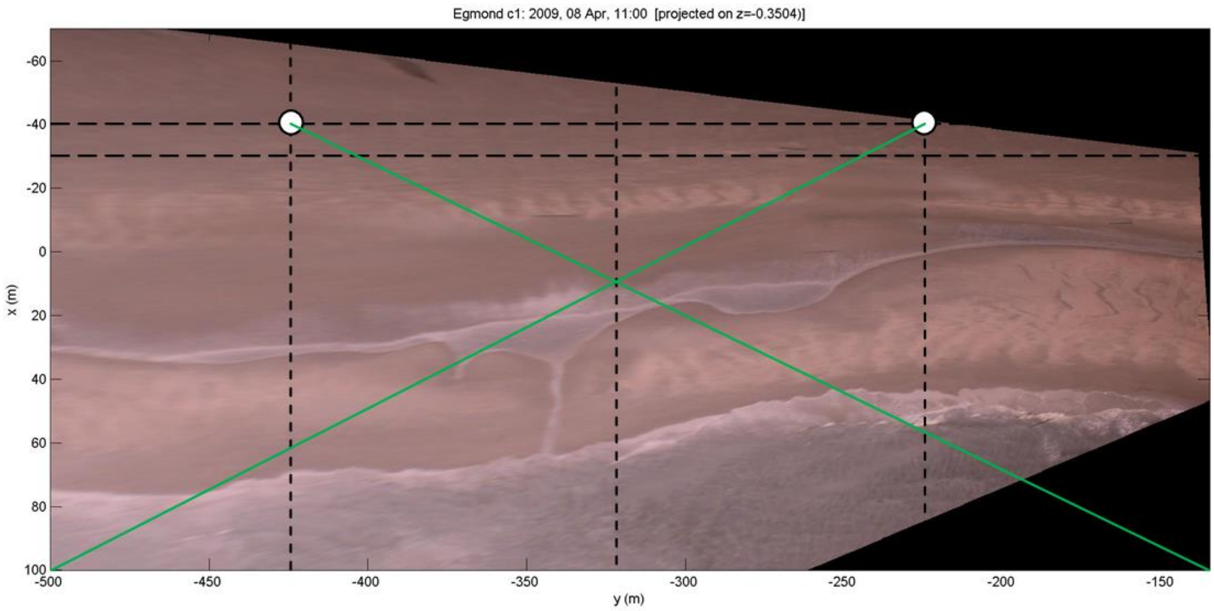

FIGURE 72: DETERMINATION OF THE THEORETICAL MAXIMUM FETCH DISTANCE THAT COULD BE SEEN ON THE RECTIFIED IMAGES. THE WHITE DOTS SHOW TWO MEASUREMENT POINTS THAT ARE OF IMPORTANCE DETERMINING THE MAXIMUM THEORECTICAL FETCH DISTANCE. THE GREEN LINES SHOW THE THEORETICAL MAXIMUM FETCH DISTANCE THAT CAN BE MEASURED.

During the rectification process, it is likewise assumed that the beach is flat, or in other words: the slope from the dune to the water level is not taken into account. This assumption might have impact on measurements of the fetch distances: the fetch distance as measured with the JavaScript program might differ from the actual fetch distance on the beach, due to the slope. In order to assess the significance of this difference in height on various points of the beach, an image is rectified with different z values. For example: high z values will represent the part of the beach close to the dune, and low z values will represent the part of the beach that is close to the sea. As is depicted in Figure 73, these varieties in height do not alter the rectified image a lot.

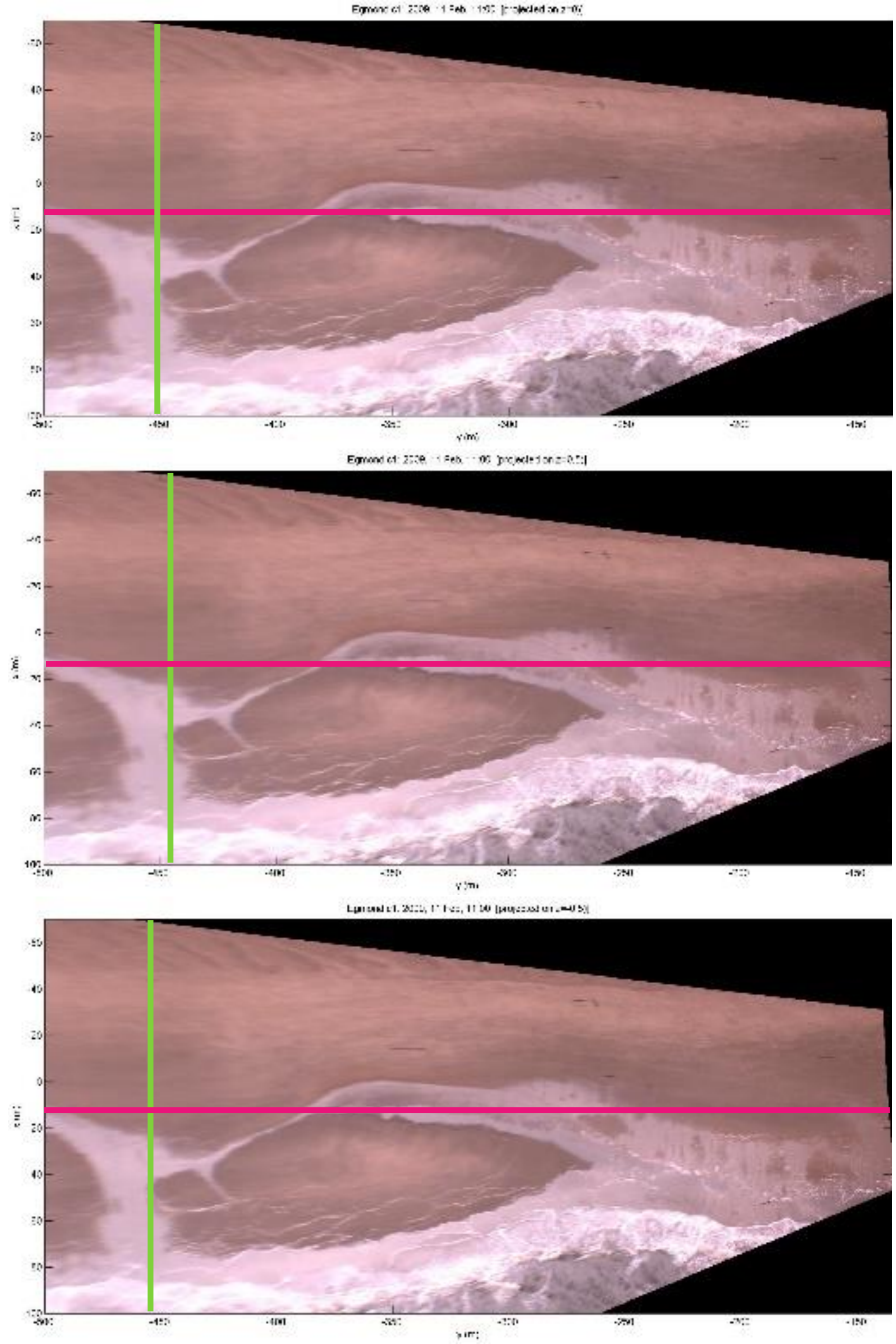

FIGURE 73: DIFFERENT RECTIFICATION LEVELS (-1M, -0.5M, 0.5M).

9.5. Cross shore component and wind directions

During the aeolian sediment transport calculation the cross shore component of the aeolian sediment transport has been calculated. This means calculating the actual amount of sediment transport per meter dune. Three measurement points next to each other on Egmond Beach were chosen on which the aeolian sediment transport rates have been calculated as explained in 3.2.3.2. Having wind approaching perpendicular to the beach the aeolian sediment transport through these three points is the aeolian sediment transport per meter that is assumed to reach the dune. If the wind approaches under an angle unequal to 90 degrees, the projection of 1 meter of wind stretches out over more than 1 meter on the dune, as can be seen in Figure 74. For this reason, the effective transport rate to the dunes decreases as the angle of the wind moves away from 90 degrees. Since the unit in which transport rate is expressed is kilograms per meter per second, the transport rate decreases as the same amount of sand per second passes through a larger width.

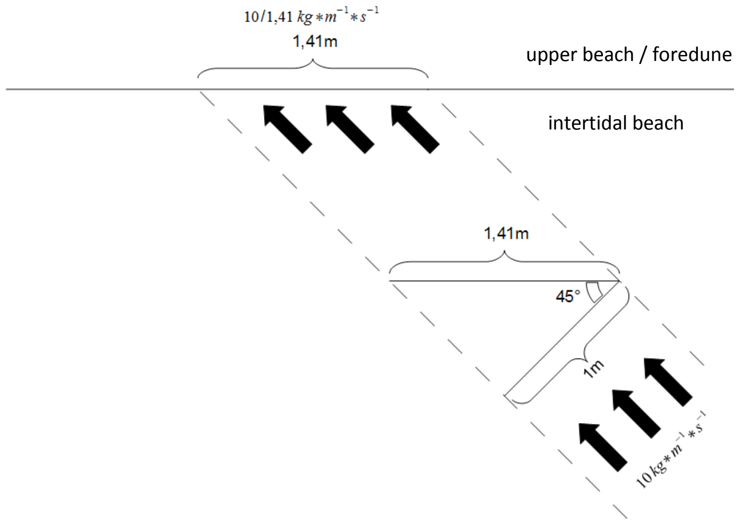

FIGURE 74: THE DEFINITION OF CALCULATING CROSS SHORE AEOLIAN SEDIMENT TRANSPORT.

Figure 75 shows the aeolian sediment transport occurrences per hour linked to the different wind directions. It appears that sediment transport mostly occurred while the wind approached from the South-West.

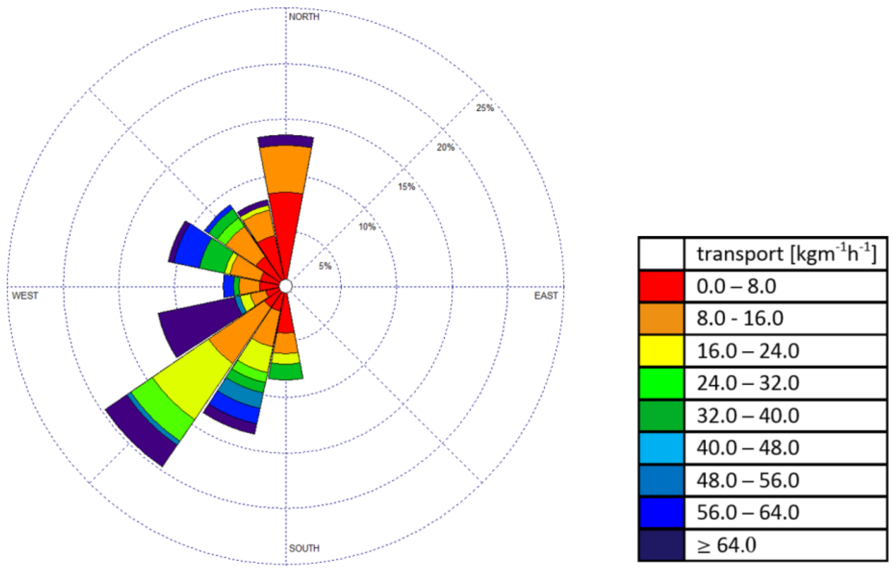

FIGURE 75: THE OCCURRENCE OF AEOLIAN SEDIMENT TRANSPORT ACCORDING TO WIND DIRECTIONS.

9.6. EXTRAPOLATION

In this section, example data is used that has no relationship with the actual data used in this study.

While extrapolating the annual aeolian sediment transport for the night, firstly, the fraction of the daytime hours when aeolian sediment transport has been identified is calculated. For example, if there are 800 daytime hours in total, and in 300 of these daytime hours, sediment movement has been observed, the fraction is equal to 300/800 = 0.375.

It is assumed that the percentage of aeolian transport hours during daytime is the same during the night. Therefore, the number of hours during the night has been multiplied by the fraction of the hours when aeolian sediment transport has been identified during daytime. This resulted in the amount of hours during the night for which aeolian sediment transport occurrences are assumed. For example, if there are 1600 night-time hours in total, the number of night-time hours in which sediment movement is assumed, is 1600*0.375 = 600. Note that this is twice the amount of daytime transport hours, since there are twice as much night-time hours than daytime hours.

Then, the total number of hours for which sediment movement is identified or assumed, is calculated by adding the number of hours where sediment transport is observed to the number of night-time hours where sediment transport is assumed. For example: Given the examples above, this would result in 300+600=900 total transport hours.

In total, there are 300 daytime hours for which transport is identified, and 900 hours for which transport is identified or assumed. If during the aforementioned 300 hours 200 kg sediment gets transported, one may assume that this would be 600 kg for 900 hours, since 900 is three times as high as 300. So the factor with which aeolian sediment transport during daytime has to be multiplied in order to calculate sediment transport during both daytime and night-time, is equal to the total number of hours for which sediment transport has been identified or assumed, divided by the number of hours for which sediment transport is identified during daytime. Given the aforementioned example, this would be 900/300 = 3.

Having calculated this factor, the annual sediment transport that is calculated using daytime data is multiplied by this factor, in order to extrapolate it to the transport during all hours in the year 2009.

9.7. Constraining factors

- During the summer month the beach is used for recreation. It was difficult to obtain visible aeolian sediment transport from the images because of people lying on the beach.
- The light conditions vary a lot throughout the day. They vary from almost too dark to obtain visible aeolian sediment transport to an almost reflecting beach were aeolian sediment was difficult to determine.
- Cars and horses were another restricting factor. Large number of tyre and horse made it almost impossible to obtain visible aeolian sediment transport on some days.
- Shadow of the dune is a limiting factor of the determination of visible aeolian sediment transport as well. When the sun comes from the East, a significant part of the beach is in shadow that made it difficult to obtain visible aeolian sediment transport on the ARGUS images.

Figure 76 shows examples of constraining factors.

THE RECREATIONAL USE DURING THE SUMMER OF EGMOND BEACH. AUGUST 5TH 2.00 PM

AN ALMOST TOO DARK BEACH TO OBTAIN VISIBLE AEOLIAN SEDIMENT TRANSPORT. DECEMBER 16TH 11.00 AM

AN ALMOST REFLECTING BEACH. MAY 28TH 1.00 PM

TOO MANY TYRE TRACKS MADE IT ALMOST IMPOSSIBLE TO OBTAIN VISIBLE AEOLIAN SEDIMENT TRANSPORT. DECEMBER 14TH 3.00 PM

FIGURE 76: CONSTRAINING FACTORS DURING THE PROCESS OF OBTAINING VISIBLE AEOLIAN SEDIMENT TRANSPORT.

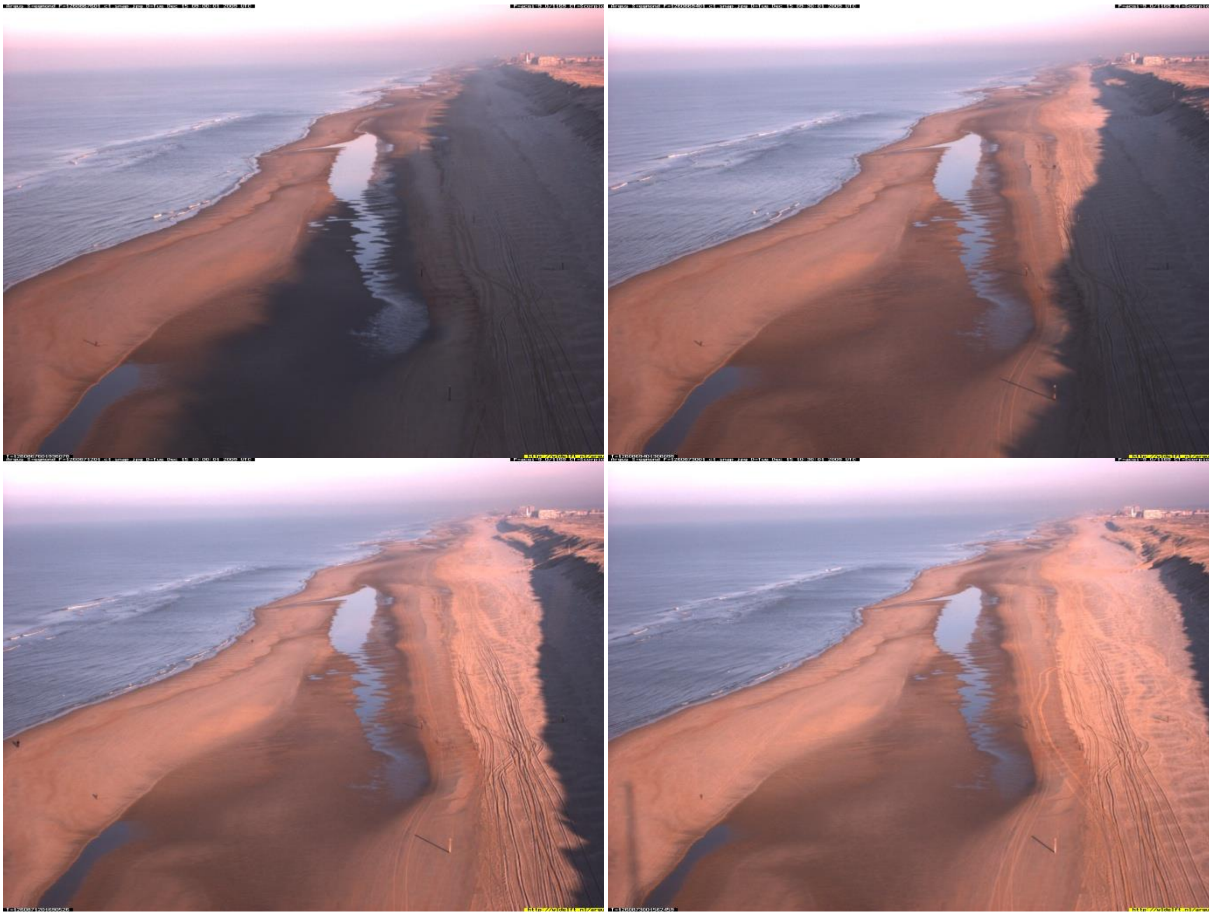

FIGURE 77: THE SHADOW OF THE DUNE AS A CONTRAINING FACTOR TO OBTAIN VISIBLE AEOLIAN SEDIMENT TRANSPORT WITHOUT UNCERTAINTIES. DECEMBER 15TH 9.30 AM UNTIL 10.30 AM

REFERENCES

Anthony Edward J., Ruz Marie-Hélène and Vanhée Stéphane Aeolian sand transport over complex intertidal bar-trough beach topography [Journal]. - [s.l.] : Geomorphology, 2009. - Vol. 105. - pp. 95-105.

Arens Bas Effecten van suppleties op duinontwikkeling [Report]. - [s.l.] : Rijkswaterstaat - Waterdienst, 2010.

Arens S. M. Rates of Aeolian Transport on a Beach in a Temperate Humid Climate [Journal] // Geomorphology. - 1996. - Vols. 17(1-3). - pp. 3-18.

Atherton Rachel J., Baird Andrew J. and Wiggs Giles F. S. Inter-tidal Dynamics of Surface Mositure Content on a Meso-tidal Beach [Journal]. - West Palm Beach (Florida) : Journal of Coastal Research, 2001. - 2 : Vol. 17. - pp. 482-489.

Attema Jisk and Lenderink Geert Mean precipitation changes and coastal effects in the ENSEMBLES regional climate model simulations [Report]. - De Bilt : KNMI, 2011.

Baas A. C. W. and Sherman D. J. The formation and behavior of aeolian streamers [Journal]. - [s.l.] : Journal of Geophysical Research, 2005. - Vol. 110.

Bagnold R. A. The physics of blown sand and desert dunes [Report]. - New York : Willian Morrow and Comp., 1941.

Bauer B. O. [et al.] Aeolian transport measurement across a beach and dune at Castroville [Journal] // Coastal Dunes: Form and Process. - 1990. - pp. 39-55.

Bauer B.O. [et al.] Aeolian sediment transport on a beach: Surface moisture, wind fetch, and mean transport [Journal] // Geomorphology. - 2009. - Vol. 105. - pp. 106-116.

Bauer Bernard O. and Davidson-Arnott Robin G.D. A general framework for modeling sediment supply to coastal dunes including wind angle, beach geometry, and fetch effects [Journal] // Geomorphology. - 2002. - Vol. 49. - pp. 89-108.

Belly Pierre-Yves Sand movement by wind [Journal]. - Berkeley : Institute of Engineering Research, July 1962. - 7 : Vol. 72.

Czitrom Veronica One-Factor-at-a-Tine versus Designed Experiments [Journal]. - [s.l.] : The American Statistician, 1999. - 2 : Vol. 53. - pp. 126-131.

Darke Ian, Davidson-Arnott Robin and Ollerhead Jeff Measurement of Beach Surface Moisture Using Surface Brightness [Journal] // Journal of Coastal Research. - [s.l.] : Coastal Education and Research Foundation, 2009. - Vol. 251. - pp. 248-256.

Davidson-Arnott Robin G. D. and Law Mark N. Measurement and Prediction of Long-Term Sediment Supply to Coastal Foredunes [Journal] // Journal of Coastal Research. - 1996. - Vol. 12(3). - pp. 654-663.

Davidson-Arnott Robin G.D. [et al.] The effect of surface moisture on aeolian sediment transport threshold and mass flux on a beach [Journal] // Earth Surface Processes and Landforms. - 2008. - Vol. 33. - pp. 55-74.

Davidson-Arnott Robin G.D., MacQuarrie Kelvin and Aagaard Troels The effect of wind gusts, moisture content and fetch length on sand transport on a beach [Journal] // Geomorphology. - 2005. - Vol. 68. - pp. 115-129.

de Vries S. [et al.] Dune behavior and aeolian transport on decadal timescales [Journal] // Coastal Engineering. - 2012. - Vol. 67. - pp. 41-53.

de Vries Sierd Physics of Blown Sand and Coastal Dunes [Report]. - Delft : [s.n.], 2013.

Delgado-Fernandez Irene A review of the application of the fetch effect to modelling sand supply to coastal foredunes [Journal] // Aeolian Research. - 2010. - Vol. 2. - pp. 61-70.

Delgado-Fernandez Irene and Davidson-Arnott Robin Meso-scale aeolian sediment input to coastal dunes: The nature of aeolian transport events [Journal] // Geomorpholgy. - 2011. - Vol. 126. - pp. 217-232.

Dong Zhibao [et al.] Aeolian sand transport: a wind tunnel model [Journal] // Sedimentary Geology. - 2003. - Vol. 161. - pp. 71-83.

Dong Zhibao, Liu Xiaoping and Wang Xunming Wind initiation thresholds of moistened sands [Journal] // Geophysical research letters. - 2002. - Vol. 29. - pp. 25-1 - 25-3.

Edwards Brandon L., Schmutz Phillip P. and Namikas Steven L. Comparison of Surface Mositure Measurements with Depth-Integrated Moisture Measurements on a Fine-Grained Beach [Journal]. - West Palm Beach (Florida) : Journal of Coastal Research, 2012.

Einstein H. A. The bed load function for sediment transportation in open channel flows [Report]. - [s.l.] : U. S. Department of Argriculture Tech. Bull, 1950.

Greeley R. and Iversen J. D. Wind as a geological process [Journal]. - Cambridge : Cambridge University Press, 1985.

Han Qingjie [et al.] Wind tunnel investigation of the influence of surface moisture content on the entrainment and erosion of beach sand by wind using sands from tropical humid coastal southern China [Article] // Geomorphology. - 2009. - Vol. 104. - pp. 230-237.

Hansen Frank V. Surface roughness lengths [Report]. - [s.l.] : U.S. Army Research Laboratory, 1993.

Hardisty J. and Whitehouse R. J. S. Evidence for a new sand transport process from experiments on Saharan dunes [Journal] // Nature. - 1988. - Vol. 332. - pp. 532-534.

Horn D. P. Beach groundwater dynamics [Journal]. - [s.l.] : Geomorphology, 2002. - Vol. 48. - pp. 121-146.

Horn D. P. Measurements and modelling of beach groundwater in the swash-zone: a review [Journal]. - [s.l.] : Continental Shelf Research, 2006. - Vol. 26. - pp. 622-652.

Hsu Shih-Ang Measurements of Shear Stress and Roughness Length on a Beach [Journal] // Journal of Geophysical Research. - [s.l.] : Coastal Studies Institute, Louisiana State University, 20 April 1971. - 12 : Vol. 76.

Iversen J. D. and White B. R. Saltation threshold on Earth, Mars and Venus [Journal] // Sedimentology. - 1982. - Vol. 29. - pp. 111-119.

Iversen James D. and Rasmussen Keld R. The effect of wind speed and bed slope on sand transport [Journal] // Sedimentology. - 1999. - Vol. 46. - pp. 723-731.

Jackson D. W. T. and Cooper J. A. G. A Review of the Effects of Surface Moisture Content on Aeolian Sand Transport [Journal]. - [s.l.] : Sedimentology, 1999. - Vol. 46. - pp. 517-522.

Jackson D. W. T. and Cooper J. A. G. Beach fetch distance and aeolian sediment transport [Journal] // Sedimentology. - 1999. - Vol. 46. - pp. 517-522.

Jackson D. W. T. and McCloskey J. Preliminary results from a field investigation of aeolian sand transport using high resolution wind and transport measurements [Journal]. - [s.l.] : Geophys. Res. Lett., 1997. - Vol. 24. - pp. 163-166.

Jackson Derek W. T. [et al.] Airflow reversal and alternating corkscrew vortices in foredune wake zones during perpendicular and oblique offshore winds [Journal] // Geomorphology. - 2013. - Vol. 187. - pp. 86-93.

Janssen G.M. and Mulder S. De ecologie van de zandige kust van Nederland [Report]. - [s.l.] : Rijkswaterstaat, 2004.

Johnson Joe W. Sand movement on coastal dunes [Conference] // Federal inter-agency sedimentation conference. - Berkeley : U.S. Department of Agriculture, 1963. - Vol. 970. - pp. 747-755.

Kadib A. A. A function for sand movement by wind [Report]. - Berkeley : Coastal Engineering Research Center, 1965.

Kadib A.A. A function for sand movement by wind [Report]. - Berkeley : Hydraulic Engineering Laboratory, 1965.

Kawamura R. Study of sand movement by wind [Report]. - Tokyo : [s.n.], 1951.

Kim Soo Wan [et al.] Detection of moving objects with a moving camera using non-panoramic background model [Journal] // Machine Vision and Applications. - New York : Springer, 2012. - 5 : Vol. 24.

Lynch Kevin, Jackson Derek W. T. and Cooper J. Andrew G. Aeolian fetch distance and secondary airflow effects: the influence of micro-scale variables on meso-scale foredune development [Journal] // Earth Surface Processes and Landforms. - 2008. - Vol. 33. - pp. 991-1005.

Mabutt J. A. Desert Landforms [Report]. - Canberra : Australian National University Press Canberra, 1977. - p. 219.

Mangor Karsten [Online] // Statistical description of wave parameters. - 24 October 2007. - 16 August 2013. - http://www.coastalwiki.org/wiki/Statistical_description_of_wave_parameters.

Mobbs Stephen University of Leeds AWS Data [U. Leeds] [Online] // Earth Observing Laboratory. - University of Leeds, 2006. - 12 September 2013. - http://data.eol.ucar.edu/codiac/dss/id=92.043.

NCAR/EOL PCAPS ISFS 1 second data [Online] // Earth Observung Laboratory. - NCAR, 2011. - 12 September 2013. - http://data.eol.ucar.edu/codiac/dss/id=233.003.

Nickling W. G. and McKenna Neuman C. Aeolian sediment transport [Book Section] // Geomorphology of Desert Environments / book auth. Parsons A. J. and Abrahams A. D.. - [s.l.] : Springer Netherlands, 2009.

Nordstorm K. F. and Jackson N. L. Effect of source width and tidal elevation changes on aeolian transport on an estuarine beach [Journal] // Sedimentology. - 1992. - Vol. 39. - pp. 769-778.

Oblinger Arnaud and Anthony Edward J. Surface Moisture Variations on a Multibarred Macrotidal Beach: Implications for Aeolian Sand Transport [Journal]. - West Palm Beach (Florida) : Journal of Coastal Research, 2008. - 5 : Vol. 25. - pp. 1194-1199.

Quartel S., Kroon A. and Ruessink B. G. Seasonal accretion and erosion patterns of a microtidal sandy beach [Journal] // Marine Geology. - [s.l.] : Marine Geology, 2008. - Vols. 250(1-2). - pp. 19-33.

Rice M. A. Grain shape effects on aeolian sediment transport [Journal] // Acta Mechanica. - 1990. - Vol. 1. - pp. 159-166.

Rijkswaterstaat [Online] // waterbase. - 2009. - 16 August 2013. - http://live.waterbase.nl/waterbase_wns.cfm?taal=nl.

Sherman D. J. and Hotta S. Aeolian sediment transport: theory and measurement [Journal] // Coastal Dunes: Form and Process. - 1990. - pp. 17-37.

Sherman Douglas J. [et al.] Wind-blown sand on beaches: an evaluation of models [Journal] // Geomorphology. - 1998. - Vol. 22. - pp. 113-133.

Sherman Douglas J. Problems of scale in the modeling and interpretation of coastal dunes [Journal] // Marine Geology. - 1995. - Vol. 124. - pp. 339-349.

Sørensen On the Rate of Aeolian Sand Transport [Conference]. - Lubbock : [s.n.], 2002.

Stout J. E. and Zobeck T. M. Intermittent saltation [Journal]. - [s.l.] : Sedimentology, 1997. - Vol. 44. - pp. 959-970.

Svasek J. N. and Terwindt J. H. J. Measurements of sand transport by wind on a natural beach [Journal]. - [s.l.] : Sedimentology, 1974. - Vol. 21. - pp. 311-322.

Taal Marcel [et al.] 15 YEARS OF COASTAL MANAGEMENT IN THE NETHERLANDS; POLICY, IMPLEMENTATION AND KNOWLEDGE FRAMEWORK [Report]. - The Hague : Rijkswaterstaat, National Institute for Coastal and Marine Management / RIKZ, 2006.

Tattelman Paul Surface Gustiness and Wind Speed Range as a Function of Time Interval and Mean Wind Speed [Journal]. - [s.l.] : Journal Of Appliesd Meteorology, October 1975. - Vol. 14. - pp. 1271-1276.

van der Wal D. Effects of fetch and surface texture on aeolian sand transport on two nourished beaches [Journal] // Journal of Arid Environments. - 1998. - Vol. 39. - pp. 533-547.

van der Wal Daphne Grain-Size-Selective Aeolian Sand Transport on a Nourished Beach [Journal]. - Amsterdam : Journal of Coastal Research, 2000. - 3 : Vol. 16. - pp. 896-908.

van Dijk Paul Aanpassingslengtes, vegetatie en modelgevoeligheid [Report] / Landscape and environmental research group. - Amsterdam : Technische adviescommissie voor de waterkeringen, 1996.

van Rijn L. C. [et al.] The predictability of cross-shore bed evolution of sandy beaches at the time scale of storms and seasons using process-based Profile models [Journal] // Coastal Engineering. - 2003. - Vol. 47. - pp. 295-327.

Vanhée Stéphane, Anthony Edward J. and Ruz Marie-Hélène Aeolian Sand Transport on a Ridge and Runnel Beach: Preliminary Results from Leffrinckoucke Beach, Northern France [Journal]. - [s.l.] : Journal of Coastal Research, 2002. - Vol. 36. - pp. 732-740.

Veerman C.P., Bakker, I.M., van Duin, J.J., Fresco, L.O. Samen Werken Met Water [Report]. - [s.l.] : Deltacommissie 2008, 2008.

von Kármán Theodore Mechanische Ähnlichkeit und Turbulenz [Report] / Fachgruppe 1 (Mathematik). - Göttingen : Nachrichten von der Gesellschaft der Wissenschaften zu Göttingen, 1930.

Wesselink Anna J. Flood safety in the Netherlands: The Dutch response to Hurricane Katrina [Journal] // Technology in Society 29. - 2007. - pp. 239–247.

Wieringa J. and Rijkoort P. J. Windklimaat van Nederland [Report]. - Den Haag : Staatsuitgeverij, 1983.

Wiggs G. F. S., Atherton R. J. and Baird A. J. Thresholds of aeolian sand transport: establishing suitable values [Journal]. - [s.l.] : Sedimentology, 2004. - Vol. 51 (1). - pp. 95-108.

Wijnberg K.M. Environmental controls on decadal morphologic behaviour of the Holland coast [Journal] // Marine Geology. - 2002. - pp. 227-247.

Yang Yanqi and Davidson-Arnott Robin G. D. Rapid Measurement of Surface Moisture Content on a Beach [Journal] // Journal of Coastal Research. - [s.l.] : Coastal Education and Research Foundation, 2005. - Vol. 213. - pp. 447-452.

Zingg A. W. Wind tunnel studies of the movement of sedimentary material [Conference] // Fifth Hydraulic Conference. - 1952.